BASIC AND APPLIED RESEARCH IN THE EARTH SCIENCES

ANALYSIS OF GROUND MOTIONS AND CLOSE-IN PHYSICAL EFFECTS, RULISON EVENT

BY

R. Q. FOOTE
C. R. CASSITY
P. C. LOUX
L. J. O'BRIEN
F. W. POWER
W. W. HAYS
R. D. LYNCH
F. R. PERCHALSKI
C. T. SPIKER
A. P. WHIPPLE

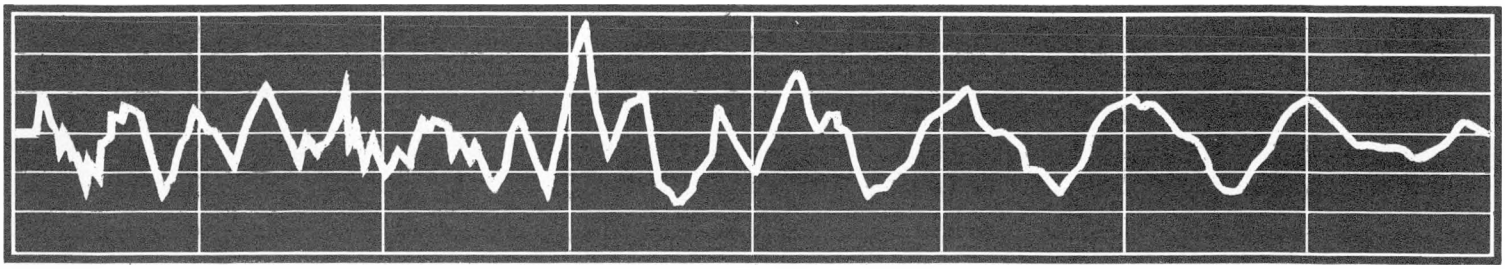

ENVIRONMENTAL RESEARCH CORPORATION
a subsidiary of computer sciences corporation

APRIL 1970

COMPUTER SCIENCES CORPORATION
ENVIRONMENTAL RESEARCH CORPORATION (702) 734-3833
2769 SOUTH HIGHLAND DRIVE · LAS VEGAS, NEVADA 89102

ERC-15845

July 30, 1971

WALTER W. HAYS
Technical Director

ERRATA
NVO-1163-206

To: Distribution

Subject: Rulison Ground Motions Recorded at the TOSCO Mine and Tower Stations

In response to a request from Mr. R. A. Johnson, Office of Effects Evaluation, USAEC, NVOO, the TOSCO mine and tower seismograms recorded from Rulison have been processed and 5% PSRV spectra have been derived for the radial and transverse components of motion recorded at the mine and the vertical and transverse components recorded at the tower. The PSRV spectra for these components and copies of the seismograms for these stations are attached. The data from these stations were not processed previously because the signals were clipped (overranged) in varying degrees on all components. The vertical component recorded at the mine and the radial component recorded at the tower were too severely clipped to be processed. Since PSRV spectra derived from overranged signals are distorted over the entire frequency band, the attached PSRV spectra for the TOSCO mine and tower stations do not correspond to the response that would have been derived if the signals had not overranged. The errors associated with the attached spectra are unknown. Although it is our opinion that the PSRV spectra derived from the TOSCO mine and tower data are probably reasonable approximations to the true response, these spectra should be used with caution recognizing that proper use of these spectra depends on the specific application.

Very truly yours,

ENVIRONMENTAL RESEARCH CORPORATION

Walter W Hays

Walter W. Hays

DLO:va

Enclosures

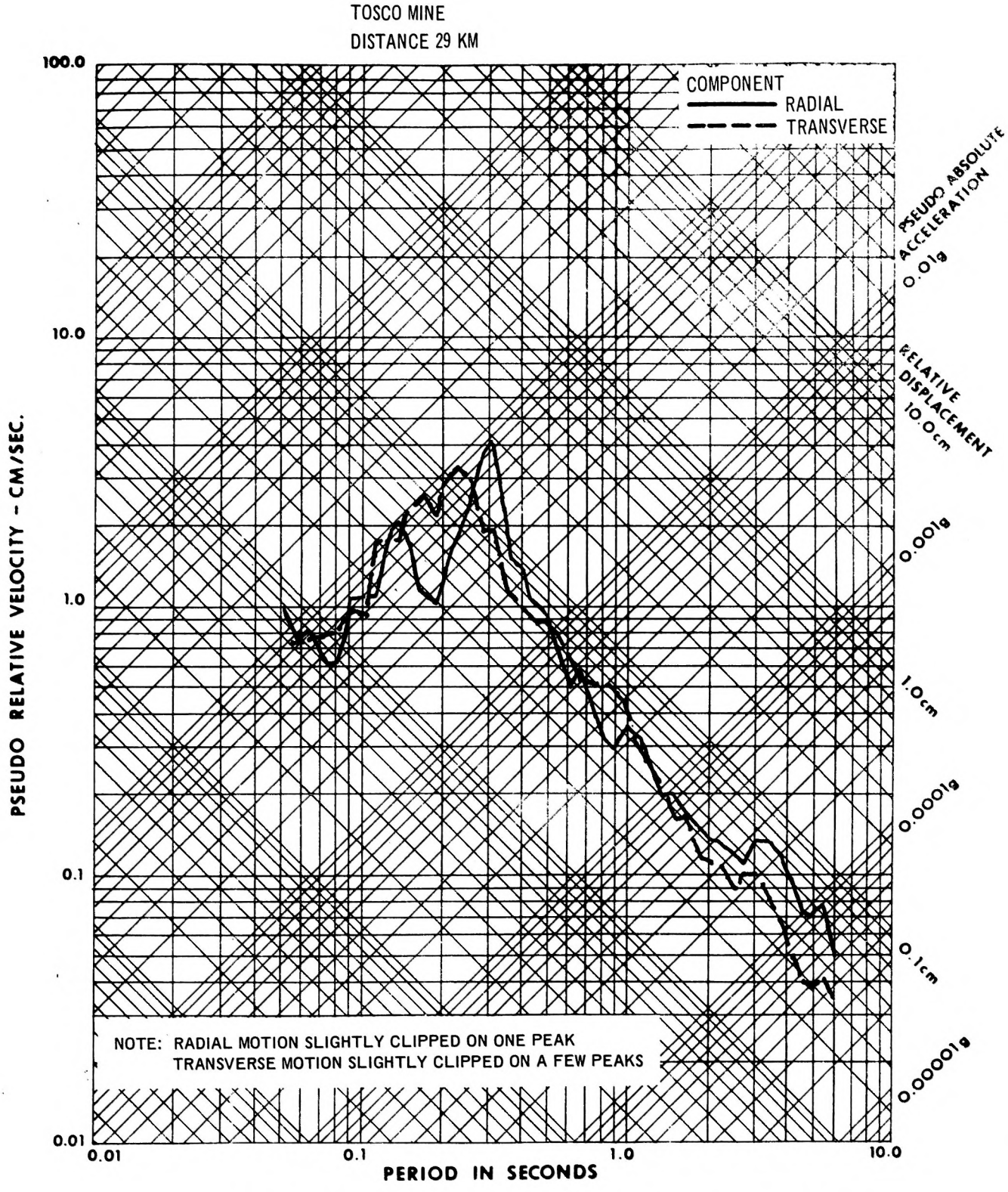

Observed 5% PSRV Spectra at TOSCO Mine, Rulison Event

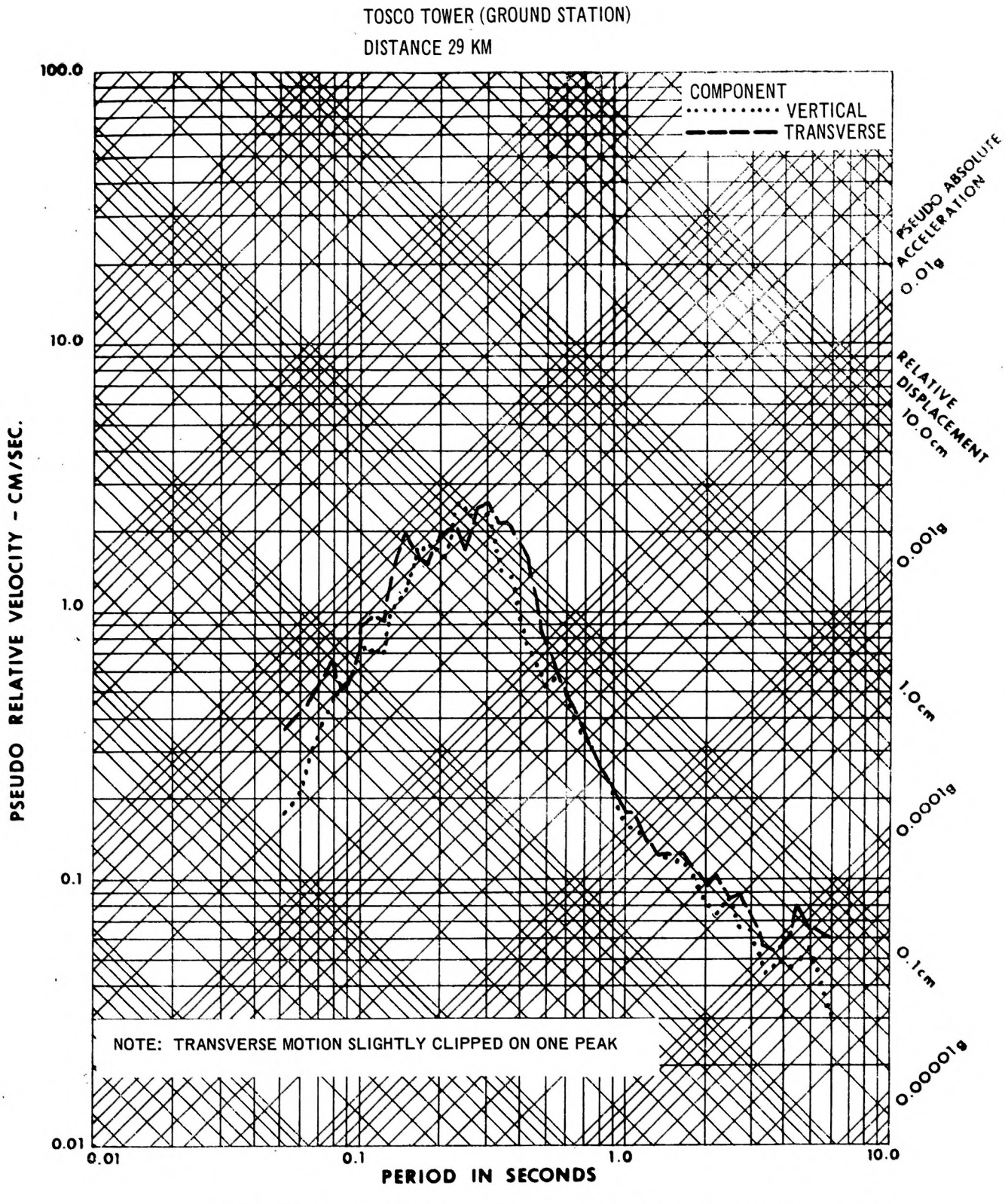

Observed 5% PSRV Spectra at TOSCO Tower (ground station), Rulison Event

VERTICAL COMPONENT

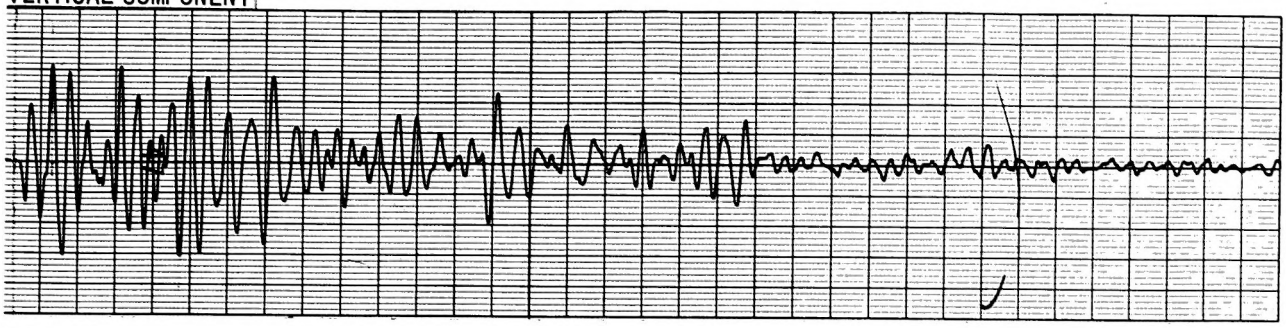

RADIAL COMPONENT

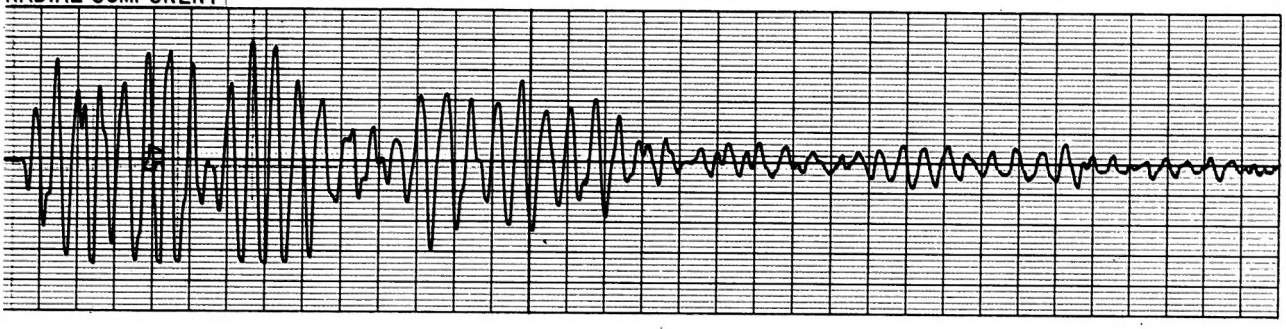

TRANSVERSE COMPONENT

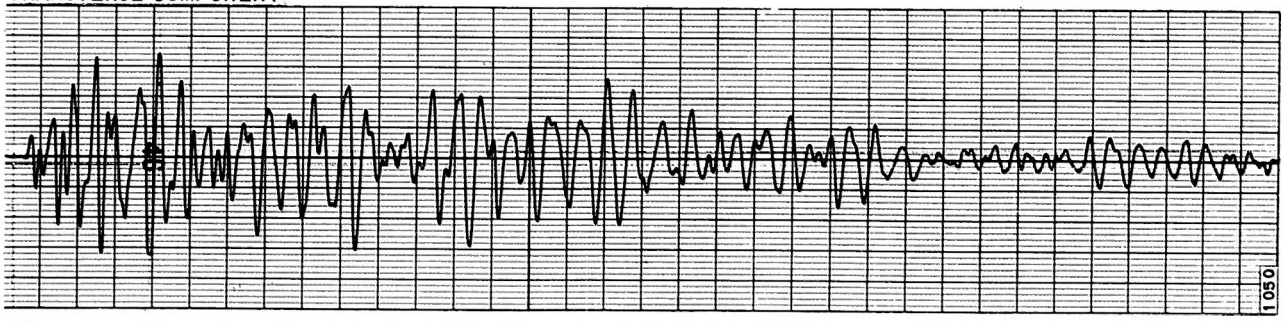

Observed Seismograms, TOSCO Tower, Rulison Event

VERTICAL COMPONENT

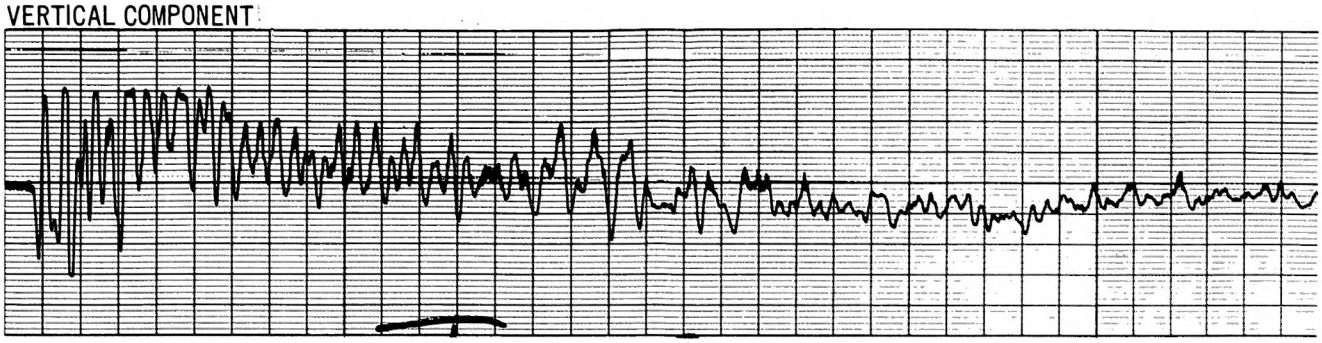

RADIAL COMPONENT

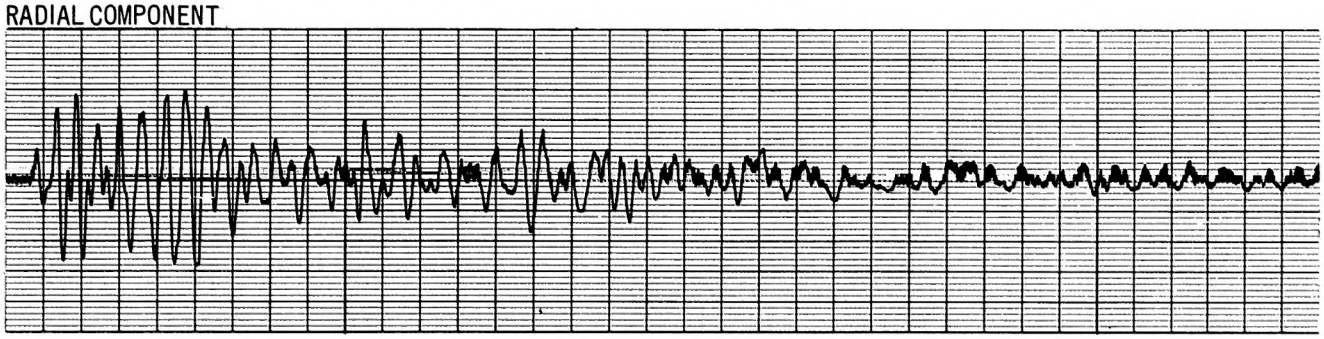

TRANSVERSE COMPONENT

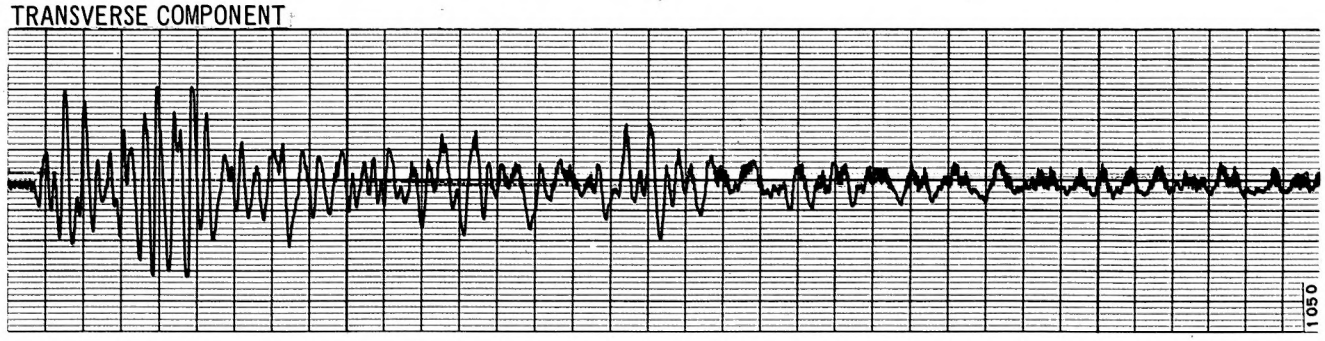

Observed Seismograms, TOSCO Mine, Rulison Event

NVO-1163-206

ANALYSIS OF GROUND MOTIONS AND CLOSE-IN PHYSICAL EFFECTS, RULISON EVENT

by

R.Q. Foote
C.R. Cassity
P.C. Loux
L.J. O'Brien
F.W. Power
W.W. Hays
R.D. Lynch
F.R. Perchalski
C.T. Spiker
A.P. Whipple

Environmental Research Corporation
813 North Royal Street
Alexandria, Virginia

Prepared Under
Contract AT(29-2)-1163
for
Nevada Operations Office
U.S. Atomic Energy Commission

TABLE OF CONTENTS

Chapter		Page
	ABSTRACT	xi
1	INTRODUCTION	1-1
	1.1 Historical Description	1-1
	1.2 Objective	1-2
	1.3 General Background	1-3
2	DATA ACQUISITION AND PROCESSING	2-1
	2.1 Instrumentation Planning	2-1
	2.2 Instrumentation	2-5
	2.3 Seismic Processing	2-6
	2.4 Peak Vector Ground Motions	2-9
	2.5 Pseudo-Relative Velocity Spectra	2-10
	2.6 Component Product Waveforms	2-11
3	NUMERICAL COMPUTATION OF CLOSE-IN PHYSICAL EFFECTS	3-1
	3.1 General Description of the Computation Technique	3-2
	3.2 Computations for Gasbuggy and Rulison	3-4
4	ANALYSIS OF THE GROUND MOTIONS	4-1
	4.1 Characteristics of the Ground Motions	4-2
	4.1.1 Peak Particle Amplitudes	4-2
	4.1.2 PSRV Spectra	4-14
	4.1.3 Explanation of the Characteristics of the Ground Motion in Terms of Scaling Theory	4-22
	4.1.4 Signal Duration	4-30
	4.2 Characteristics of the Seismic Waves	4-31
	4.2.1 Shear (SH) Waves	4-46
	4.2.2 Characteristics of the First Arrival (P Wave)	4-49
	4.2.3 Attenuation of Seismic Waves in the Earth's Crust	4-54
	4.3 Frequency Dependent Amplification of Ground Motion	4-60

TABLE OF CONTENTS
(Continued)

Chapter		Page
	4.3.1 Analysis of the Ground Motions at Harvey Gap Dam	4-73
	4.4 Azimuthal Variation of Ground Motions	4-81
	4.5 Seismic Energy Efficiency	4-88
5	SUMMARY AND RECOMMENDATIONS FOR ADDITIONAL WORK	5-1
	5.1 Summary of Conclusions	5-1
	5.2 Prediction Methodology for Future Detonations	5-7
	5.3 Recommendations for Additional Work	5-16
	REFERENCES	R-1
Appendix		
A	GEOLOGIC ENVIRONMENT	A-1
	A.1 Introduction	A-1
	A.2 Regional Geologic Environment of the Rulison Detonation	A-1
	A.3 Geology of the Source Region	A-4
	A.3.1 Location and Topography	A-4
	A.3.2 Stratigraphy and Lithology	A-4
	A.3.3 Physical Properties	A-6
	A.3.4 Structure	A-8
	A.3.5 Hydrology	A-8
	A.4 Geology of the Elastic Wave Transmission Region	A-8
	A.5 Geologic Environment of Recording Sites	A-9

LIST OF ILLUSTRATIONS

Figure		Page
2-1	Map Showing Location of 30 Station Instrument Plan, Rulison Event.....	2-2
2-2	Map Showing Location of 17 Additional Instrument Stations, Rulison Event.....	2-4
2-3	Generalized Block Diagram Showing Recording and Processing of Ground Motion Data, Rulison Event.	2-7
3-1	Pressure Profiles Calculated for the Gasbuggy and Rulison Detonations.....	3-8
3-2	The Calculated Cracking Front, Cavity Radius and Regions of Cracking as a Function of Time, Rulison Detonation.....	3-11
4-1	Peak Vector Particle Acceleration Observed from the Rulison Detonation, Hard Rock Sites.....	4-3
4-2	Peak Vector Particle Velocity Observed from the Rulison Detonation, Hard Rock Sites.....	4-4
4-3	Peak Vector Particle Displacement Observed from the Rulison Detonation, Hard Rock Sites.....	4-5
4-4	Peak Vector Particle Ground Motions Observed at Alluvium Sites outisde the Piceance Creek Basin, Rulison Detonation.....	4-8
4-5	Peak Particle Acceleration and Velocity Observed at Hard Rock Sites, Rulison Detonation.....	4-9
4-6	Ratio of Peak Component Acceleration Amplitude to Peak Vector Acceleration Amplitude as a Function of Distance, Rulison Event.....	4-11
4-7	Ratio of Peak Component Velocity Amplitude to Peak Vector Velocity Amplitude as a Function of Distance, Rulison Event.....	4-12

LIST OF ILLUSTRATIONS
(Continued)

Figure		Page
4-8	Ratio of Peak Component Displacement Amplitude to Peak Vector Displacement Amplitude as a Function of Distance, Rulison Event.....	4-13
4-9 to 4-15	Comparison of Observed 5% PSRV Spectrum with the Predicted Spectrum and the Spectrum Expected on the Basis of Nevada Test Site Experience.....	4-15 to 4-21
4-16	Comparison of the Observed Gasbuggy and Rulison Peak Particle Accelerations with the Accelerations Expected on the Basis of Nevada Test Site Experience and on the Basis of Scaling Theory...	4-25
4-17	Comparison of the Observed Gasbuggy Spectra at Three Distances with the Spectra Expected on the Basis of NTS Experience and on the Basis of Scaling for Depth of Burial.....	4-27
4-18	Comparison of the Observed Gasbuggy Spectra at Two Distances with the Spectra Expected on the Basis of Scaling to the Rulison Yield and Device Depth of Burial.....	4-29
4-19	Particle Velocity Seismogram Observed at Lemon Ranch, Rulison Detonation.....	4-32
4-20	Particle Velocity Seismogram Observed at Rulison, Rulison Detonation.....	4-33
4-21	Particle Velocity Seismogram Observed at DeBeque School No. 2, Rulison Detonation.....	4-34
4-22	Particle Velocity Seismogram Observed at DeBeque Canyon, Rulison Detonation.....	4-35

LIST OF ILLUSTRATIONS
(Continued)

Figure		Page
4-23	Particle Velocity Seismogram Observed at Denver, Colorado, Rulison Detonation.....	4-36
4-24	First Arrival Time as a Function of Station Distance, Rulison Detonation.....	4-37
4-25	Contour Maps of the Thickness of Crust and Propagation Velocity of P_n in the United States.....	4-39
4-26	Comparison of Peak Vector Velocity in P, S, and Surface Wave Time Windows with the Regression Line Derived from the Peak Vector Particle Velocity, Rulison Event, Piceance Creek Basin Sites.....	4-43
4-27	Variation of the Peak Particle Velocity of P_g with Distance, Rulison Detonation.....	4-50
4-28	Smoothed Fourier Amplitude Spectra of the P Wave Time Window Observed at Various Recording Sites, Rulison Detonation.....	4-52
4-29	Radial Component of Particle Velocity Observed at Stations on the BPF Line, Boxcar Detonation	4-57
4-30	Smoothed Fourier Amplitude Spectra Corresponding to the P Wave Time Window Observed at Stations on the BPF Line, Boxcar Detonation...	4-58
4-31	The Relationship between Amplitude, Q, and Frequency for Three Fixed Distances.....	4-59
4-32	Frequency Dependent Amplification Observed at Tonopah, Nevada from Underground Nuclear Detonations.....	4-62
4-33 to 4-35	Interpretation of Refraction Surveys at Selected Rulison Sites.....	4-64 to 4-66

LIST OF ILLUSTRATIONS
(Continued)

Figure		Page
4-36 & 4-37	Theoretical Transfer Functions Calculated for Selected Rulison Sites.....	4-67 & 4-68
4-38	Comparison of the Observed and Predicted PSRV Spectra at Harvey Gap Dam, Rulison Detonation.	4-70
4-39	Comparison of the Observed and Predicted PSRV Spectra at Rifle, Rulison Detonation.....	4-71
4-40	Frequency Dependent Amplification Observed at Rangely, Colorado, and Farmington, New Mexico.....	4-72
4-41	Cross-Sectional View of Harvey Gap Dam.....	4-74
4-42	Finite Element Representation of Harvey Gap Dam.....	4-75
4-43	Amplification Versus Frequency Close to Crest of Harvey Gap Dam, Rulison Event.....	4-77
4-44	Amplification Versus Frequency, Harvey Gap Dam (Node 56), Rulison Event.....	4-78
4-45	Comparison of Seismograms and PSRV Spectra, Harvey Gap Dam.....	4-82
4-46	Azimuthal Variation of the Peak Vector Particle Acceleration, Rulison Detonation.....	4-84
4-47	Azimuthal Variation of the Peak Vector Particle Velocity, Rulison Detonation.....	4-85
4-48	Azimuthal Variation of the Peak Vector Particle Displacement, Rulison Detonation.....	4-86
4-49	Smoothed Fourier Amplitude Spectra of P Wave Time Windows Observed at Selected Sites, Gasbuggy and Rulison Detonations.....	4-92

LIST OF ILLUSTRATIONS
(Continued)

Figure		Page
5-1	Ground Motion Levels Predicted for an Arbitrary 80 kt Detonation Buried at 12,000 ft, Using Observed Rulison Data as the Basis.....	5-13
5-2	5% PSRV Spectra Predicted for an Arbitrary 80 kt Detonation Buried at 12,000 ft, Using Observed Rulison Data as the Basis.....	5-14
A-1	Regional Geological and Structure Map of Piceance Creek Basin, Northwestern Colorado, Showing Rulison Site.....	A-2
A-2	Generalized Cross-Section Across the Piceance Creek Basin, Colorado.....	A-3

LIST OF TABLES

Table		Page
1-1	Characteristics of the Data Samples which Define the Average Seismic Response Characteristics of Nevada Test Site.....	1-5 & 1-6
1-2	Regression Equations Relating the Parameter of Observed Ground Motion to Distance, Gasbuggy Event.....	1-11
1-3	Regression Equations for Band-Pass Filter Velocity Amplitudes Versus Distance, Gasbuggy Event.....	1-12
2-1	Table Showing Stations and Components not Processed by ERC.....	2-8
3-1	Effect of Failure Parameters (5 kt Yield in Granite—no Overburden Pressure).....	3-3

LIST OF ILLUSTRATIONS
(Continued)

Table		Page
3-2	Input Parameters Used in the Numerical Simulation of the Gasbuggy and Rulison Detonations.....	3-5 & 3-6
3-3	Output Parameters for the Numerical Simulation of the Gasbuggy and Rulison Detonations.....	3-7
4-1	Correlation of Peak Ground Motion Parameter with Wave Mode Time Windows, Rulison Event.....	4-41
4-2	Correlation of Peak Ground Motion Parameter with Wave Mode Time Windows, Gasbuggy Event.....	4-44
4-3	Rulison Sites which Recorded Significant SH Ground Motion.....	4-47
4-4	Seismic Energy Efficiency.....	4-94
5-1	Regression Equations Relating the Parameter of Observed Ground Motion to Distance (km), Rulison Event.....	5-8
5-2	Regression Equations Relating the Observed PSRV Amplitude at Each Period to Distance (km), Rulison Event.....	5-9
A-1	General Sequence of Rocks Overlying the Rulison Gas-Bearing Formation (Mesaverde).....	A-5
A-2	Physical Properties of the Rulison W.P. Medium (First 1,000 Feet over the W.P.—Mesaverde Formation).....	A-7
A-3	Description of the Geologic Characteristics of Selected Rulison Instrument Sites.....	A-11 to A-13

ABSTRACT

The Rulison event, a 40 kt Plowshare nuclear detonation in the Rulison gas field of the Piceance Creek Basin, Colorado, provided an opportunity to analyze the ground motions and the close-in physical effects of a deeply buried detonation. Ground motions were recorded at 36 sites over a distance of about 4 to 367 km. These data were evaluated and the primary conclusions are:

- The level of the peak vector velocities and displacements observed from Rulison agree with the predicted levels. However, the peak vector accelerations are slightly higher than predicted. The observed peak vector accelerations and velocities significantly exceed the level expected from a normally buried 40 kt contained device detonated on the Nevada Test Site (NTS).

- The PSRV spectra calculated from Rulison ground motions agree well with the spectra predicted on the basis of scaling theory, accounting for differences in yield and device depth of burial. The peak spectral response exhibits a higher level and occurs at shorter periods (0.1 - 0.4 second) than that of the spectral response expected from a normally buried 40 kt contained device detonated on the Nevada Test Site.

The Rulison experiment provides useful experience which will materially advance the safety and scientific objectives of the Plowshare Program.

RULISON

CHAPTER 1

INTRODUCTION

1.1 HISTORICAL DESCRIPTION

Project Rulison is a joint experiment sponsored by Austral Oil Company, Incorporated, Houston, Texas, the U.S. Atomic Energy Commission and the Department of the Interior, with the Program Management provided by CER Geonuclear Corporation of Las Vegas, Nevada, under contract to Austral. Its purpose is to study the economic and technical feasibility of using underground nuclear explosions to stimulate production of natural gas from the low productivity, gas bearing Mesaverde formation in the Rulison Field.

The nuclear explosive for Project Rulison was detonated successfully at 3:00 P.M. plus or minus 0.1 second Mountain Daylight time, September 10, 1969, at a depth of 8,425.5 feet below ground level and was completely contained. Preliminary results indicate that the Rulison device behaved about as expected; i.e., with a yield of 40^{+20}_{-4} kt. The wellhead of the emplacement well, Hayward 25-95A, is at an elevation of 8,154 feet above mean sea level (MSL) and is located 1,976.31 feet

east of west line and 1,813.19' north of south line of Section 25, Township 7 South, Range 95 West of 6th P.M., Garfield County, Colorado. This corresponds to geodetic coordinates of longitude 107° 56' 53" West and latitude 39° 24' 21" North.

1.2 OBJECTIVE

The objective of this report is to relate the characteristics of the observed ground motions and close-in physical effects at specific recording stations to source, transmission path, and station site variables. Various functional analyses were performed to accomplish this objective. These analyses included:

1. Numerical simulation of close-in physical effects, such as cavity radius, cracking radius, and the energy input into the elastic region (Chapter 3).

2. Comparison of the peak amplitude of ground motion and the pseudo-relative velocity (PSRV) spectral response observed at selected recording stations with the corresponding parameter of ground motion expected on the basis of Nevada Test Site (NTS) experience and the experience gained from analysis of the ground motions from the Gasbuggy detonation (Chapter 4).

3. Comparison of the duration of the seismic energy observed from Rulison with that observed from Gasbuggy and from events at NTS (Chapter 4).

4. Assessment of the adequacy of scaling theory to predict the amplitude and frequency composition of the ground motions expected from an overburied detonation in a sedimentary basin (Chapter 4).

5. Identification of the elastic wave types observed on seismograms from Rulison and determination of the contribution of each wave type to the observed peak particle ground motion (Chapter 4).

6. Determination of the specific dissipative (Q) characteristics of the earth's crust in the Piceance Creek Basin (Chapter 4).

7. Determination of the frequency dependent amplification experienced at local sites and assessment of the adequacy of the techniques employed to predict its characteristics (Chapter 4).

8. Calculation of the seismic energy efficiency of the Rulison detonation and a comparison with that determined for Gasbuggy and selected NTS detonations (Chapter 4).

9. Specification of the properties and characteristics of the geologic environment of the source, transmission path, and recording site (Appendix A).

1.3 GENERAL BACKGROUND

As prediction equations are derived on an empirical and theoretical basis from analysis of the ground motions observed from previous detonations, it will be useful to review briefly the history of ground motion predictions. This review will deomonstrate how prediction techniques were applied to extrapolate from NTS experience to the San Juan Basin for the Gasbuggy event and from Gasbuggy and NTS experience to the Piceance Creek Basin for the Rulison event.

Since 1961, Environmental Research Corporation (ERC) has been under contract to the United States Atomic Energy Commission (AEC) to provide scientific and engineering support to the Office of Effects Evaluation, Nevada Operations Office (NVOO) by predicting ground motions for nuclear events and processing and analyzing the observed data resulting from the detonations. In fulfilling contractual obligations, ERC has compiled and analyzed the comprehensive ground motion data sample summarized in Table 1-1. These analyses, involving data measured at approximately 500 different instrument stations, have produced more than 2,900 peak resultant vector surface particle acceleration, velocity, and displacement data points. Band-Pass Filter (BPF) spectra, approximations of Fourier amplitude spectra, were derived from the recorded horizontal ground motion for 20 NTS events, Table 1-1. Statistically derived equations were developed from the observed spectra to obtain predictions of BPF spectra as a function of yield and distance, or for selected stations, as a function of yield. Multiplication of the predicted BPF spectrum by an appropriate factor (6.4) produces an estimate of the 5% damped Pseudo-Relative Velocity Spectrum (Loux and Davis, 1969). A direct method of predicting PSRV spectra was

TABLE 1-1. CHARACTERISTICS OF THE DATA SAMPLES WHICH DEFINE THE AVERAGE SEISMIC RESPONSE CHARACTERISTICS OF NEVADA TEST SITE

GROUND MOTION PARAMETER	CHARACTERISTICS OF THE DATA SAMPLE				STANDARD ERROR OF ESTIMATE (σ)
	Station Geology	Number of Data Points	Range of Yield(kt)	Range of Distance(km)	
Peak Vector Ground Motion A. Acceleration (Murphy and Lahoud, 1969)	Hard Rock and Alluvium	1207 (99 events)	About 1 to 1200	About 0.25 to 600	2.33
	Alluvium	819 (99 events)	About 1 to 1200		2.13
	Hard Rock	388 (99 events)	About 1 to 1200		2.54
B. Velocity (Murphy and Lahoud, 1969)	Hard Rock and Alluvium	509 (99 events)	About 1 to 1200	About 0.25 to 600	2.13
	Alluvium	400 (99 events)	About 1 to 1200		1.97
	Hard Rock	109 (99 events)	About 1 to 1200		2.42
C. Displacement (Murphy and Lahoud, 1969)	Hard Rock and Alluvium	1072 (99 events)	About 1 to 1200	About 0.25 to 600	2.29
	Alluvium	767 (99 events)	About 1 to 1200		2.20
	Hard Rock	305 (99 events)	About 1 to 1200		2.19

TABLE 1-1. CHARACTERISTICS OF THE DATA SAMPLES WHICH DEFINE THE AVERAGE SEISMIC RESPONSE CHARACTERISTICS OF NEVADA TEST SITE (CONTINUED)

GROUND MOTION PARAMETER	CHARACTERISTICS OF THE DATA SAMPLE				STANDARD ERROR OF ESTIMATE (σ)
	Station Geology	Number of Data Points	Range of Yield (kt)	Range of Distance (km)	
Spectra					
A. Band-Pass Filter (Loux and Davis, 1969)	Hard Rock and Alluvium	20 Pahute Mesa & Yucca Flat Events (108 Stations) 200 Points/Frequency 12 Frequencies (0.4-11.3 Hz)	16 to 825	40 - 200	2.0-2.5
B. Pseudo-Relative Velocity (Lynch, 1969)	Hard Rock and Alluvium	11 Pahute Mesa Events (64 Stations) 260 Points/Period 40 Periods (0.05-2.5 secs)	About 20-1200	4.4-551.0	2.5-3.0

developed by Lynch (1969). In that study, PSRV spectra (to be discussed in more detail in Chapter 2) were derived from the horizontal ground motions shown in Table 1-1. Multiple regression analysis of the derived data were used to obtain the PSRV prediction equations and to establish the standard error of estimate (σ), a measure of uncertainty.

By statistical analysis of this comprehensive NTS data sample, an average seismic response and a measure of the uncertainty (σ) have been established as a function of yield and distance from the source to the recording station. The average seismic response, defined by regression analysis, is refined by continued statistical analysis of the total data sample as additional peak vector ground motion data (accelerations, velocities, and displacements) and spectral measurements (Band-Pass Filter and Pseudo-Relative Velocity), are added from successive events. The characteristics of the data sample and the measurements of the uncertainty which relate to the average seismic response based on NTS experience are summarized in Table 1-1.

Peak resultant vector surface particle ground motions (defined in Chapter 2) are predicted and used in comparative analyses, because they characterize the seismic energy in a

systematic fashion and can be correlated on a one-to-one basis with the seismogram in an economical manner. PSRV spectra are used almost exclusively, both for predictions and analyses, because they approximate (for small damping) Fourier amplitude spectra more closely than BPF spectra.

The effect of the physical properties of the detonation medium on a nuclear explosion has been well documented for certain geologic formations at NTS; the effects of other formations, both on and off NTS, are less well known. All contained events at NTS have been detonated in tuffs, rhyolite, or alluvium with the exception of two detonations in dolomite and three in granite. Off the NTS, underground events have been detonated in a salt dome in Mississippi (Salmon event), bedded salt (Gnome event) and shale (Gasbuggy event) in New Mexico, tuff in central Nevada (Faultless event) and granite in western Nevada (Shoal event). Since the shale and sandstone surrounding the Rulison explosion probably have properties similar to those found at Gasbuggy and between those of granites and tuffs at NTS, the Rulison physical effects predictions (see Weetman, et al., 1969, for details) were based upon an average of these physical properties.

The nature of the geology underlying the instrument station has a pronounced effect on the ground motions. Experience has indicated that recording sites should be subdivided, even if on a somewhat subjective basis, as hard rock and alluvium sites in order to characterize the responses accurately. Therefore, the regression equations derived by Murphy and Lahoud (1969) are applicable for these two general classes of recording site geology.

Ground motion predictions were made for the Gasbuggy event (Environmental Research Corporation, 1967). This was a Plowshare event designed to stimulate the flow of natural gas by a nuclear detonation (device depth of burial - 4240 feet), below the base of the Pictured Cliffs formation, San Juan Basin, New Mexico. As Gasbuggy represented the first underground nuclear detonation in a sedimentary basin, the prediction methodology was based on Nevada Test Site experience. For Gasbuggy, a comparison of the physical properties of the proposed detonation medium with those for a range of detonation media of Nevada Test Site showed that the physical properties at the Gasbuggy site correspond best with those of the media at Pahute Mesa on NTS. Accordingly, ground motion predictions for Gasbuggy were made using the prediction equations applicable

(at that time) for Pahute Mesa detonations.

Ground motion predictions for the Rulison event (Weetman, et al., 1969) were based upon the recorded motions of the Gasbuggy event (Foote, et al., 1969). The primary reasons for applying the ground motion data observed from Gasbuggy (in the San Juan Basin) to Rulison (in the Piceance Creek Basin) are: (1) the two basins have quite similar geologic environments, and (2) both detonations were greatly overburied; device depths of burial were 4240 and 8425 feet, respectively. Peak particle ground motion amplitude predictions for stations within the Piceance Creek Basin were based on regression lines derived from the observed Gasbuggy data, combining hard rock and alluvium sites (Weetman, et al., 1969). This was done because the peak ground motions and spectra observed at Gasbuggy stations with thin alluvium cover did not differ significantly (except for a few sites) from corresponding data observed at adjacent hard rock stations (Foote, et al., 1969). The regression lines derived from the Gasbuggy data (see Tables 1-2 and 1-3) were scaled to the Rulison yield, using scaling exponents derived from NTS experience (Murphy and Lahoud, 1969). The peak amplitude predictions for stations located on alluvium outside the Piceance Creek Basin

TABLE 1-2. REGRESSION EQUATIONS RELATING THE PARAMETER OF OBSERVED GROUND MOTION TO DISTANCE, GASBUGGY EVENT

GROUND MOTION PARAMETER	REGRESSION EQUATION	DATA SAMPLE	RANGE (R) ON DATA SAMPLE
ACCELERATION			
1. Peak Vector Acceleration	$a = 3.55 \times 10^{6} R^{-1.83}$ $\sigma = 1.59$	Hard Rock	1.5-90.0 km
2. Peak Vector Acceleration	$a = 1.61 \times 10^{8} R^{-2.19}$ $\sigma = 1.59$	Alluvium	1.9-90.0 km
3. Peak Vector Acceleration	$a = 9.50 \times 10^{6} R^{-1.93}$ $\sigma = 1.62$	Hard Rock & Alluvium	1.5-90.0 km
4. Peak Horizontal Acceleration	$a = 5.70 \times 10^{5} R^{-1.69}$ $\sigma = 1.74$	Hard Rock & Alluvium	1.8-90.0 km
5. Peak Vertical Acceleration	$a = 1.10 \times 10^{6} R^{-1.75}$ $\sigma = 1.95$	Hard Rock & Alluvium	1.5-90.0 km
VELOCITY			
1. Peak Vector Velocity	$u = 9.95 \times 10^{7} R^{-1.82}$ $\sigma = 1.66$	Hard Rock	4.3-90.0 km
2. Peak Vector Velocity	$u = 7.89 \times 10^{10} R^{-2.42}$ $\sigma = 1.59$	Alluvium	20.1-90.0 km
3. Peak Vector Velocity	$u = 1.65 \times 10^{8} R^{-1.86}$ $\sigma = 1.62$	Hard Rock & Alluvium	4.3-90.0 km
4. Peak Vector Velocity	$u = 4.60 \times 10^{7} R^{-1.74}$ $\sigma = 1.59$	Hard Rock & Alluvium*	1.3-90.0 km
DISPLACEMENT			
1. Peak Vector Displacement	$d = 2.88 \times 10^{6} R^{-1.72}$ $\sigma = 1.45$	Hard Rock	1.5-90.0 km
2. Peak Vector Displacement	$d = 3.47 \times 10^{7} R^{-1.94}$ $\sigma = 1.41$	Alluvium	1.9-90.0 km
3. Peak Vector Displacement	$d = 4.17 \times 10^{6} R^{-1.75}$ $\sigma = 1.45$	Hard Rock & Alluvium	1.5-90.0 km

*Including data from W.R. Perret, Sandia Corporation, Personal Communication, January, 1968.

TABLE 1-3. REGRESSION EQUATIONS FOR BAND-PASS FILTER VELOCITY AMPLITUDES VERSUS DISTANCE, GASBUGGY EVENT

FREQUENCY (Hz)	REGRESSION EQUATION	STANDARD ERROR OF ESTIMATE, σ
0.41	$Vb = 2.79 \times 10^{0} R^{-1.27}$	1.66
0.55	$Vb = 3.97 \times 10^{0} R^{-1.32}$	1.55
0.75	$Vb = 6.41 \times 10^{0} R^{-1.42}$	1.55
1.00	$Vb = 1.33 \times 10^{1} R^{-1.54}$	1.70
1.35	$Vb = 2.99 \times 10^{1} R^{-1.70}$	1.70
1.85	$Vb = 3.32 \times 10^{1} R^{-1.63}$	2.35
2.50	$Vb = 7.86 \times 10^{1} R^{-1.76}$	2.04
3.40	$Vb = 1.24 \times 10^{2} R^{-1.84}$	2.09
4.60	$Vb = 1.12 \times 10^{2} R^{-1.83}$	2.04
6.20	$Vb = 5.20 \times 10^{1} R^{-1.73}$	1.82
8.40	$Vb = 2.33 \times 10^{1} R^{-1.66}$	2.00
11.30	$Vb = 8.38 \times 10^{0} R^{-1.48}$	2.04

Vb = peak band-pass filter velocity (cm/sec)
R = slant distance (km)
Range of Data Sample = 5-90 km (hard rock and alluvium sites)

Note: Approximations of the 5% damping PSRV spectra can be obtained by multiplying each equation by the factor 6.4.

(Salt Lake City, Utah, and Denver, Colorado) were derived by applying appropriate amplification factors, derived from NTS experience, to the yield-scaled Gasbuggy regression equations.

Pseudo-Relative Velocity (PSRV) predictions were made at thirteen selected locations in the Piceance Creek Basin (see Weetman, et al., 1969 for details). The predicted response spectra at the selected locations were determined as follows: (1) regression lines, derived from the Gasbuggy Band-Pass Filter (BPF) data sample, were converted to PSRV (5% damping) and used to generate spectra at each site for the Rulison yield; (2) frequency-dependent factors to scale for the difference in depth of burial (4240 vs 8425 feet) of the devices were derived and applied to each spectrum in (1); and (3) amplification factors, based on the results of analytical amplification modeling, using as input the physical parameters derived from refraction surveys at Gasbuggy and Rulison sites, were applied, as required, at seven of the thirteen sites.

The results of the Rulison project will be described in the following chapters.

CHAPTER 2

DATA ACQUISITION AND PROCESSING

2.1 INSTRUMENTATION PLANNING

In Grand Junction, Colorado, on March 19 and 20, 1969, a safety instrumentation plan was formulated at a joint meeting of representatives from Austral Oil Company, (represented by CER Geonuclear), John A. Blume & Associates (JAB), United States Coast & Geodetic Survey (USC&GS), Atomic Energy Commission/Nevada Operations Office (NVOO), and Environmental Research Corporation (ERC). After a detailed field inspection of sites where injury to people or damage to property was considered possible, the representatives approved an instrumentation plan of 30 carefully selected sites (Figure 2-1). The two primary goals of this instrumentation plan were:

1. To document the nuclear-generated ground motions at populated locales or at specific structures.

2. To record on magnetic tape a history of the ground motions so that this information could be fully utilized for theoretical studies.

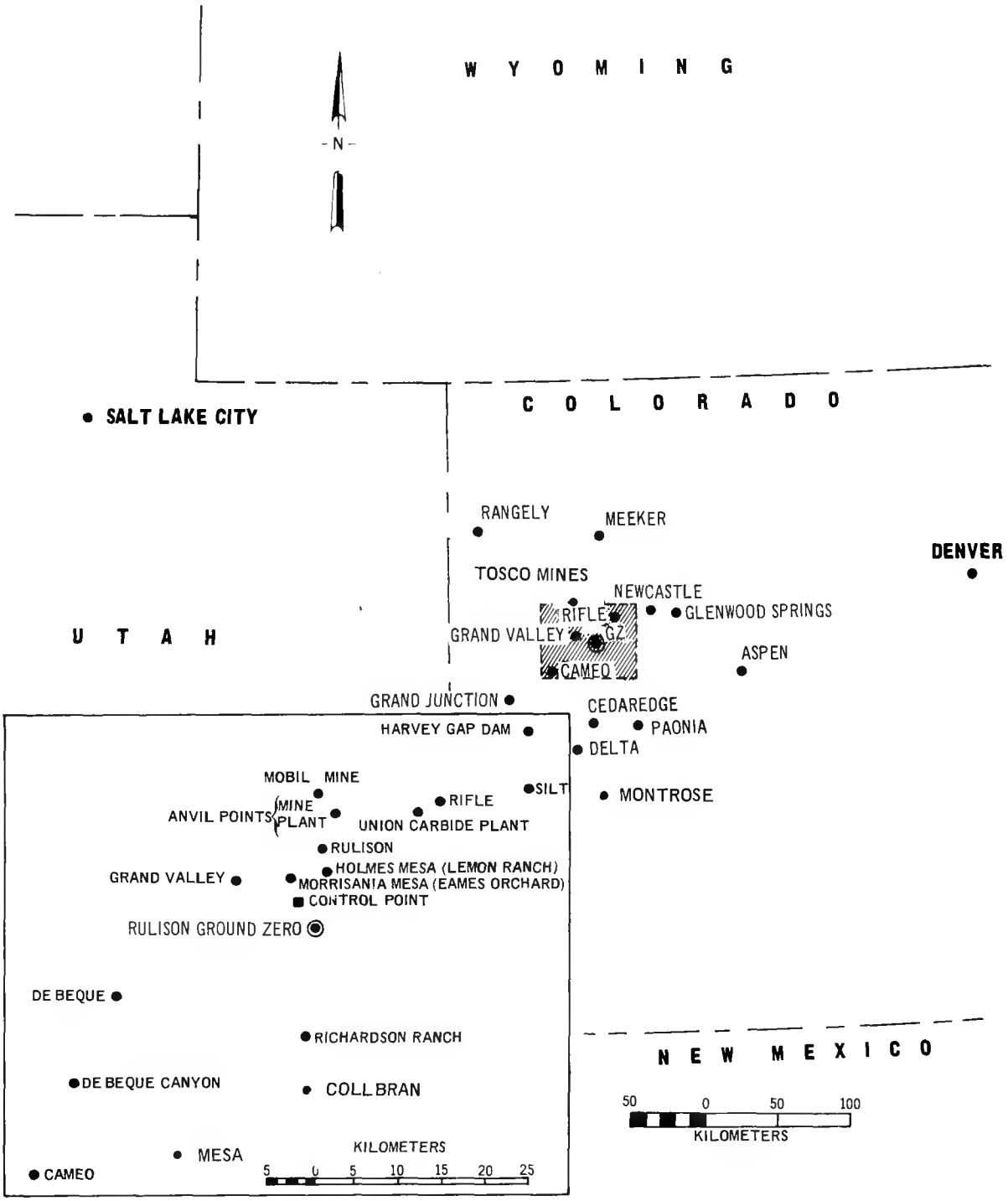

Figure 2-1. Map Showing Location of 30 Station Instrument Plan, Rulison Event

Subsequently, seventeen additional instrument stations were approved (Figure 2-2) for the purpose of more fully documenting and analyzing the Rulison event ground motions, both in and outside the Piceance Creek Basin. Twelve of the additional stations were on four radial lines extending from the Rulison site, Piceance Creek Basin, to other basins. The intent of these lines was to provide valuable regional information on wave propagation.

Three of the additional instruments stations were incorporated to provide supplemental documentation of the ground motions, as follows:

1. In the deepest part of the Piceance Creek Basin (White River).

2. In Dinosaur National Monument (Greystone)

3. In the northeastern part of the San Juan Basin (Pagosa Springs)

Two of the additional stations were added to document the ground motions at the Control Point and Battlement Resevoir Dam near surface ground zero (SGZ).

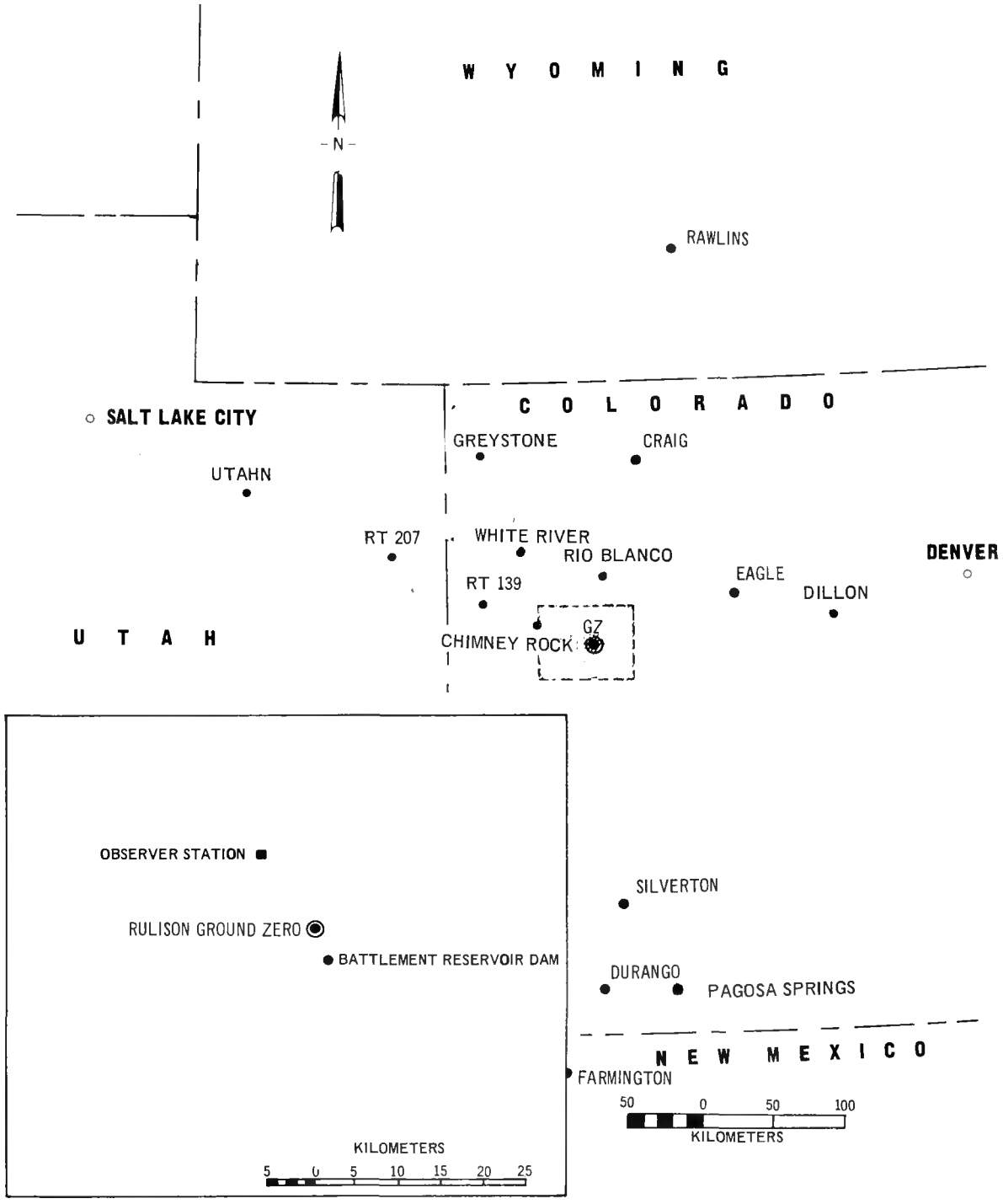

Figure 2-2. Map Showing Location of 17 Additional Instrument Stations, Rulison Event

At Rangely, Colorado, and Farmington, New Mexico, recordings were made with two sets of instruments, one located on hard rock and the other on alluvium. The purpose of these stations was to provide measurements for determination of station site amplification.

2.2 INSTRUMENTATION

Specific data were provided by the Special Projects Party of the United States Coast and Geodetic Survey (USC&GS) (December, 1969). This data, for each recording site, included:

1. Location (Latitude and Longitude)
2. Elevation
3. Slant Distance in kilometers from the Working Point, (W.P.), or detonation depth, to instrument stations.
4. Bearing in degrees from surface ground zero (SGZ).

The installation and operation of the instruments was the responsibility of the USC&GS. The L-7 recording system, consisting of L-7 seismometers, integrating amplifiers, time code generator, and frequency modulation (FM) magnetic tape recorder, was used to record the ground motions at all stations. A detailed description of the L-7 recording system,

which records three orthogonal components of velocity, is provided by King (1969).

Four stations were located at the Harvey Gap Dam; one at each end and one, each, at the top center and bottom center of the dam. The intent of this instrumentation was to provide measurements of the response of an earth fill dam to nuclear generated ground motions so that a detailed analysis could be performed.

A list of the instrument stations processed by ERC are shown in Table 4-1. A detailed description and photographs of all instrument stations for the Rulison event can be found in the report by Navarro and Wuollet (1969).

2.3 SEISMIC PROCESSING

A generalized block diagram illustrating the sequence followed in the recording and processing of the ground motion data for the Rulison event is shown in Figure 2-3.

The output of the L-7 seismometers, containing both seismic signals and noises, were filtered by the L-7 amplifier to eliminate noise outside the frequency range of interest before being recorded on FM tapes (King, 1969).

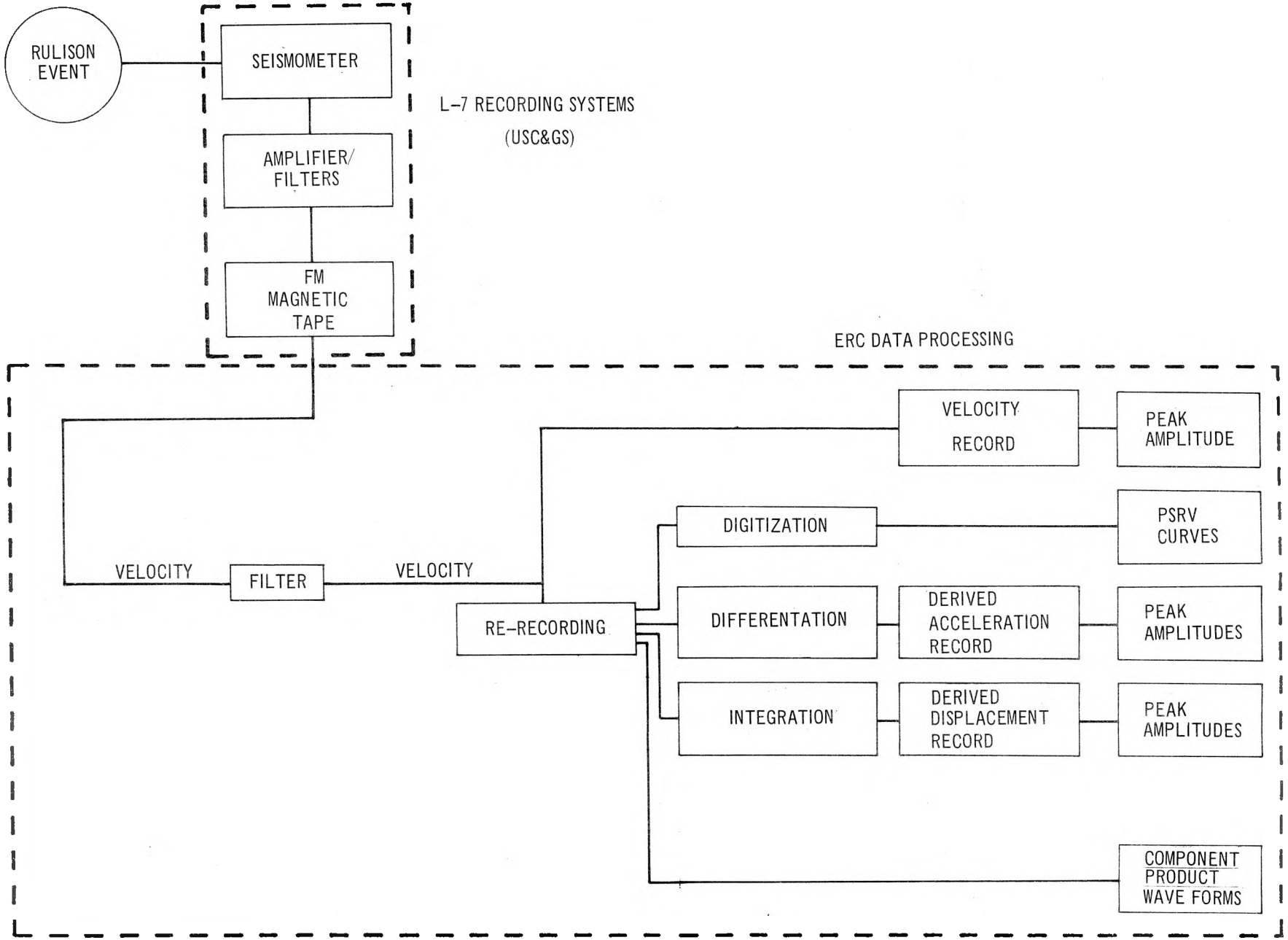

Figure 2-3. Generalized Block Diagram Showing Recording and Processing of Ground Motion Data, Rulison Event

As the field magnetic tapes were re-recorded, the filtered velocity data were also recorded onto paper records. During processing, no corrections were necessary for frequency-response because the L-7 instrument response is flat from 0.1 to approximately 34 Hz. The limiting value on the upper range is governed by the tape speed.

Data were processed from all stations which recorded useable signals. Stations on which all components were not processed or where there were no recordings are shown in Table 2-1.

TABLE 2-1. TABLE SHOWING STATIONS AND COMPONENTS NOT PROCESSED BY ERC

Instrument	Components not Processed			Remarks
	R	T	Z	
Control Point	X	X	X	No record, power failure*
Observer Point	X	X	X	No calibration*
Collbran	X	X	X	Power failure after first arr.
Tosco Mine (Ground)	X	X	X	All signals clipped
Tosco Mine Unit 118	X	X	X	60 Hz superimposed on data
Tosco Mine (Tower)	X	X	X	Calibration no good
Silt		X	X	Signals clipped
Mesa	X	X	X	Power failure after first arr.
Harvey Gap Dam				
West End	X	X	X	Dead channel & no calibration
Top Center	X	X	X	Signals clipped
Base	X	X	X	Signals clipped
Chimney Rock	X	X	X	Power failure after first arr.
Route 139	X	X	X	No record, power failure*
Montrose	X	X	X	Not recorded*
Route 207	X	X	X	Signals undetectable in noise
Ridgeway	X	X	X	Not recorded*
Utahn	X	X	X	Power failure after first arr.
Rawlins, Wyo.	X			Channel very noisy
Salt Lake City, Utah	X			Transient spike and noise

*R. Navarro, USC&GS personal communication, 1969.

Particle acceleration and displacement time histories were derived by differentiation and integration of the velocity traces, respectively, with respect to time, using the techniques described by Lynch (1965).

2.4 PEAK VECTOR GROUND MOTIONS

At each station, peak values of surface particle acceleration, velocity and displacement were determined for each of the three components; vertical, radial and transverse. In addition, peak values of the resultant vectors of surface particle motion were obtained to determine the maximum value of ground motion. Peak resultant vector surface particle magnitudes were calculated by analyzing instantaneous values of the three components of motion. The peak resultant vector surface particle motion is defined as the largest instantaneous value of the square root of the sum of the squares of the amplitudes for the three components.

$$V_p(t) = \sqrt{Z^2(t) + R^2(t) + T^2(t)} \qquad (2\text{-}1)$$

where $V_p(t)$ = peak resultant vector of surface particle motion*

$Z(t)$ = vertical component of surface particle motion

$R(t)$ = radial component of surface particle motion

$T(t)$ = transverse component of surface particle motion

*Called the peak vector throughout the report.

The peak vector values of the ground motion observed at hard rock and alluvium sites for the Rulison event are shown in a report by Environmental Research Corporation, 1969.

2.5 PSEUDO-RELATIVE VELOCITY SPECTRA

The pseudo-relative velocity (PSRV) spectrum, an approximation of the Fourier amplitude spectrum, represents the peak response to ground motion of a series of single-degree-of-freedom system (mass-spring system with velocity damping). PSRV spectra are useful in the analysis of ground motions, because they provide a means of determining the spectral composition of the ground motion. They are also used by the Structural Contractor in approximating the response of certain structures to ground motions. The PSRV spectrum is derived digitally from a seismic trace, f(t), containing a broad spectrum of frequencies. This trace is transformed into another trace containing a restricted range of frequencies by filtering with narrow band-pass filters (BPF) centered at selected frequencies. The filters (BPF) are logarithmically spaced and a sufficient number of frequencies are sampled to cover the frequency range from 0.41 to 11.3 Hz. A value of the velocity damping is incorporated to produce the resultant spectra. Typical values of damping utilized are 2%, 5%,

and 10%; the spectrum for 2% damping is the best approximation to the Fourier spectrum.

A detailed description of PSRV and band-pass filter (BPF) spectra has been provided by Loux and Davis (1969), and Lynch (1965 and 1969).

2.6 COMPONENT PRODUCT WAVEFORMS

The component product waveform is a useful tool for identifying elastic wave types on a seismogram (Sutton and Pomeroy, 1963). The waveform representing the product of the radial and vertical components has the greatest utility, for its characteristics can be related to the P, SV (vertically polarized shear wave), and the Rayleigh wave. The basic characteristics of the product waveform which, in theory, correspond to these wave types are as follows:

1. P Wave — The radial-vertical component product waveform displays a positive amplitude for the elastic wave which propagates through the earth as a P wave.

2. SV Wave — The radial-vertical component product waveform displays a negative amplitude for the SV wave.

3. Rayleigh Wave — The radial-vertical component product waveform is a sinusoidal oscillation with twice the frequency of the incident wave.

In practice, the characteristics displayed by the component product waveforms are usually not as straightforward as indicated above due to the complex signature which the heterogeneous character of the earth imparts. However, this relatively simple tool does provide useful information about the elastic waves composing the seismogram.

CHAPTER 3

NUMERICAL COMPUTATION OF CLOSE-IN PHYSICAL EFFECTS

The ground motion in the region immediately surrounding an underground nuclear detonation and extending radially outward for some distance is extremely non-linear and complex. Approximately 50% of the available energy, about 10^{-6} seconds after the explosion, feeds a shock wave which propagates radially outward from the wall of the shot cavity. The detailed characteristics of the intense shock wave and the resultant growth of the underground cavity are a function of the explosive yield as well as the emplacement cavity geometry and the properties of the rock media in which wave propagation takes place. These characteristics are complex and are the subject of continuing research by many individuals: Bishop (1963), Beaudet, et al. (1969), Cherry (1966 and 1967), Reily (1967), Germain and Kahn (1969), and others. As the shock wave propagates outward, the dissipative characteristics of the rock and the radial expansion reduce the loading intensity to the point where the elastic properties of the medium begin to play a significant role.

The objective of this chapter is to describe the close-in physical effects calculated for the Gasbuggy and Rulison detonations.

3.1 GENERAL DESCRIPTION OF THE COMPUTATION TECHNIQUE

A one-dimensional, spherically symmetric Lagrangian model has been developed to calculate the close-in effects of underground nuclear detonations (Beaudet, et. al., 1969, Cassity, et. al., 1969). This model, which takes into account the effects of plastic or brittle failure of the material, can be applied to determine the dimensions of cracking and cavity radii and to estimate the energy input into the elastic region.

The principal variables required in the model to define the complex physical situation include:

1. The yield of the device.
2. The depth of burial.
3. The parameters characterizing the equations-of-state of both the earth medium and the cavity gas.
4. The Mohr-Coulomb failure criterion of the in-situ earth medium, before and after cracking.

The failure criterion is particularly important and is characterized by four parameters: (1) the tensile strength, (2) the cohesive strength, (3) the angle of internal friction, and (4) the ultimate strength under high confining pressure. The cohesive strength and the ultimate strength under high confining pressure are the most sensitive failure parameters. These parameters for the unfailed rock primarily affect the magnitude of the cracking radius, whereas, for failed rock, they affect the magnitude of the cavity radius (Cassity, et al., 1969). Table 3-1 illustrates the computed effect of varying of these two parameters for a 5 kt detonation in granite.

* * * * * * *

TABLE 3-1

EFFECT OF FAILURE PARAMETERS
(5 kt yield in granite) - no overburden pressure)

UNFAILED ROCK		FAILED ROCK		PHYSICAL EFFECT	
Cohesive Strength (Mb)	Ultimate Strength (Mb)	Cohesive Strength (Mb)	Ultimate Strength (Mb)	Cavity Radius(m)	Cracking Radius(m)
$2x10^{-4}$	$5x10^{-4}$	$2x10^{-4}$	$5x10^{-4}$	15.5	222
$4x10^{-4}$	10^{-3}	$4x10^{-4}$	10^{-3}	12.6	190
$4x10^{-4}$	10^{-3}	$2x10^{-4}$	$5x10^{-4}$	15	196

3.2 COMPUTATIONS FOR GASBUGGY AND RULISON

Numerical computations were made with the 1-D code to simulate the Gasbuggy and Rulison detonations. Input parameters used in each simulation are listed in Table 3-2. Two sets of values for the ultimate strength under high confining pressure were used to determine the effect of greater material strength on the parameters of interest, i.e., the cavity radius, the radius of cracking, and the stress input into the elastic region.

The parameters of primary interest which represent the output of the computer code (using the input parameters listed in Table 3-2) are given in Table 3-3. It should be emphasized that these values are not intended to be meaningful in an absolute sense. Because they represent the result of simulating complex physical phenomena, using various numerical and physical approximations, they are estimates of a physical effect. Thus, the values obtained by numerical simulation should be interpreted in a relative sense instead of an absolute sense.

TABLE 3-2. INPUT PARAMETERS USED IN THE NUMERICAL SIMULATION OF THE GASBUGGY AND RULISON DETONATIONS**

PHYSICAL PARAMETER	DETONATION	
	Gasbuggy	Rulison
Device Yield/Depth of Burial	26 kt/4240'	40 kt/8425.5'
Radius of Vaporization	592 cm	684 cm
Material Density	2.6 gm/cm^3	2.6 gm/cm^3
Poisson's Ratio	0.25	0.25
Hugoniot Equation -		
if $1 \leq \frac{V_o^*}{V} \leq 1.08675$ then C_1	0.176 Mb	0.176 Mb
B_1	4.6	4.6
if $\frac{V_o}{V} > 1.08675$ then C_1	0.403 Mb	0.403
B_1	1.045	1.045
Constants Modifying Hugoniot equation -		
A_1	0.66	1
B	10^6	10^6

* $\frac{V_o}{V}$ = ratio of the initial to the current specific volume.

$C_1, B_1 \equiv$ Constants determined empirically from Hugoniot (pressure-volume) data for given rocks to best fit the curve for the non-linear region

$$p = \frac{C_1 \xi}{(1-B_1\xi)^2}$$

where $\xi = 1 - \frac{V}{V_o}$, p = pressure

$A_1, B \equiv$ Empirically determined constants to transfer from the elastic to the non-linear region with the relation

$$p = \frac{C_1 \xi}{(1-B_1\xi)^2} \cdot \frac{A_1 + B\xi^3}{1 + B\xi^3}$$

**See Cassity, et al., 1969, for a discussion of the numerical simulation.

TABLE 3-2. INPUT PARAMETERS USED IN THE NUMERICAL SIMULATION OF THE GASBUGGY AND RULISON DETONATIONS
(Continued)

PHYSICAL PARAMETER	DETONATION	
	Gasbuggy	Rulison
Failure Criteria-- Initial Failure:		
Tensile Strength	-5×10^{-5} (Mb)	-5×10^{-5} (Mb)
Cohesive Strength	2×10^{-4} (Mb)	2×10^{-4} (Mb)
Tangent of Angle of Internal Friction	1	1
Ultimate Strength under High Confining Pressure	2×10^{-3} (Mb)	Case I 1×10^{-3} (Mb) Case II 2×10^{-3} (Mb)
Later Fail Later Failure		
Tensile Strength	-10^{-5} (Mb)	-10^{-5} (Mb)
Cohesive Strength	10^{-4} (Mb)	10^{-4} (Mb)
Tangent of Angle of Internal Friction	1	1
Ultimate Strength under High Confining Pressure	2×10^{-3} (Mb)	Case I 5×10^{-4} (Mb) Case II 10^{-3} (Mb)
Gaseous Equation-of-State		
Alpha (cm^3/gm)	0.0166	0.0166
Gamma	1.08	1.08

* * * * * *

TABLE 3-3.

OUTPUT PARAMETERS FOR THE NUMERICAL SIMULATION OF THE GASBUGGY AND RULISON DETONATIONS

PHYSICAL PARAMETER	DETONATION		
	Gasbuggy	Rulison	
		Case I	Case II
Final Cavity Radius	35 m	$58^{+(2)}$ m	48 m
Outer Limit of Cracking	290 m	$273^{+(2)}$ m	289 m
Maximum Radial Pressure at 50 m	0.040 Mb	0.053 Mb	0.053 Mb
Maximum Radial Pressure at 100 m	0.007 Mb	0.010 Mb	0.010 Mb
Maximum Radial Pressure at 200 m	0.0029 Mb	0.0033 Mb	0.0033 Mb
Energy Transmitted to the Elastic Region	2%	$6^{(1)}$%	3%
Maximum Velocity at Ground Zero	44cm/sec[3]	Not calculated	Not calculated

(1) Extrapolated from 100 msec. Kinetic energy at 100 msec is twice that of Case II.

(2) Extrapolated from data at 100 msec. Case I was stopped at 100 msec, the cavity growth and material cracking process was not complete.

(3) Extrapolation from the calculated velocity at 420 m; hence, highly unreliable.

* * * * * *

Figure 3-1 illustrates pressure profiles calculated at three distances for the Gasbuggy and Rulison detonations. Unfortunately, no measured values are available for comparison.

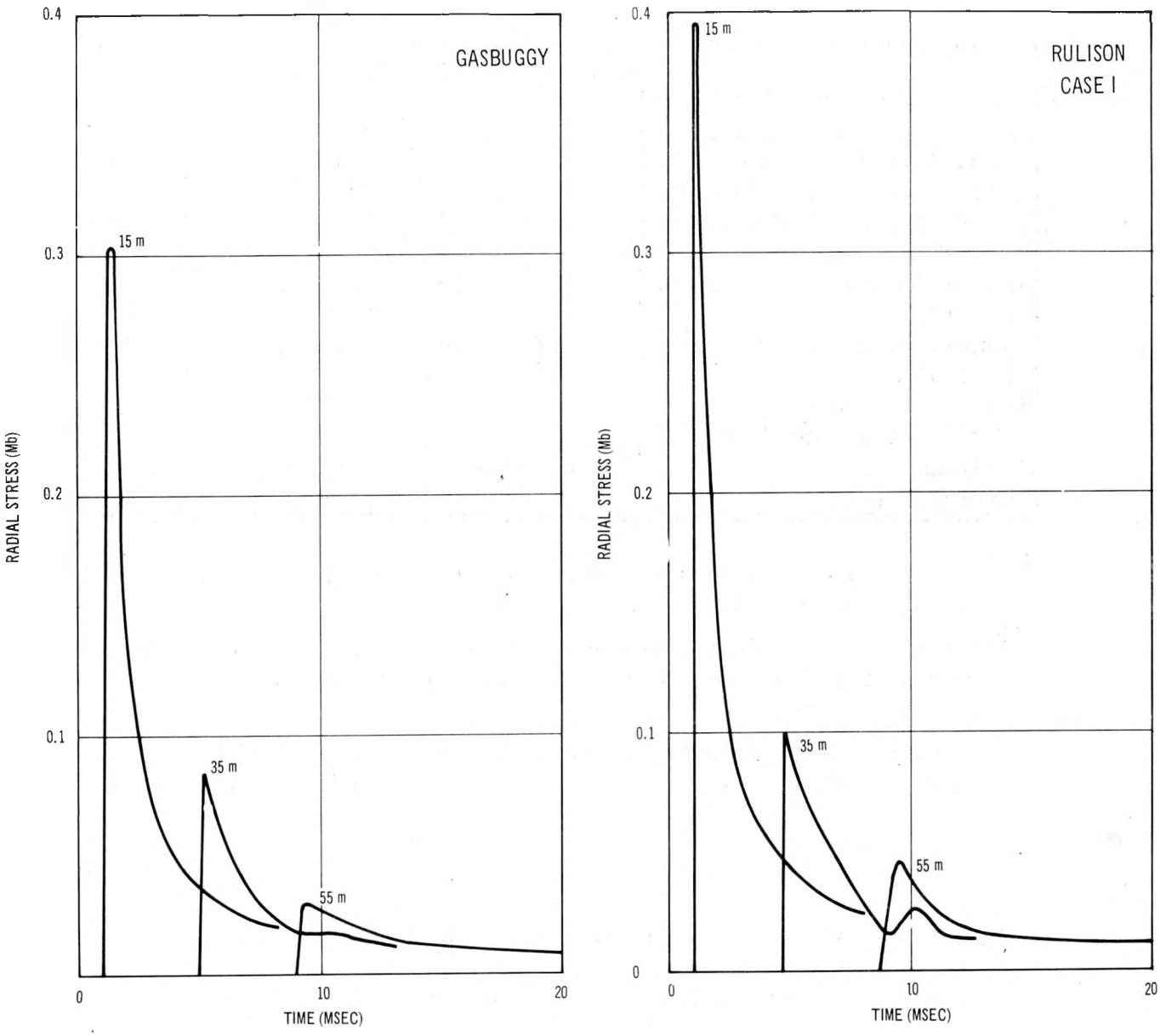

Figure 3-1. Pressure Profiles Calculated for the Gasbuggy and Rulison Detonations

It should be noted that predictions of the cavity radius and the radius of cracking based on empirical methods (Foote, et al., 1969; Weetman, et al., 1969) give smaller values than those calculated (see Table 3-3) for the Gasbuggy and Rulison detonations. For example, the prediction of the cavity and cracking radii for Rulison are, respectively, 102 ± 20 feet and 440 ± 66 feet, whereas, the calculated values (for Case II) are 157 and 950 feet. As noted earlier, the results of the numerical simulation should be interpreted in a relative rather than an absolute sense. However, some explanation for the value calculated for the cracking radius can be given. Being spherically symmetric, the one-dimensional calculation can only determine whether a given spherical shell has suffered cracking at a given time step, without regard to the severity of the cracking. That is, the crack in the simulated spherical shell may be a single small crack or many large cracks and the basic interpretation by the code is the same. The progress of the cracking front provides some insight to this basic question, however. The calculated progress of the cracking front for Rulison is:

Time (msec):	10	20	30	40	50	60	70	80	110
Cracking Distance (m):	61	97	124	146	172	187	215	238	289

Hence, the cracking front progresses at approximately a constant velocity. Detailed examination of the ensemble of cells

at various time steps to determine if the failure criterion is satisfied provides additional insight; namely (see Figure 3-2), that as time progresses fewer cells in a radial line undergo cracking. Hence, the severity of cracking decreases with time and distance. It is quite plausible that the indicated cracking by the outermost cells in the code is so mild that experimental determination of the cracked region would not sense it; thereby leading to larger calculated values than are actually observed. The dimension of the cracked region is an important parameter for gas stimulation experiments like Gasbuggy and Rulison. (Calculations of the elastic radius using measurements in the seismic region also provide insight into the dimensions of the cracked region, see Section 4.5.)

It should be noted that the radius of cracking calculated in the one-dimensional computer code is approximately equivalent to the elastic radius, the region where the material exhibits only elastic behavior. The relative values calculated for Gasbuggy and Rulison are roughly equivalent to those determined on the basis of seismic energy efficiency calculations, using the characteristics of the observed seismic data. This technique, along with other aspects of the observed seismic motions, will be discussed in Chapter 4.

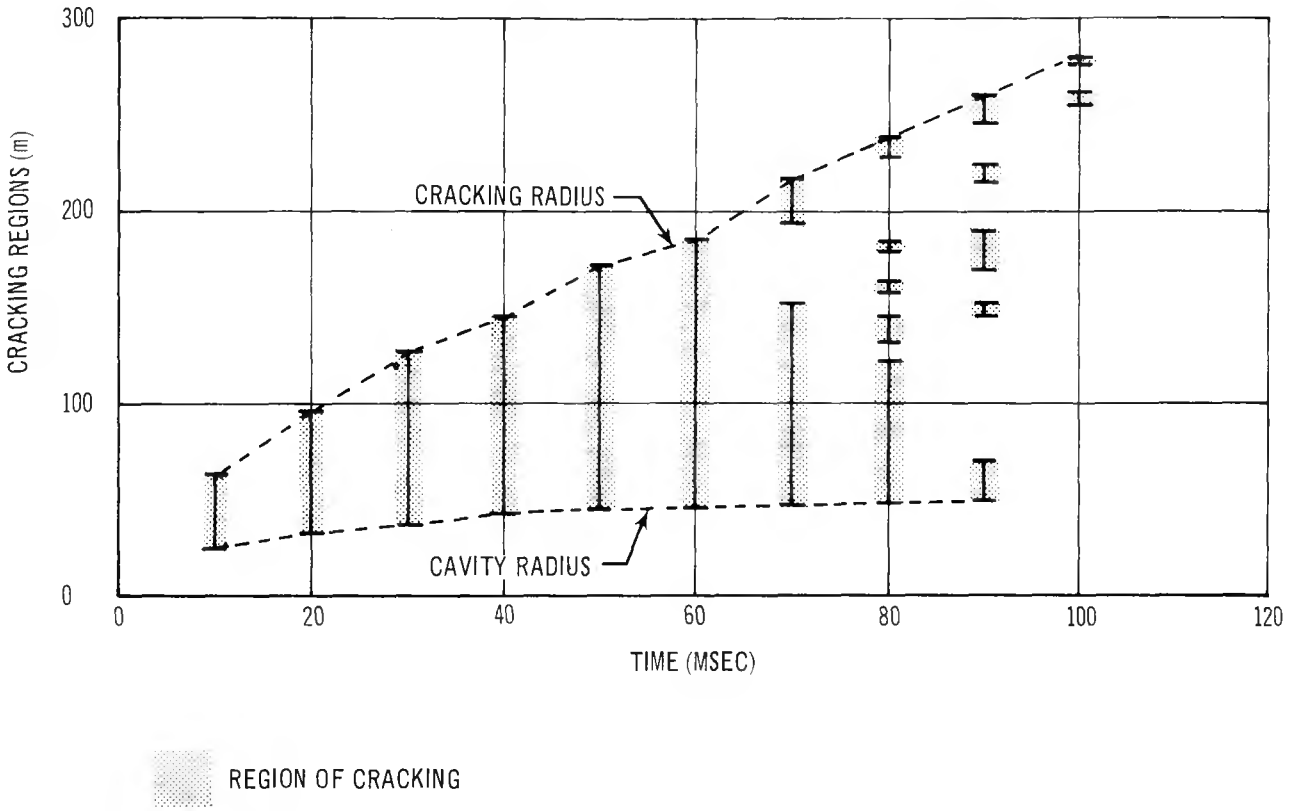

Figure 3-2. The Calculated Cracking Front, Cavity Radius and Regions of Cracking as a Function of Time, Rulison Detonation

CHAPTER 4

ANALYSIS OF THE GROUND MOTIONS

The ground motion which a site experiences following an underground nuclear detonation is related in a complex manner to the forcing function acting at the source, the geological and geophysical properties along the various paths which the energy follows from the source to the receiver, and the physical properties and configuration of the near-surface materials underlying the receiver. Consequently, the amplitude and frequency composition of the ground motion recorded at each individual site is a complex function of variables related to (1) the source region, (2) the transmission path, and (3) the recording site. Source variables include the yield of the device, the depth of burial, the nature of the emplacement hole, and physical parameters (rock type, elastic properties, moisture content, porosity, etc.) of the source and near-source media. Transmission path variables include the physical parameters of each individual transmission path between the source and the receiver, the geometric travel path, and the type of propagating

elastic wave. Recording site variables include the physical parameters (thickness, elastic properties, rock type, etc.) of the near-surface materials, the coupling between the seismograph and the earth, and the instrument response characteristics.

The objective of this chapter is to describe the characteristics of the ground motion observed at various recording sites and to relate these characteristics to parameters of the source, transmission path, and recording site.

4.1 CHARACTERISTICS OF THE GROUND MOTIONS

4.1.1 Peak Particle Amplitudes

Figures 4-1 through 4-3 illustrate, respectively, the peak resultant vector particle acceleration, velocity, and displacement observed (derived in the case of acceleration and displacement) at each hard rock recording site. Each figure shows: (1) the corresponding level of ground motion which would be expected on the basis of Nevada Test Site (NTS) experience (Murphy and Lahoud, 1969) for the 40 kt Rulison yield, (2) the level of ground motion predicted for 40 kt on the basis of Gasbuggy experience (Weetman, et al., 1969; Foote, et al., 1969), and (3) the level of ground motion expected when differences in device depth of burial between

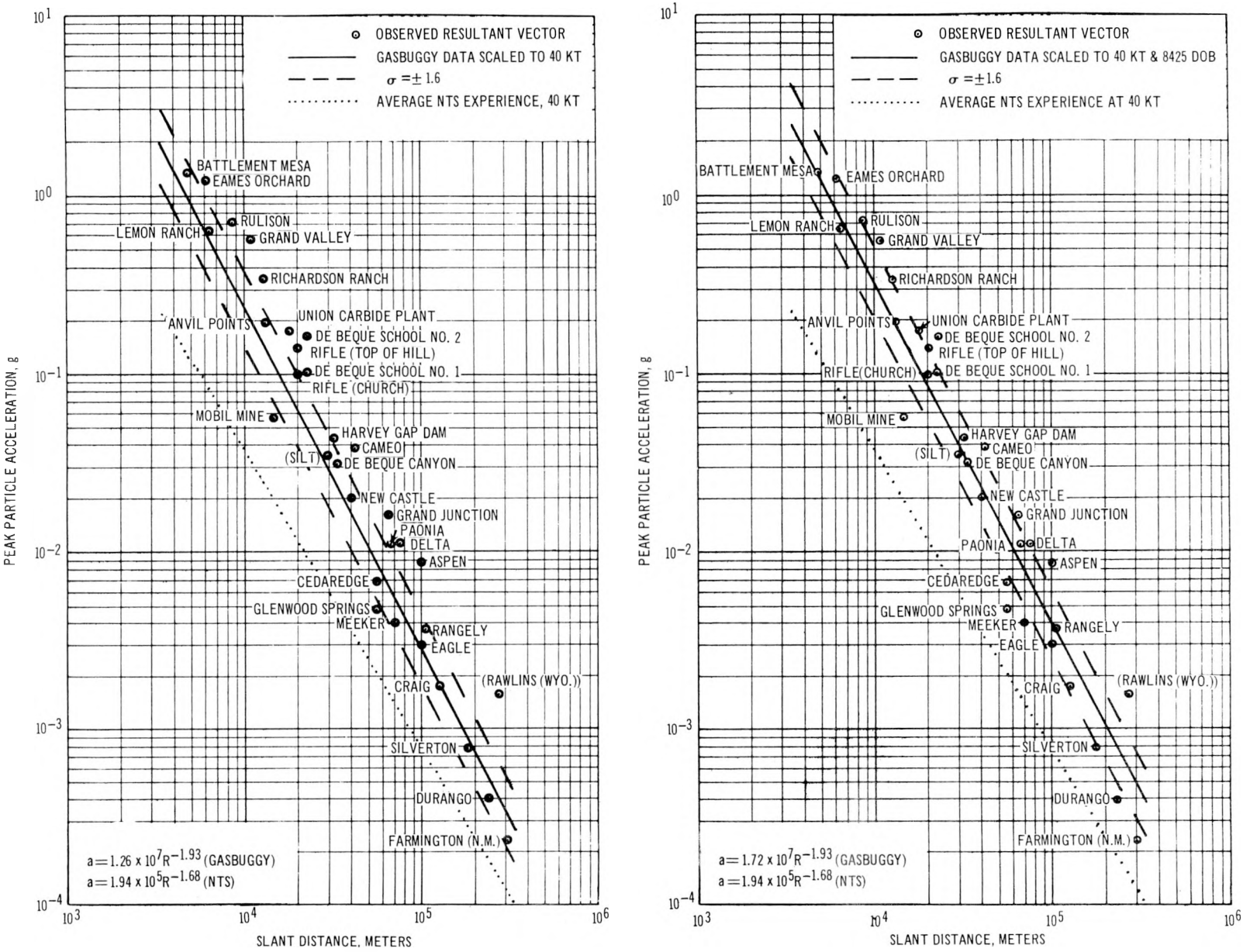

Figure 4-1. Peak Vector Particle Acceleration Observed from the Rulison Detonation, Hard Rock Sites

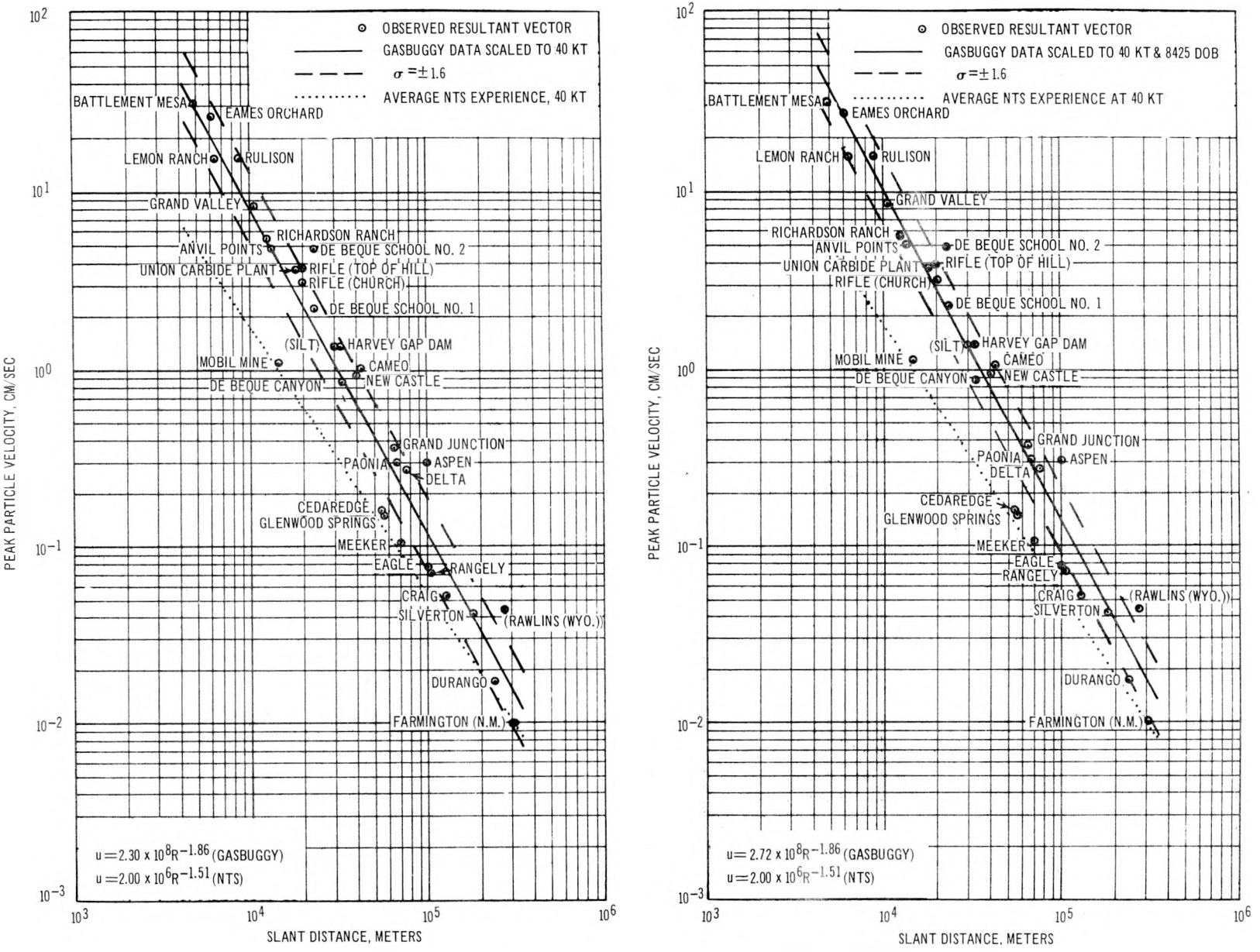

Figure 4-2. Peak Vector Particle Velocity Observed from the Rulison Detonation, Hard Rock Sites

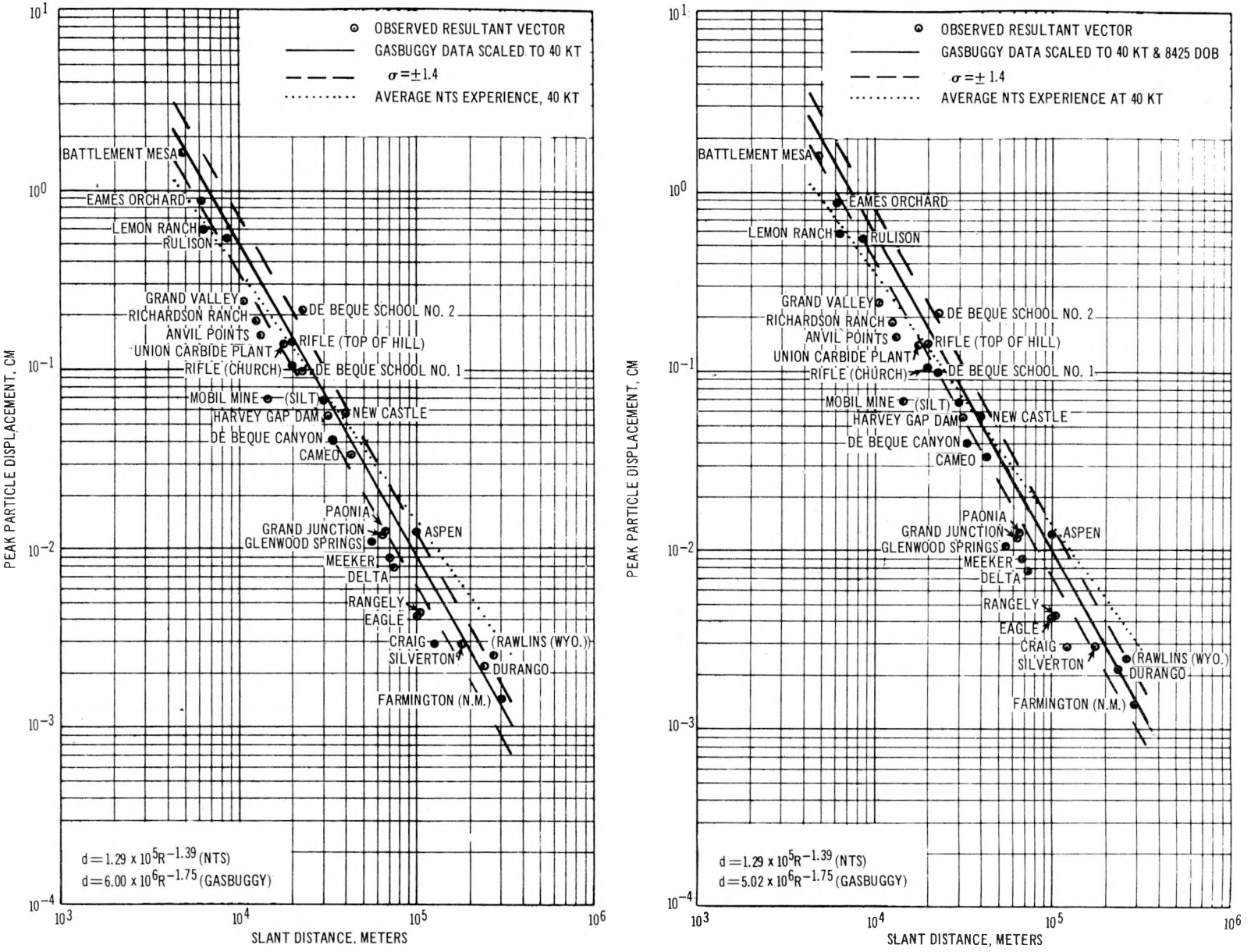

Figure 4-3. Peak Vector Particle Displacement Observed from the Rulison Detonation, Hard Rock Sites

Gasbuggy and Rulison are taken into account (Mueller, 1969a). The data of these figures illustrate the following:

1. The observed peak vector particle velocities and displacements agree well with the predicted levels obtained by scaling Gasbuggy data to 40 kt, the Rulison yield, whereas, the observed peak vector accelerations are slightly higher than predicted.

2. The level of peak vector particle acceleration and velocity significantly exceed the level expected on the basis of NTS experience. The peak vector particle displacement at 10 km is about 0.8 times the level expected at that distance from a normally buried 40 kt detonation on the NTS (an explanation for these effects will be discussed in Section 4.1.3).

3. The observed peak vector ground motions agree best with the corresponding levels expected on the basis of scaling Gasbuggy ground motion data for differences in yield (26 kt vs 40 kt) and device depth of burial (4240 ft vs 8425 ft).

It should be noted that the recording sites shown in Figure 4-1 through 4-3 are grouped together as hard rock sites. This grouping is not correct in the strictest sense of the word, but was made for several reasons. (1) The ground motion predictions were based upon the Gasbuggy event data sample, a sample of data from 34 recording stations in the San Juan Basin, located on both hard rock and alluvium, over the distance range of 5 - 90 km. The alluvium cover at Gasbuggy is typically so thin (50 feet or less) that the frequencies

generated are too high to be of significance in changing the peak values. (2) The alluvium cover is also fairly thin at many of the sites in Piceance Creek Basin instrumented for Rulison, as shown on pages 4-64 through 4-66. (3) Refraction surveys (to be discussed in Section 4.3) at several selected critical sites provided evidence that amplification would occur at only a few sites and would be virtually absent or very minimal at many other sites.

Figure 4-4 shows the peak vector ground motions recorded at sites located on alluvium outside the Piceance Creek Basin. The level of ground motion expected at these sites on the basis of Gasbuggy data, scaled for yield and incorporating NTS amplification experience, is shown for comparison.

Figure 4-5 shows the peak particle acceleration and velocity recorded on the radial, transverse, and vertical components. Regression lines, derived on the basis of the data, are shown on each graph for reference. The peak accelerations observed on the three components contribute

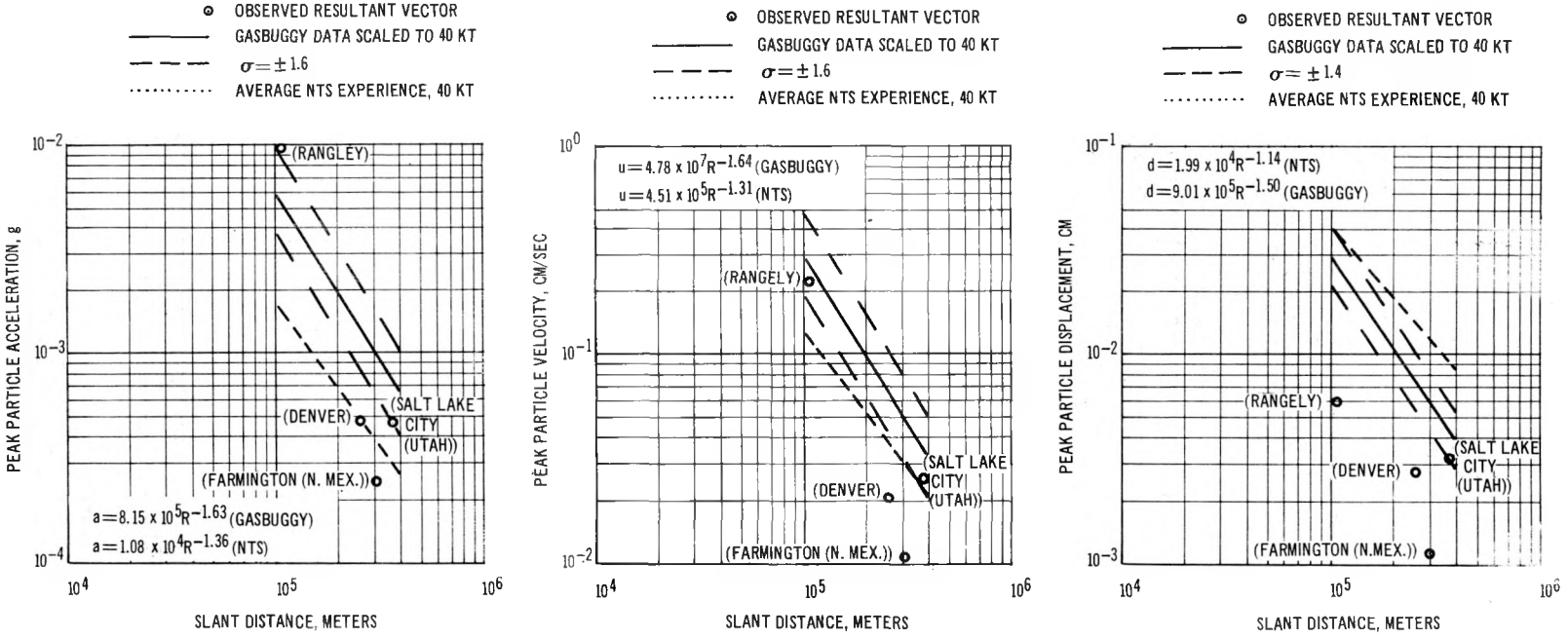

Figure 4-4. Peak Vector Particle Ground Motions Observed at Alluvium Sites outside the Piceance Creek Basin, Rulison Detonation

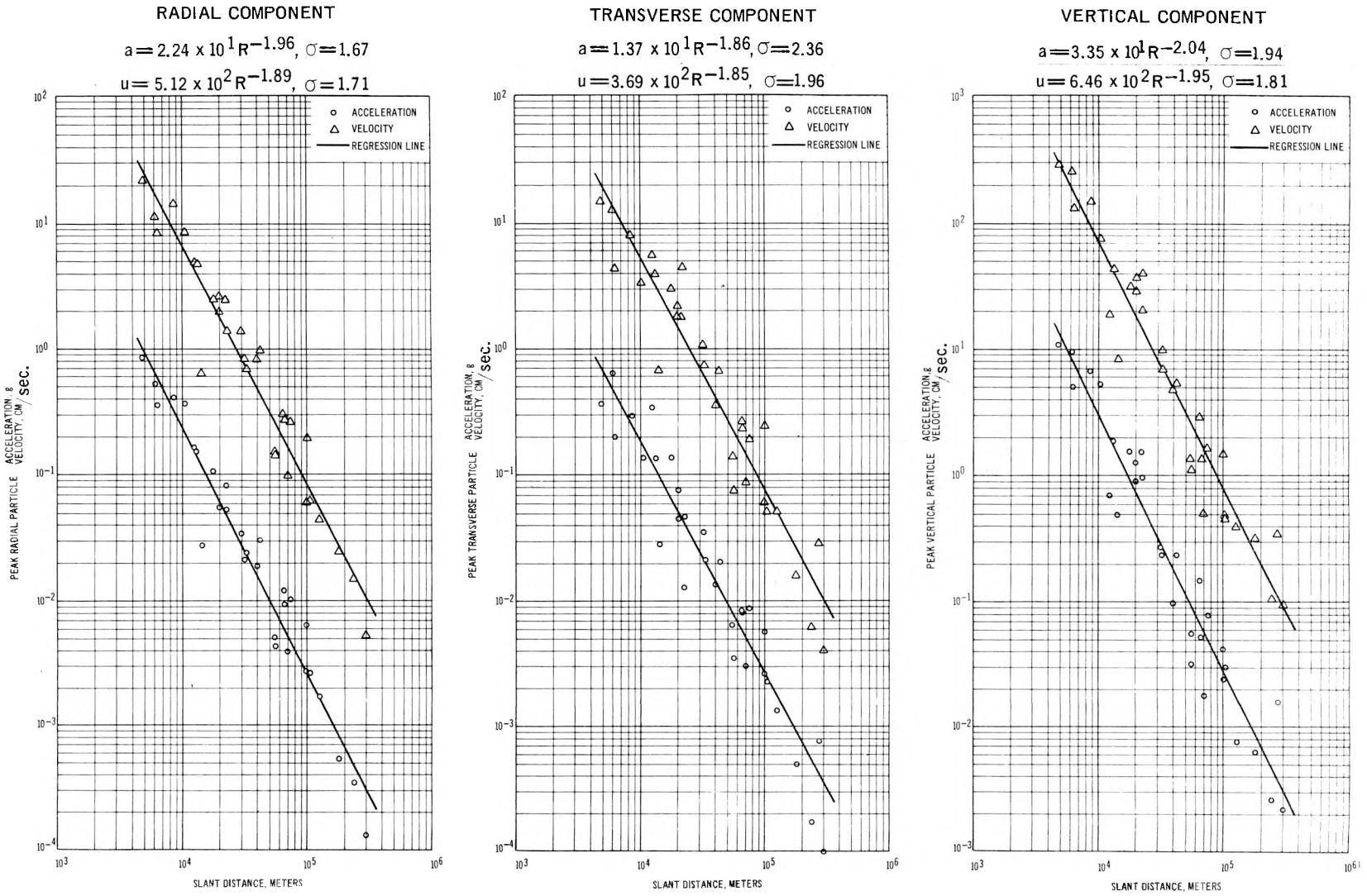

Figure 4-5. Peak Particle Acceleration and Velocity Observed at Hard Rock Sites, Rulison Detonation

varying amounts to the resultant vector, with distance, as was expected. The vertical component acceleration (Figure 4-6) contributes about 0.8 of the resultant vector magnitude inside 8 km. From about 8 km to about 23 km, the percentage contribution increases to values in excess of 0.9, on an average, of the resultant vector, a rather high value on the basis of simple geometric considerations. The contribution decreases to 0.6 in the 23 to 40 km range and then the data points show considerable scatter. The radial component acceleration contributes an average of 0.5 to 0.6 of the resultant vector inside 20 km, then, the percentage contribution increases with increased distance. The transverse component acceleration shows an increasing contribution to the resultant vector from the closest station to about 100 km. Beyond that distance, the contribution diminishes rapidly.

The vertical component velocity (Figure 4-7) contributes in excess of 0.9 of the resultant vector magnitude inside about 8 km. The percentage contribution is somewhat lower, or about 0.8 to 0.9 (except for the Richardson Ranch instrument station at 12.7 km), from about 10 to approximately 18 km. The percentage contribution "peaks" at approximately 20 km and then decreases with increased distance. The relationships of the radial and transverse component velocities to the

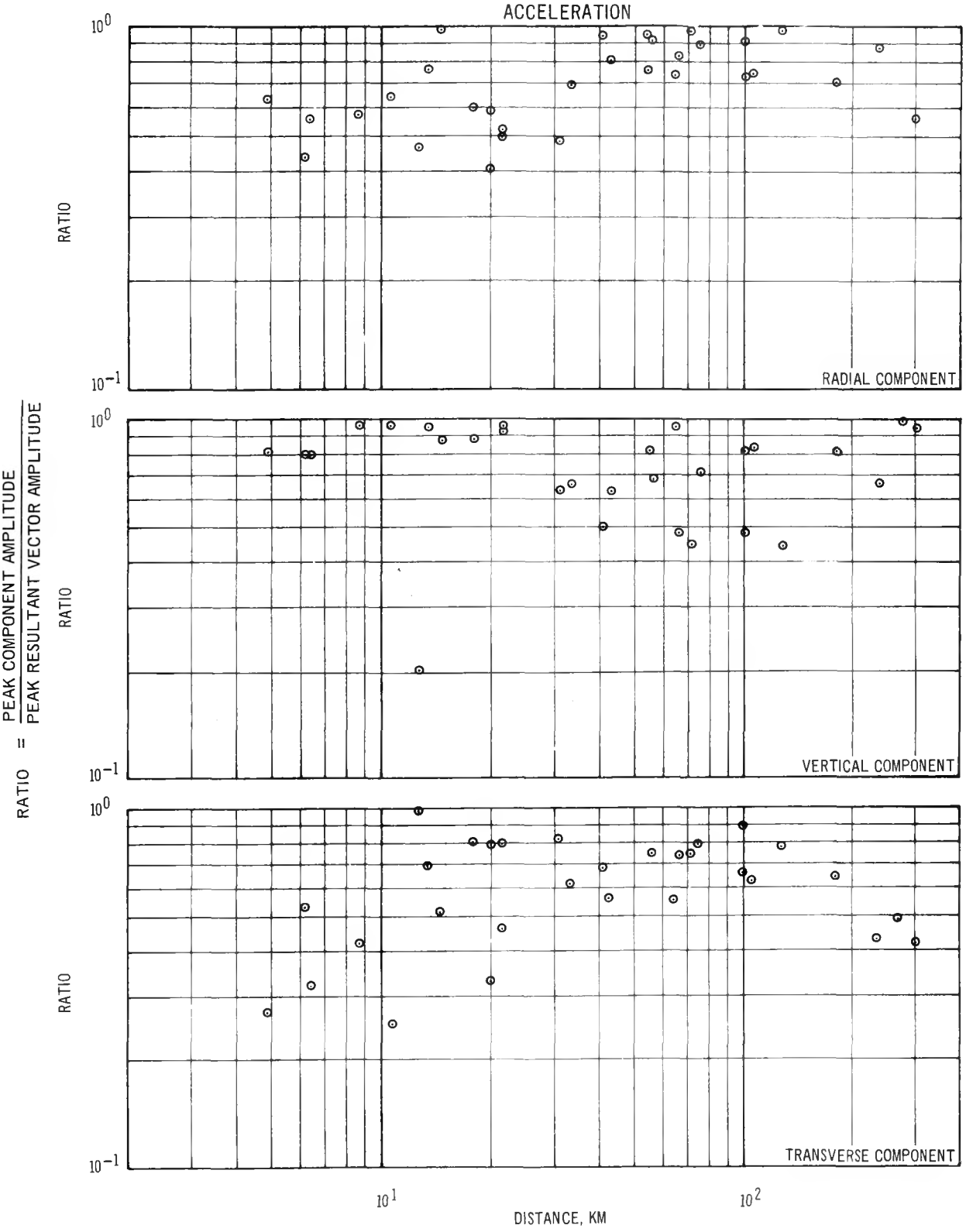

Figure 4-6. Ratio of Peak Component Acceleration Amplitude to Peak Vector Acceleration Amplitude as a Function of Distance, Rulison Event

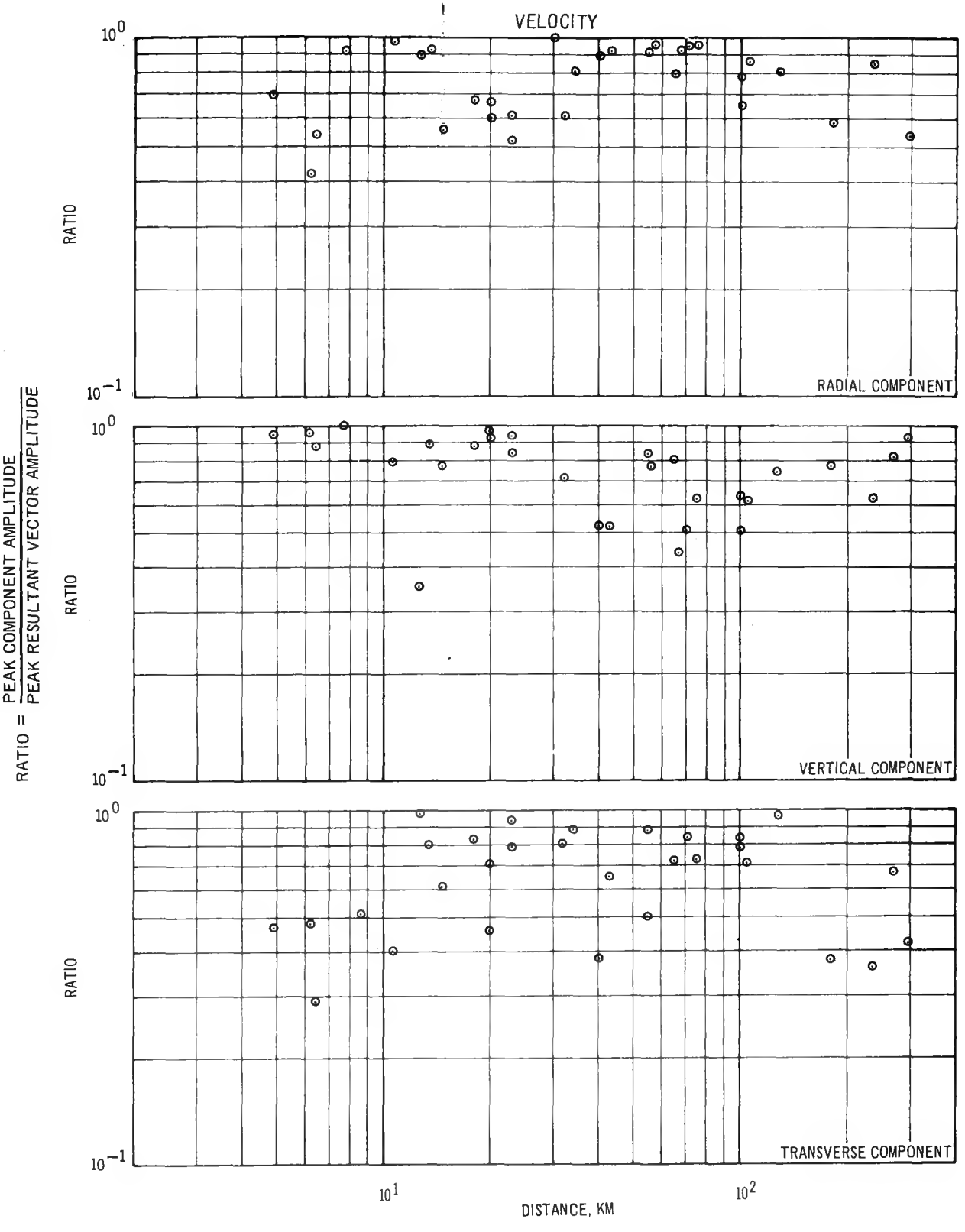

Figure 4-7. Ratio of Peak Component Velocity Amplitude to Peak Vector Velocity Amplitude as a Function of Distance, Rulison Event

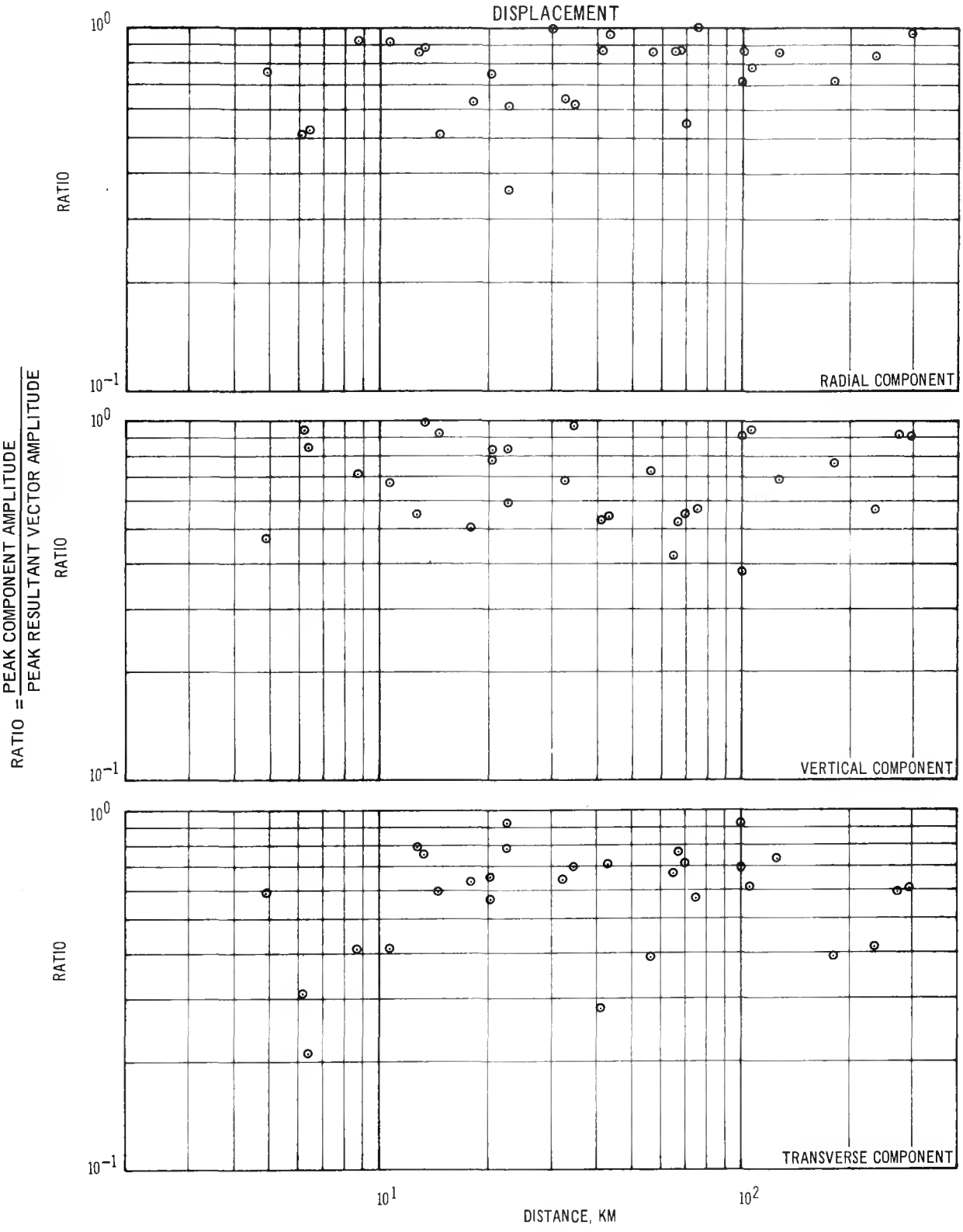

Figure 4-8. Ratio of Peak Component Displacement Amplitude to Peak Vector Displacement Amplitude as a Function of Distance, Rulison Event

resultant vectors are approximately the same as shown for the accelerations.

The relative contributions of the radial, vertical, and transverse components of displacement (Figure 4-8) to the resultant vector are approximately equivalent at all distances. Both the radial and vertical component displacements average in excess of 0.5 contribution, whereas, the contribution of the transverse component velocity is slightly lower.

The contribution of each component of motion to the peak resultant vector is a complex subject which will be studied in detail in the future.

4.1.2 PSRV Spectra

Figures 4-9 through 4-15 show for selected Rulison stations the pseudo-relative velocity (PSRV) spectra with 5% damping, derived from the measured horizontal component of ground motion having the peak response. PSRV spectra represent the response of a series of single-degree-of-freedom systems having viscous damping to a ground motion input. PSRV spectra, for small damping (5 percent), are reasonably close approximations to Fourier amplitude spectra. The spectra shown in Figures 4-9 through 4-15 are compared to: (1) the spectra expected on the basis of Gasbuggy experience,

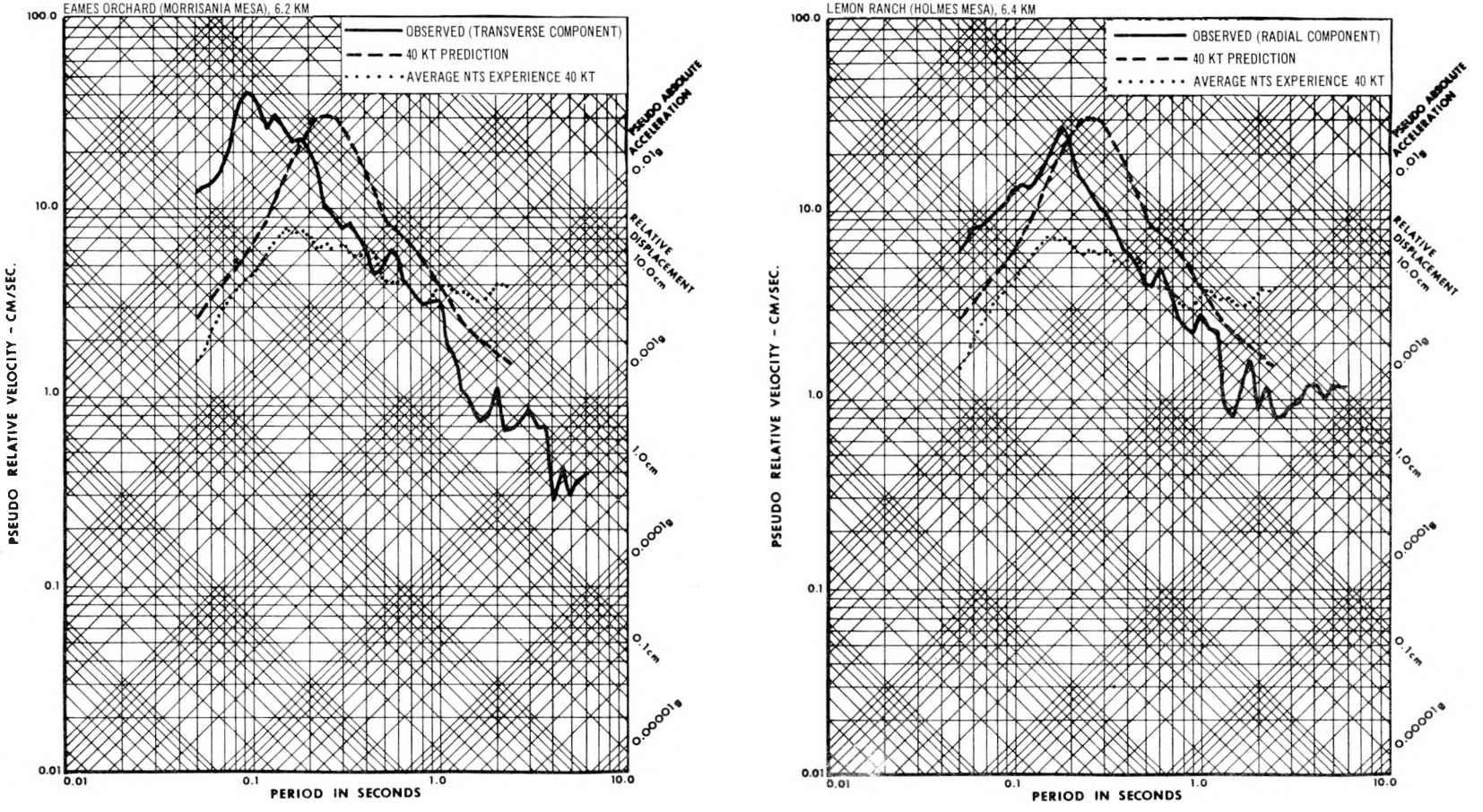

Figure 4-9. Comparison of Observed 5% PSRV Spectrum with the Predicted Spectrum and the Spectrum Expected on the Basis of Nevada Test Site Experience.

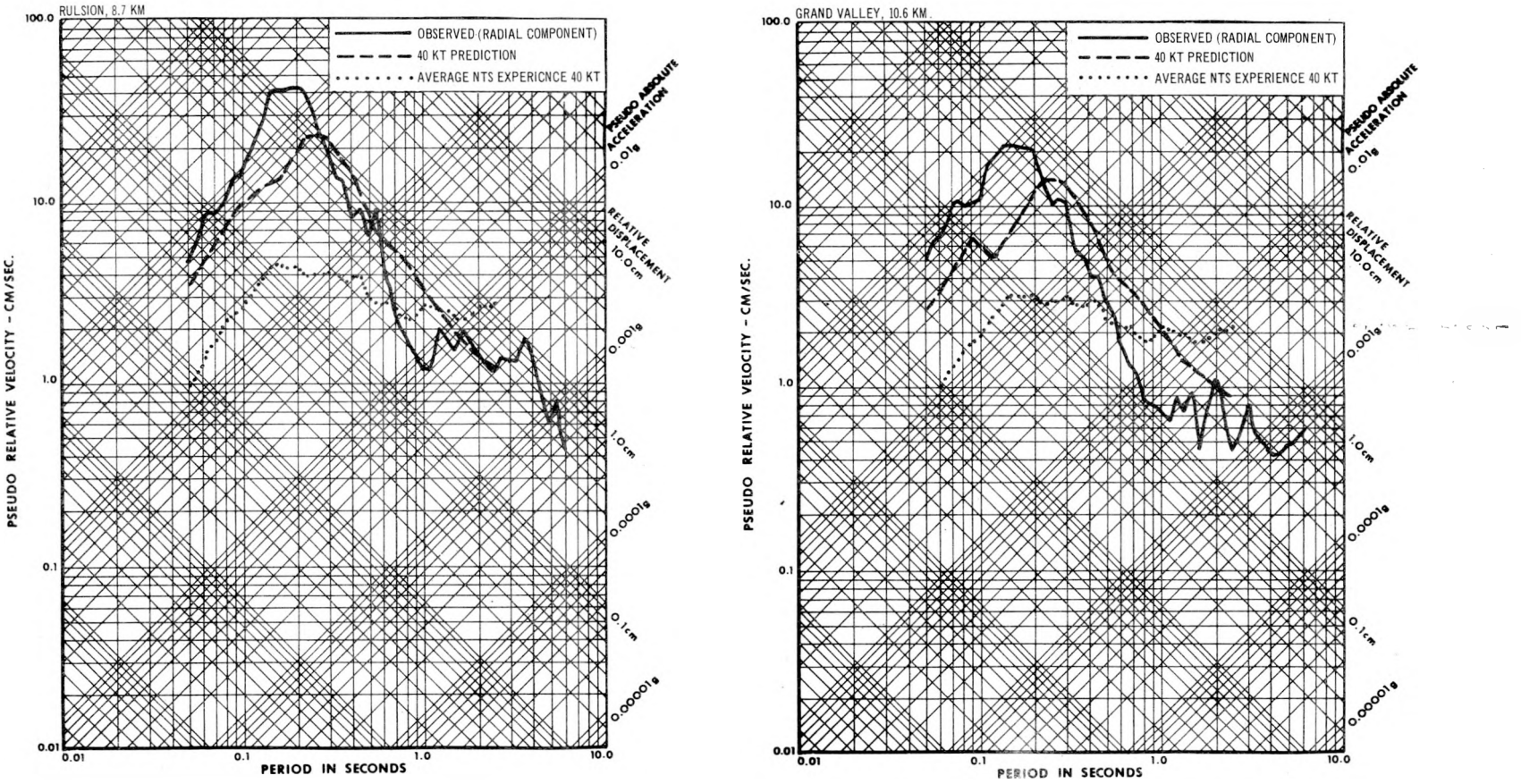

Figure 4-10. Comparison of Observed 5% PSRV Spectrum with the Predicted Spectrum and the Spectrum Expected on the Basis of Nevada Test Site Experience.

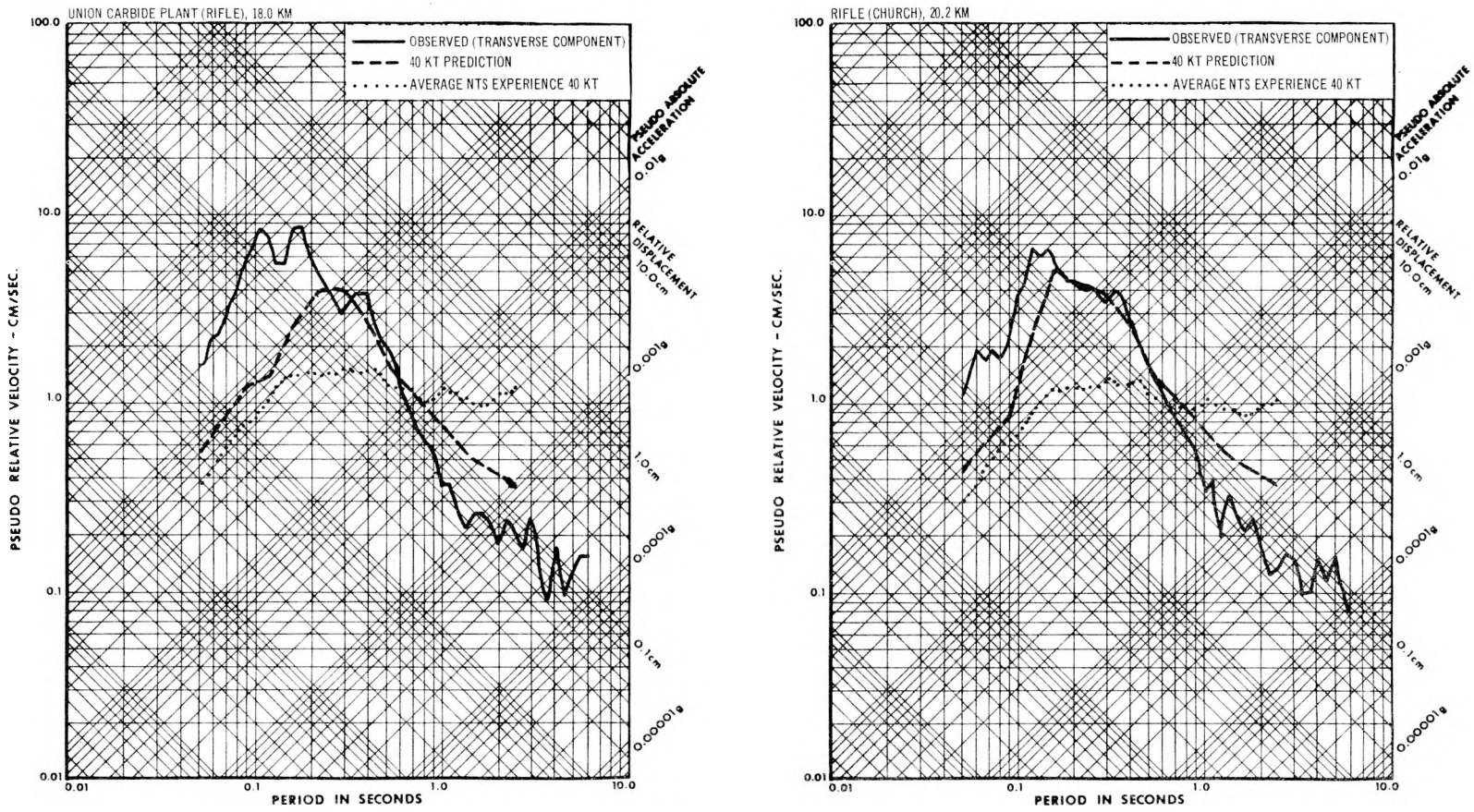

Figure 4-11. Comparison of Observed 5% PSRV Spectrum with the Predicted Spectrum and the Spectrum Expected on the Basis of Nevada Test Site Experience.

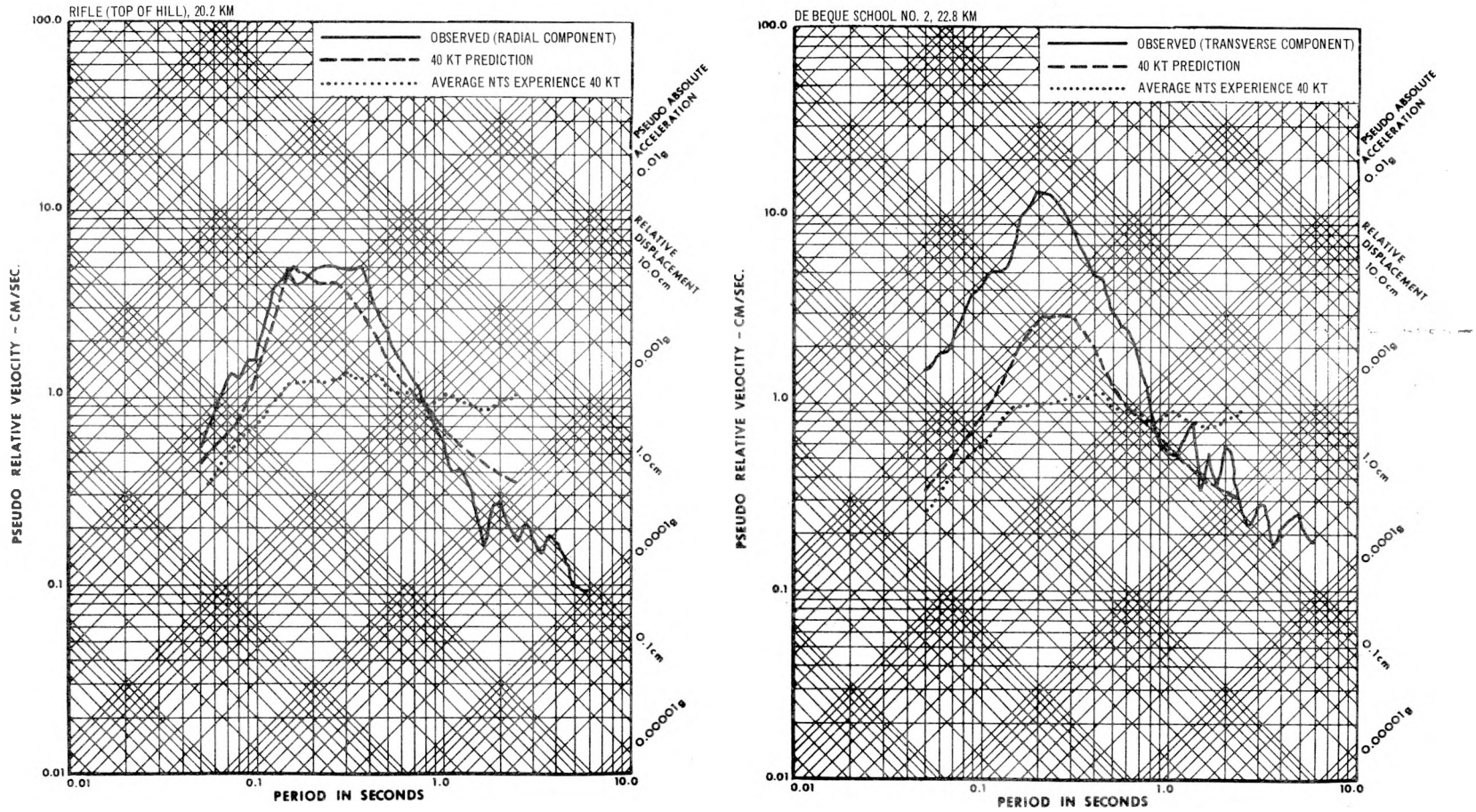

Figure 4-12. Comparison of Observed 5% PSRV Spectrum with the Predicted Spectrum and the Spectrum Expected on the Basis of Nevada Test Site Experience.

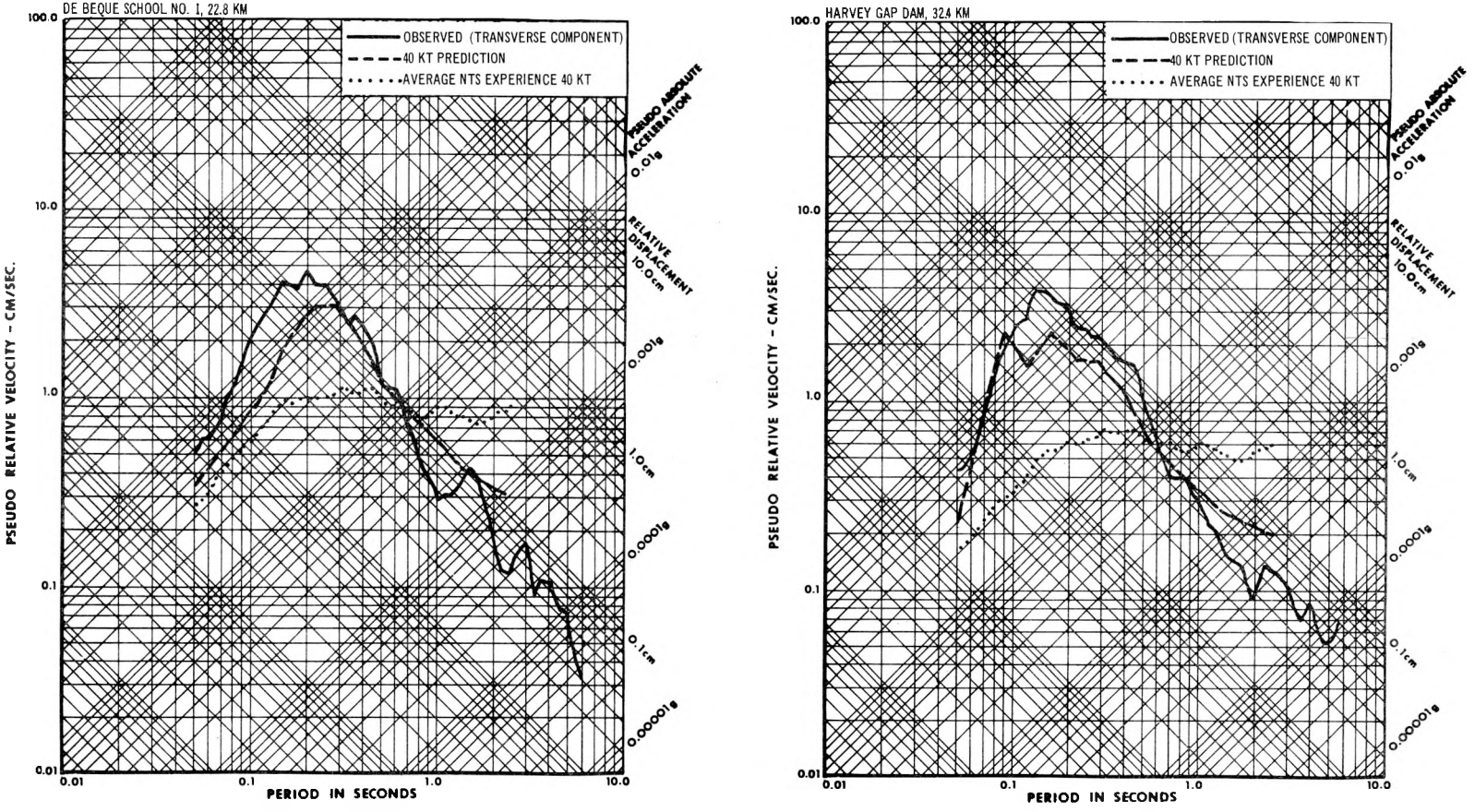

Figure 4-13. Comparison of Observed 5% PSRV Spectrum with the Predicted Spectrum and the Spectrum Expected on the Basis of Nevada Test Site Experience.

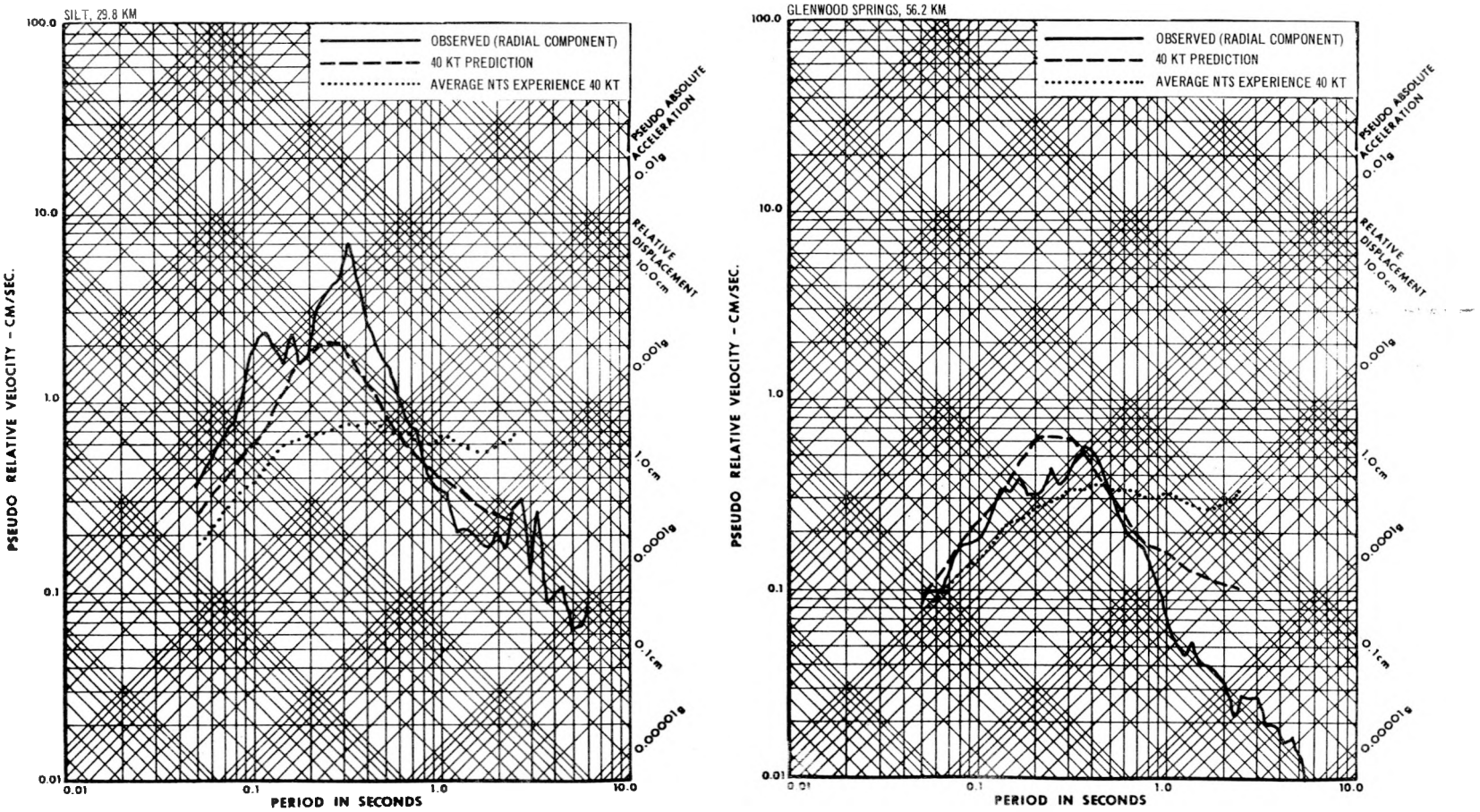

Figure 4-14. Comparison of Observed 5% PSRV Spectrum with the Predicted Spectrum and the Spectrum Expected on the Basis of Nevada Test Site Experience.

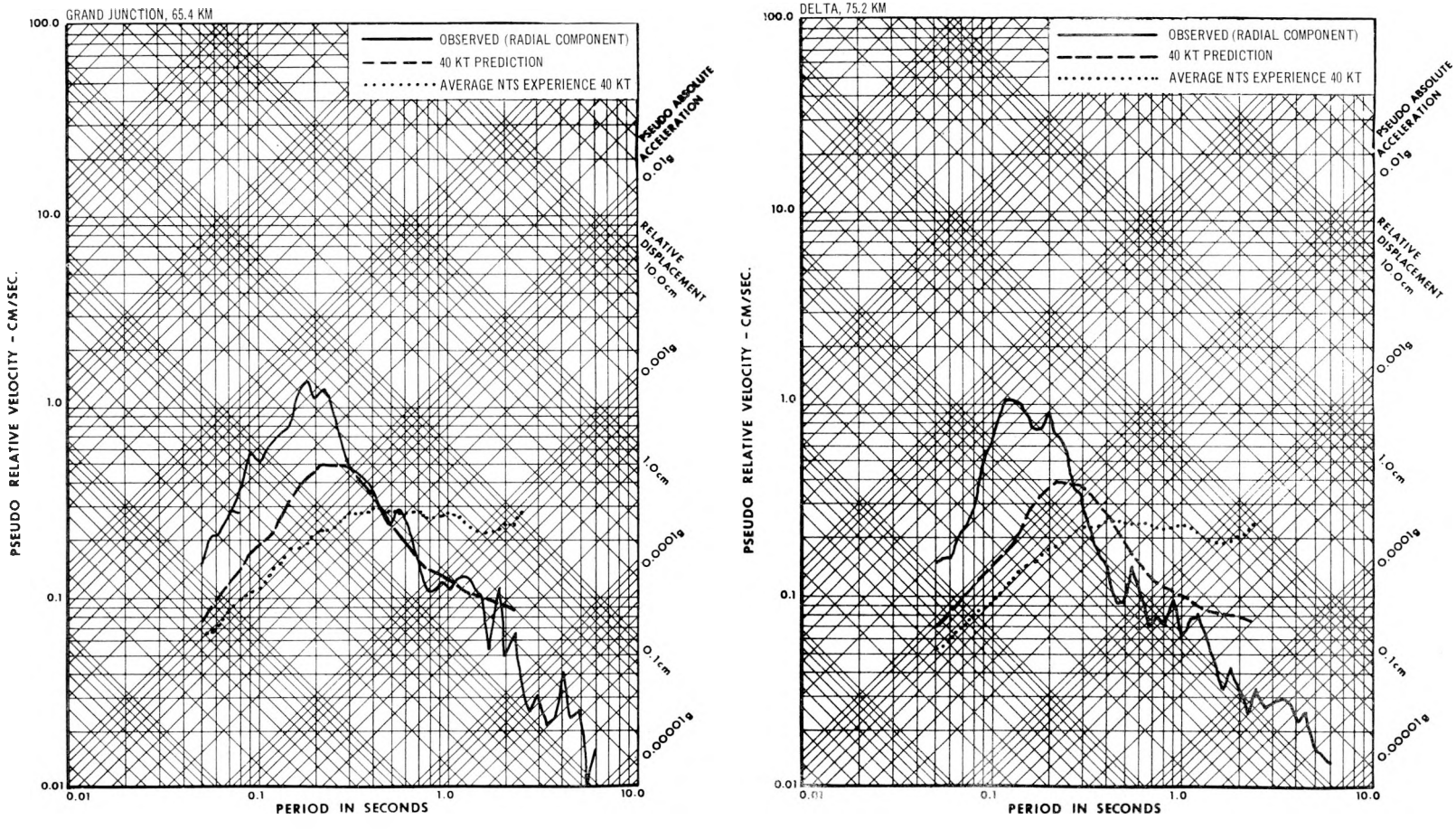

Figure 4-15. Comparison of Observed 5% PSRV Spectrum with the Predicted Spectrum and the Spectrum Expected on the Basis of Nevada Test Site Experience.

scaling the Gasbuggy spectra for differences in yield, device depth of burial, and, for some stations, modified for acoustic impedance contrast (Weetman, et al, 1969; Mueller, 1969a), and (2) the spectra expected on the basis of Nevada Test Site experience (Lynch, 1969) for a typical 40 kt detonation. The data for Figures 4-9 through 4-15 substantiate the following facts:

1. The horizontal spectra observed at Rulison sites are significantly different from the spectra expected on the basis of a typical 40 kt detonation at NTS. On the above mentioned figures, representing selected Rulison stations, the peak spectral response occurs between 0.1 - 0.4 seconds. This is somewhat shorter than the period of the peak spectral response typically observed for a 40 kt NTS detonation.

2. The Rulison spectra exhibit characteristics which are comparable to those expected on the basis of Gasbuggy experience and scaling theory; differences are greatest at distances inside 30 km. These differences include a slightly higher peak spectral response (a difference of less than a factor of 2 at most stations) than expected and a relative shift of the period of maximum spectral response to the short period end of the spectrum (the Gasbuggy maximum spectral response typically occurred at periods of 0.2 - 0.5 second).

4.1.3 Explanation of the Characteristics of the Ground Motion in Terms of Scaling Theory

Relative differences in the characteristics of the seismic response (peak amplitude and PSRV spectra) observed from the Rulison and Gasbuggy detonations and the average

response expected on the basis of NTS experience can be partially explained in terms of a general scaling theory developed by Mueller (1969a). The theory, based on an extension of work by Sharpe (1947) and Latter, et al. (1959), shows that scaling of amplitude spectra of seismic waves generated by an underground nuclear detonation is, in general, dependent on frequency, yield, depth of burial, and medium. In the case of the Gasbuggy and Rulison detonations, two major parameters, the device depth of burial and the physical properties of the sedimentary rocks (sand-shale) of the source environment, are significantly different from Nevada Test Site experience for 26 kt and 40 kt detonations. Both the Gasbuggy and Rulison devices were greatly overburied (factors of 3.8 and 6.2, respectively) relative to the depth of burial which would be employed at NTS for typical containment of these yields. An effect of the device overburial is to cause the distance to the point where the medium begins to behave elastically (the elastic radius) to be relatively smaller (see Section 4.5 on seismic energy efficiency). The elastic radius may be thought of as representing a resonant cavity whose characteristic frequency is determined by its radius. Consequently, the larger the elastic radius, the lower is the dominant frequency of generation for elastic waves. Conversely, the smaller the elastic radius, the higher is the dominant frequency of generation for the elastic waves. Thus, the smaller elastic radii (see Section 4-5) for Gasbuggy and

Rulison results in a higher dominant frequency of generation for the elastic waves than expected on the basis of typical NTS experience. An effect of the higher frequency content is to enhance greatly the peak vector particle accelerations, to enhance slightly the peak vector particle velocities, and to decrease the peak vector particle displacements, as noted earlier.

The Gasbuggy and Rulison detonations both occurred in sedimentary formations (Lewis shale for Gasbuggy and Mesaverde sandstone and shale for Rulison), whereas, most detonations at NTS have occurred in tuff and rhyolite, rocks of igneous origin. Detonation at a greater depth in dense, competent sedimentary rocks, such as these, which have a high sonic velocity (partially due to the greater depth of burial) relative to the NTS tuffs and rhyolites leads to an increased efficiency in coupling the energy into the elastic or seismic region.

Two source parameters, depth of burial and detonation medium, cause a higher level and spectral composition of the ground motions for the Gasbuggy and Rulison detonations relative to the average NTS experience. Figure 4-16 shows the observed Gasbuggy and Rulison peak vector particle accelerations (grouping all recording sites in the basin together) compared to the accelerations expected for 40 kt, based on NTS experience. When differences in the depth of burial and the emplacement medium are considered, the scaling theory

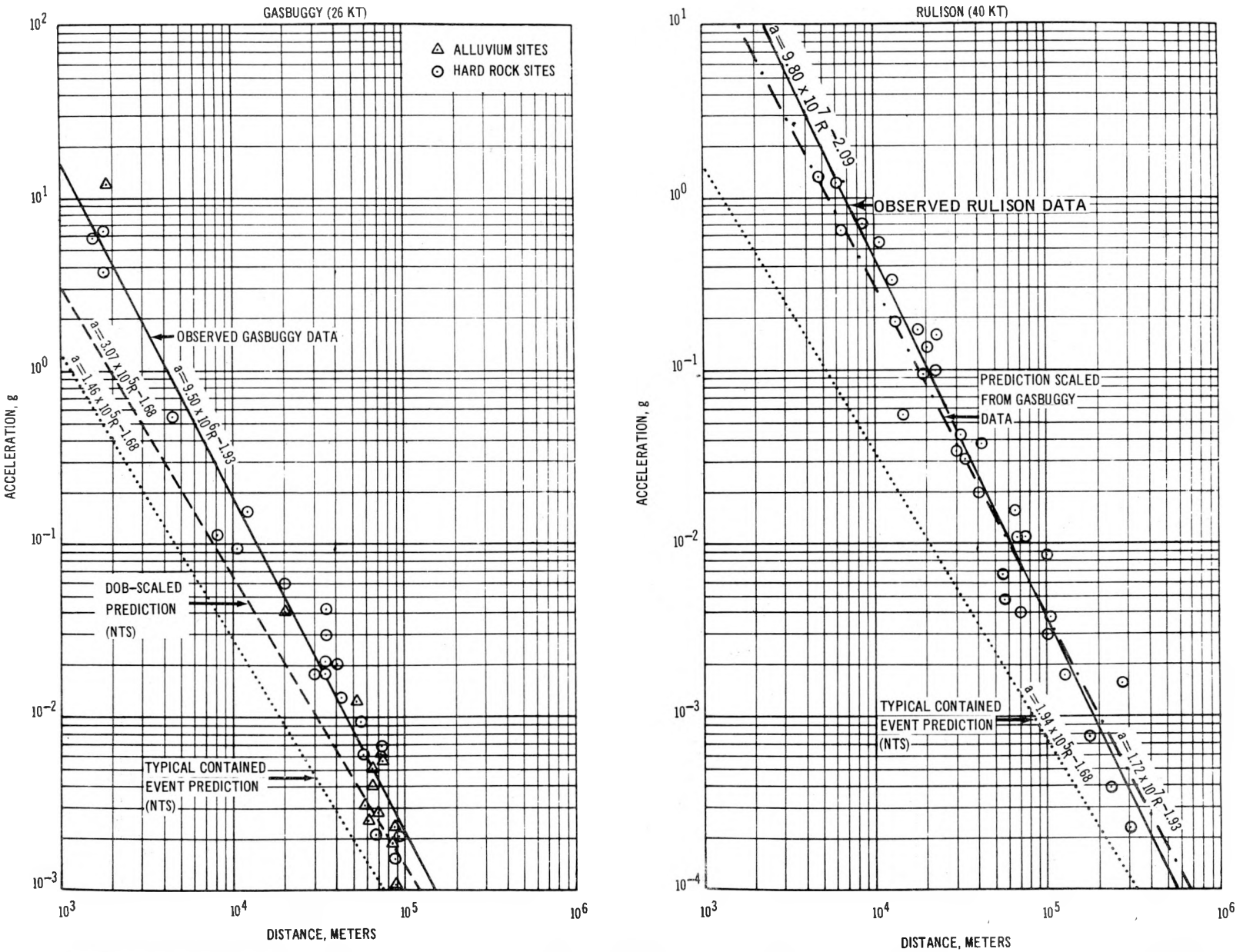

Figure 4-16 Comparison of the Observed Gasbuggy and Rulison Peak Particle Accelerations with the Accelerations Expected on the Basis of Nevada Test Site Experience and on the Basis of Scaling Theory

(Mueller, 1969a) predicts a considerably higher level of peak vector particle acceleration than expected on the basis of average NTS experience. Thus, these two source variables account for much, but not all, of the observed differences between Gasbuggy and Rulison and the peak vector particle accelerations expected on the basis of NTS experience.

Figure 4-17 illustrates the effect, for the Gasbuggy detonation, which scaling for depth of burial has on the PSRV spectra. This figure shows, for distances of 10, 40, and 80 km, the relationship of three different spectra: (1) the average spectra expected on the basis of NTS experience for a 26 kt contained detonation, (2) the average 26 kt spectra based on NTS experience scaled for the difference in depth of burial between Gasbuggy and the average NTS detonation, and (3) the average of Gasbuggy PSRV spectra observed at the corresponding distance. As noted in the figure, scaling the spectrum based on NTS experience for depth of burial produces a spectrum which is enhanced at the short periods (<1 second) and reduced at the long periods (>1 second). The shape and spectral level of the scaled spectra compare well with the observed spectra, particularly at 40 and 80 km. However, the differences in the spectra based on NTS experience and Gasbuggy spectra are not

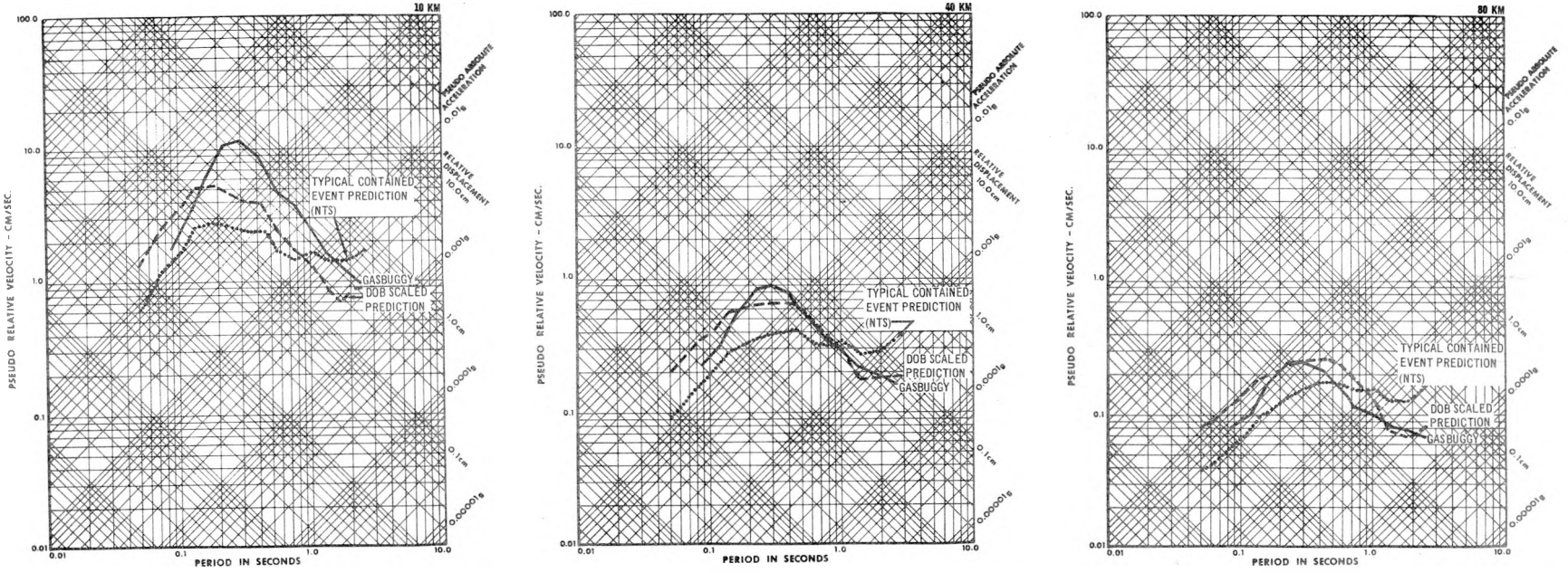

Figure 4-17. Comparison of the Observed Gasbuggy Spectra at Three Distances with the Spectra Expected on the Basis of NTS Experience and on the Basis of Scaling for Depth of Burial

completely explained by scaling for depth of burial, especially at close-in distances. Other variables related to the source, the transmission path, and the recording site, although probably not as important as the two cited, exert some influence in shaping the observed amplitude spectra.

Figure 4-18 illustrates clearly the effect of scaling for differences in yield (26 kt vs 40 kt) and device depth of burial (4240 feet vs 8425 feet) between the Gasbuggy and Rulison detonations. The Gasbuggy spectra (based on regression equations) at two distances, 10 km and 80 km, are compared to: (1) the spectra at these distances scaled to 40 kt, the Rulison yield, and (2) spectra at these distances scaled to 40 kt and the Rulison depth of burial (8425 feet). The latter spectrum, in each case, represents the general spectral prediction for Rulison at these distances. Comparison of these spectra shows:

1. Scaling to a higher yield enhances the long period spectral composition more than the short period spectral composition, a well known fact (Lynch, 1969).

2. Scaling to a greater depth of burial enhances the short period spectral components and reduces the long period spectral components (Mueller, 1969a).

On the basis of the preceding discussion of the effect of source variables, it is reasonable to expect characteristics of the

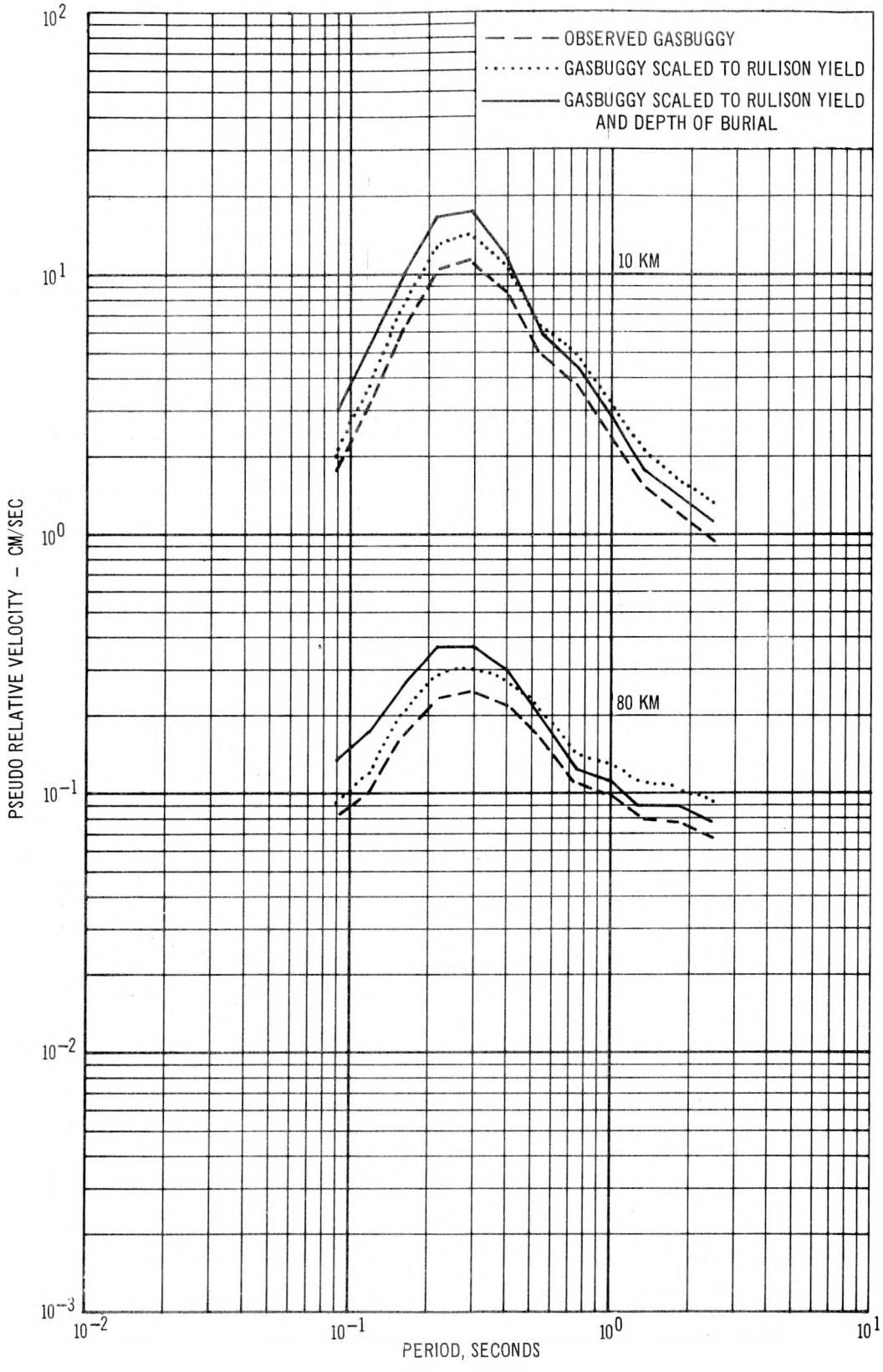

Figure 4-18. Comparison of the Observed Gasbuggy Spectra at Two Distances with the Spectra Expected on the Basis of Scaling to the Rulison Yield and on the Basis of Scaling to the Rulison Yield and Device Depth of Burial

seismic response observed from Rulison to be more comparable to the response characteristics observed from Gasbuggy than to the average NTS response characteristics. The difference in depth of burial between the Gasbuggy and Rulison devices was much less than the difference between that corresponding to average NTS experience and Gasbuggy or Rulison. The Gasbuggy and Rulison detonations occurred in similar sedimentary media. Also, the recording sites are located on hard rock or thin alluvial layers (see Appendix A). The depth of burial, the detonation medium, and geology of the recording sites affected the seismic waves generated by Gasbuggy and Rulison in a similar manner.

4.1.4 Signal Duration

In an earlier study (Lynch, 1968), the relative amplification factor between PSRV (2 percent damped) and BPF spectra for NTS events was shown to frequency independent and to average 8.54 in the period range of 0.1 to 2.5 seconds. Through the transient characteristics of the PSRV and BPF generating process, it was determined that a set of seismic pulses distributed over this period range and having a duration of approximately 4 cycles would account for the observed amplitude ratio. Examination of these and additional NTS data show that the energy in the neighborhood of a given frequency band persists on an average for 3.90 cycles, independent of frequency, within the time history of measured seismograms.

The duration of the ground motion observed at Gasbuggy and Rulison sites was determined, using 2% PSRV spectra and BPF spectra. These spectra should exhibit a distinct parallelism across the frequency domain, if the duration is independent of frequency. This phenomenon was observed for both Gasbuggy and Rulison. The mean ratios between the 2% PSRV and BPF spectra were, respectively, 7.38 and 8.16. These amplitude ratios correspond, respectively, to sine waves of unit amplitude and durations 2.75 and 3.25 cycles, values which are somewhat different from NTS experience of 3.90 cycles.

4.2 CHARACTERISTICS OF THE SEISMIC WAVES

Figures 4-19 through 4-23 illustrate representative particle velocity seismograms recorded at several sites from the Rulison detonation. The radial-vertical component product waveform is displayed as the bottom trace on each seismogram. Inspection of the seismogram and the component product waveform in conjunction with travel time data and derived particle acceleration and displacement seismograms permits the P(compressional), SV and SH(shear), and Rayleigh(surface) waves to be identified (Hays, 1968 and 1969).

Figure 4-24 displays the first arrival time observed from Rulison as a function of the horizontal distance from the energy source to the recording site. The first arrival times

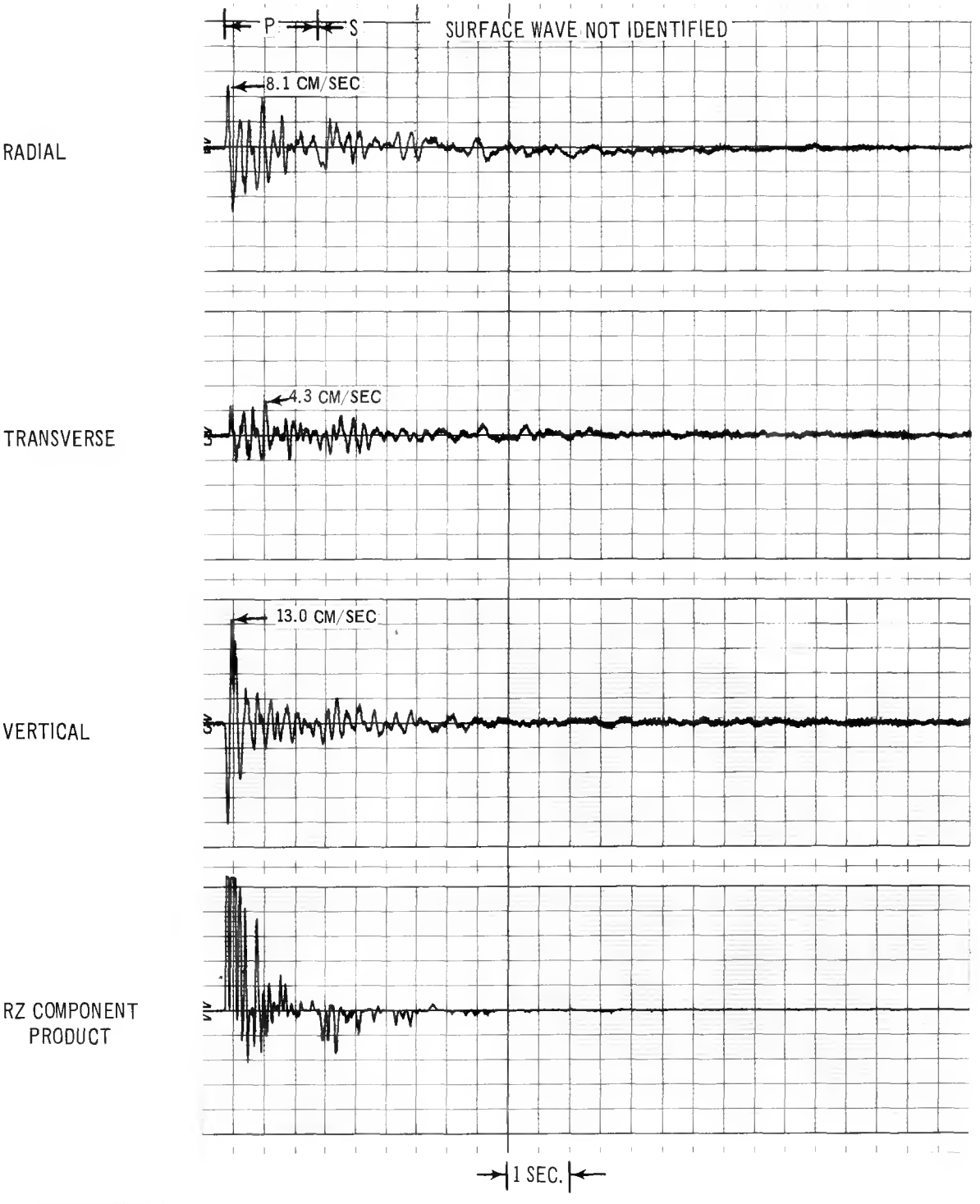

Figure 4-19. Particle Velocity Seismogram Observed at Lemon Ranch, Rulison Detonation

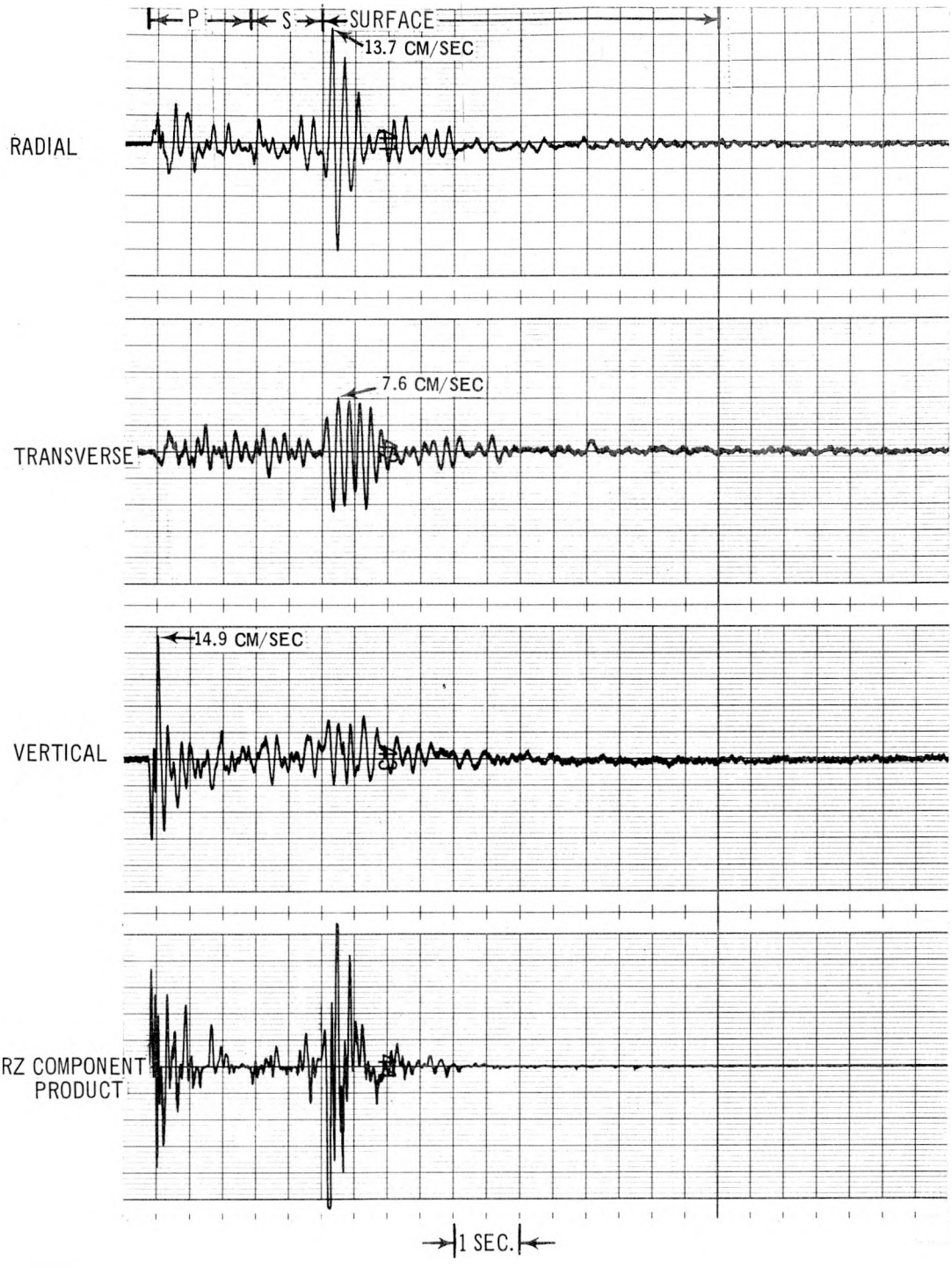

Figure 4-20. Particle Velocity Seismogram Observed at Rulison, Rulison Detonation

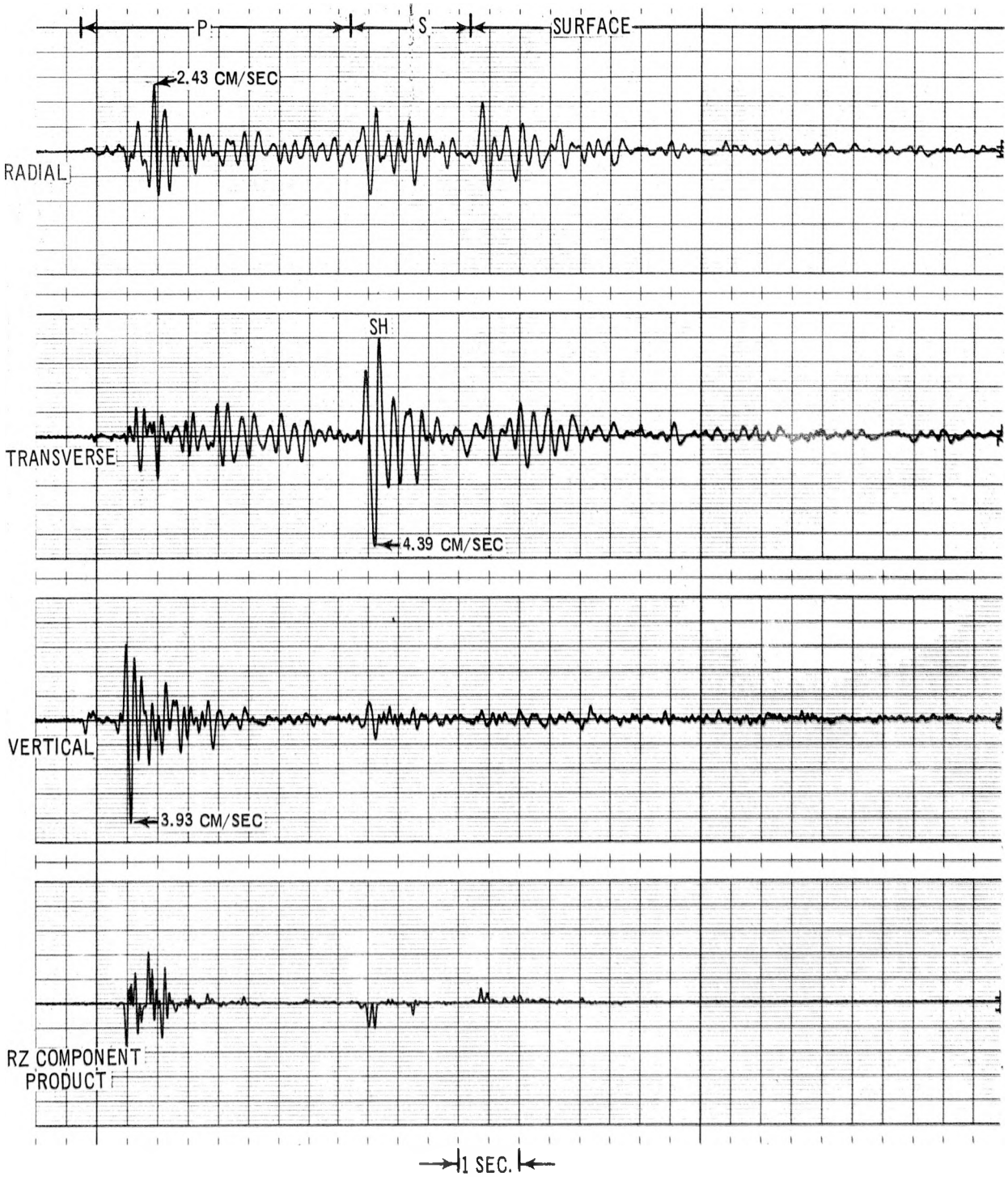

DE BEQUE SCHOOL NO. 2
Δ = 22.8 KM
RULISON EVENT

FIRST ARRIVAL TIME:
5.8 SEC

Figure 4-21. Particle Velocity Seismogram Observed at DeBeque School No. 2, Rulison Detonation

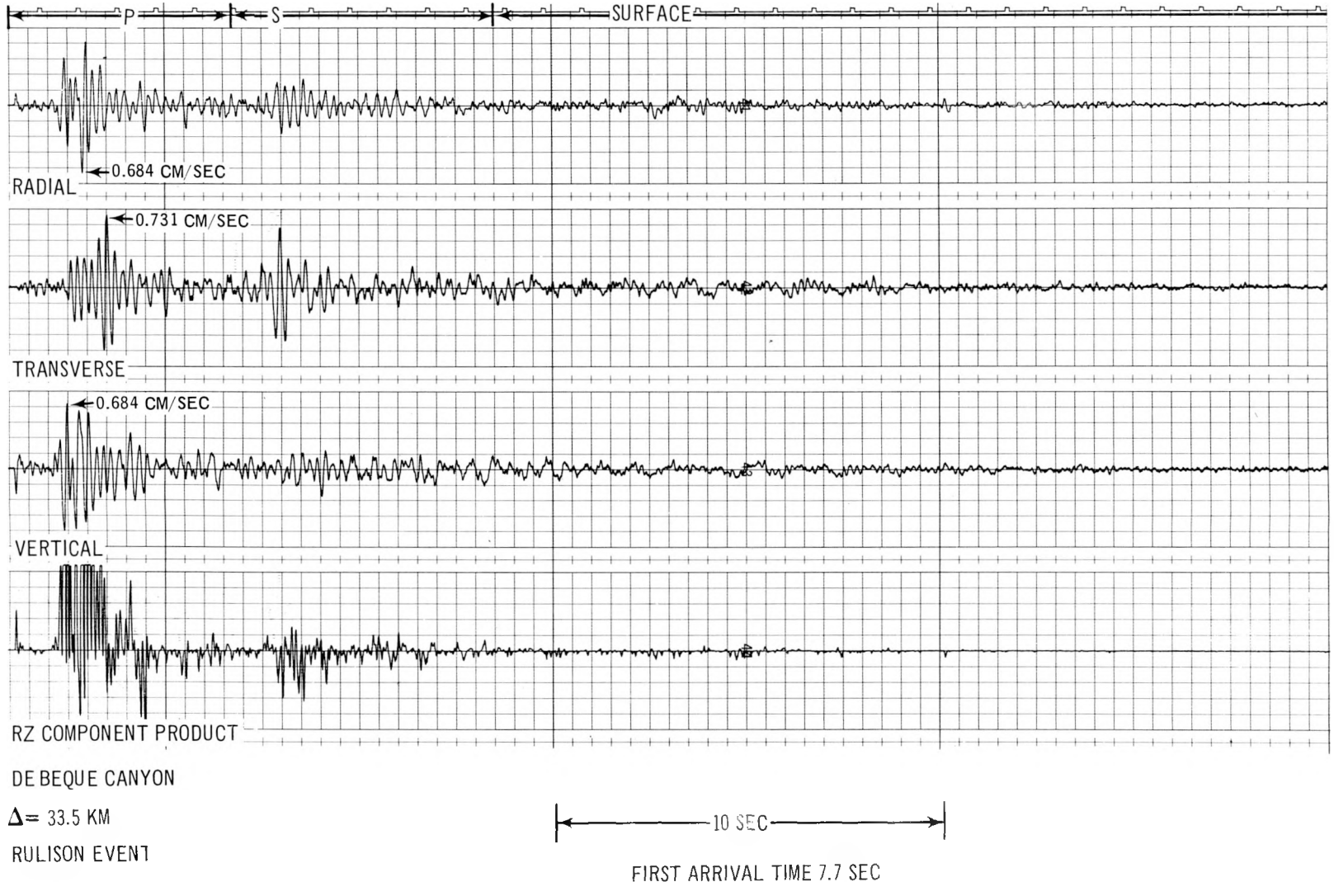

Figure 4-22. Particle Velocity Seismogram Observed at DeBeque Canyon, Rulison Detonation

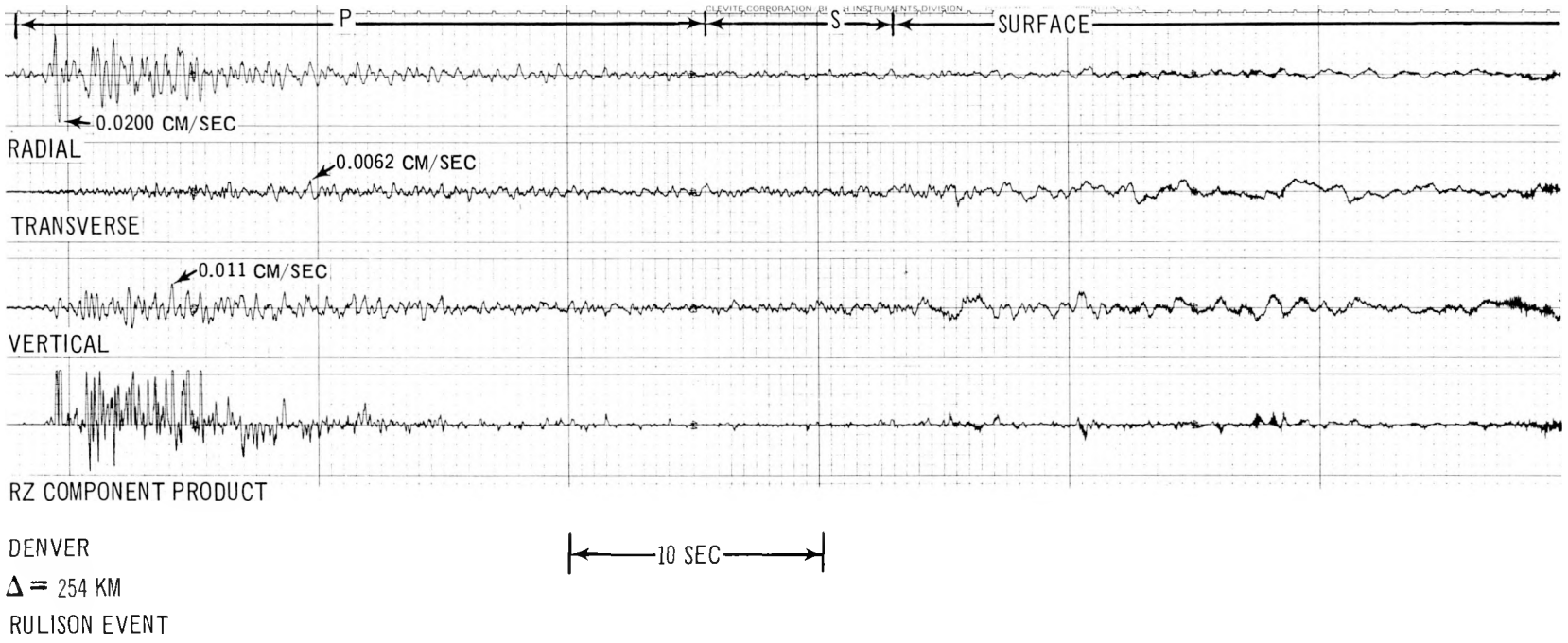

Figure 4-23. Particle Velocity Seismogram Observed at Denver, Colorado, Rulison Detonation

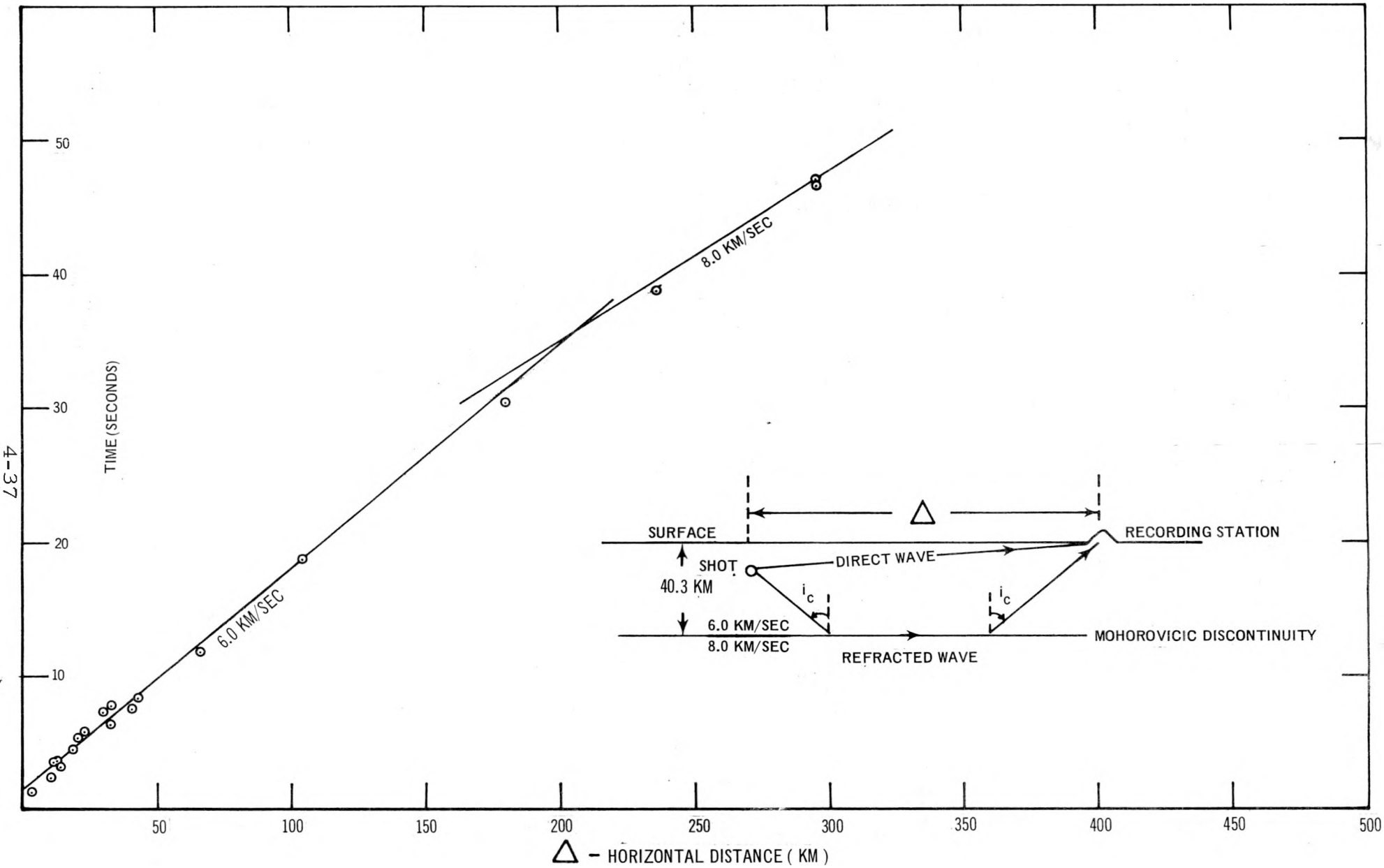

Figure 4-24. First Arrival Time as a Function of Station Distance, Rulison Detonation

can be approximated by two straight line segments. The first line, for distances less than 200 km (the critical distance), indicates a propagation velocity for P_g, the direct P wave, of approximately 6.0 km/sec. The second line, defined by only 3 data points beyond 200 km, indicates a propagation velocity of approximately 8.0 km/sec for P_n, the P wave critically refracted from the Mohorovicic discontinuity. These values of propagation velocity, although based on a very limited number of observations, are not inconsistent with the results of other investigators such as Stuart, et al. (1964) and Herrin (1969). These data lead to a crustal model with a thickness of about 40 km, a value which is slightly less than expected on the basis of data reported by Herrin (1969) (see Figure 4-25). A more definitive crustal model may have been possible if the time-distance curve for P_n were defined by more than 3 observations and reverse profiles were available to determine the structural attitude of the Mohorovicic discontinuity (an absolute requirement to establish the best value for P_n).

On the basis of travel time data and the radial-vertical component product waveforms, the time history of a typical seismogram can be divided into three time windows:

1. A P wave window (beginning with the first arrival and extending to the first S wave arrival).

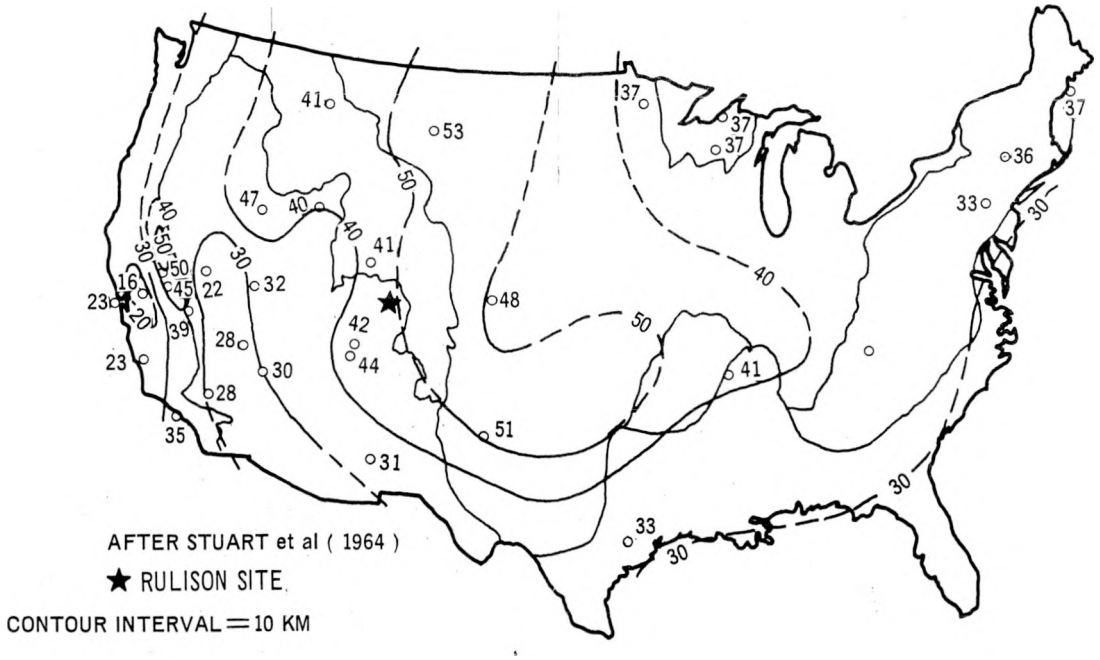

CONTOUR MAP OF CRUSTAL THICKNESS IN THE UNITED STATES

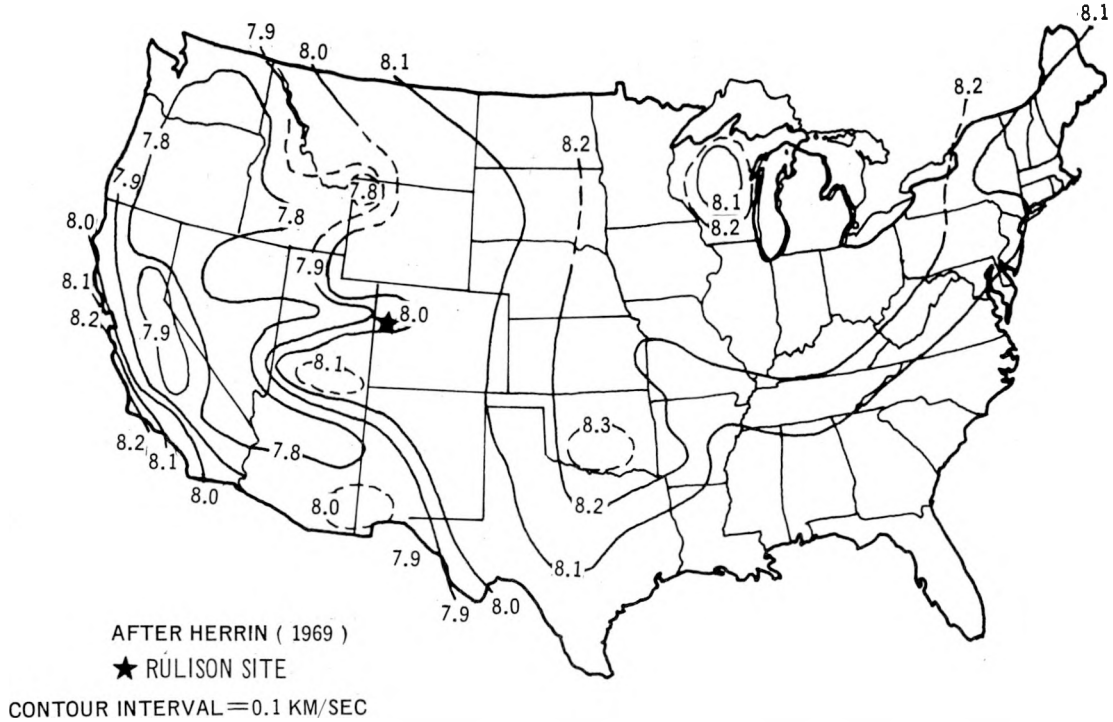

CONTOUR MAP OF ESTIMATED P_n VELOCITY IN THE UNITED STATES

Figure 4-25. Contour Maps of the Thickness of Crust and Propagation Velocity of P_n in the United States

2. An S wave window (beginning at the first S wave arrival; i.e., at a time about 1.7 times the first arrival time, and extending to the onset of the surface wave train).

3. A surface wave window (beginning with the onset of the long period surface wave and extending to the end of the significant motion on the seismogram).

These wave mode time windows are necessarily generalized and vary in length and complexity according to factors such as: (1) the distance of the station from the source, (2) the geologic layering at the recording site, and (3) the many complex geological and geophysical parameters of the earth's crust which impress their signature upon the propagating waves. The P wave, for example, contains the direct wave, the wave critically refracted from the Mohorovicic (M) discontinuity and the reflection from the M discontinuity in an order which depends upon the source-to-station distance relative to the depth of the M discontinuity.

The particle velocity seismograms measured from Rulison and the corresponding derived acceleration and displacement seismograms were analyzed to determine the correlation of the peak vector ground motion and the component of ground motion with the elastic wave type time window. Table 4-1 lists the results of this analysis and illustrates the following general facts:

TABLE 4-1.

CORRELATION OF PEAK GROUND MOTION PARAMETER
WITH WAVE MODE TIME WINDOWS,
RULISON EVENT

RECORDING STATION	SITE GEOLOGY	SLANT DISTANCE	FIRST ARRIVAL TIME	WAVE MODE WINDOW WHERE THE PEAK VECTOR PARTICLE MOTION OCCURS			WAVE MODE WINDOW AND COMPONENT WHERE THE PEAK PARTICLE MOTION OCCURS		
				ACCELERATION	VELOCITY	DISPLACEMENT	ACCELERATION	VELOCITY	DISPLACEMENT
Battlement Mesa	HR	4.9	1.2	(?)surface*	(?)surface*	(?)surface*	P(Z)	P(Z)	S(R)
Eames Orchard	HR	6.2	-	P	P	P	P(Z)	P(Z)	P(Z)
Lemon Ranch	HR	6.4	-	P	P	P	P(Z)	P(Z)	P(Z)
Rulison	HR	8.7	-	P	P	surface	P(Z)	P(Z)	surface (R)
Grand Valley	HR	10.6	2.3	P	surface	**	P(Z)	surface (R)	**
Richardson Ranch	HR	12.7	3.8	P	S	**	P(T)	S(T)	**
Anvil Points	HR	13.3	3.8	P	S	P	P(Z)	P(Z)	P(Z)
Mobil Mine	HR	14.6	3.2	P	P	surface	P(Z)	P(Z)	surface (Z)
Union Carbide	HR	18.0	4.5	NR	NR	NR	NR	NR	NR
Rifle (church)	HR	20.2	5.3	P	P	P	P(Z)	P(Z)	P(Z)
Rifle (top of hill)	HR	20.2	5.4	P	P	P	P(Z)	P(Z)	P(Z)
Debeque (school #1)	HR	22.8	5.8	P	P	S	P(Z)	P(Z)	S(T)
Debeque (school #2)	HR	22.8	5.8	P	S	S	P(Z)	S(T)	S(T)
Silt	HR	29.8	7.2	**	**	**	**	S(R)	**
Harvey Gap Dam	HR	32.4	6.2	P	P	P	P(Z)	P(Z)	P(Z)
Debeque Canyon	HR	33.5	7.7	P	P	P	P(R)	P(T)	P(Z)
New Castle	HR	40.4	7.3	P	P	P	P(R)	P(R)	P(R)
Cameo	HR	42.8	8.3	P	P	P	P(R)	P(R)	P(R)
Cedaredge	HR	55.4	-	P	S	-	S(T)	S(R)	-
Glenwood Springs	HR	56.2	-	P	P	P	P(R)	P(Z)	P(R)
Grand Junction Motel	HR	65.4	11.9	P	surface	surface	P(Z)	surface	surface
Paonia	HR	66.8	-	S	surface	surface	surface (R)	surface (R)	surface (R)
Meeker	HR	70.4	-	surface	surface	surface	surface (R)	surface (R)	surface (T)
Delta	HR	75.2	-	P	P	P	P(R)	P(R)	P(R)
Eagle	HR	100	-	S	P	surface	P(R)	P(T)	surface (Z)
Aspen	HR	100	-	P	P	S(?)	P(T)	P(T)	P(T)
Rangely	Alluv.	104	18.7	surface	surface	surface	surface (T)	surface (T)	surface (R)
Rangely	HR	104	18.7	P	surface	surface	P(Z)	surface (R)	surface (Z)
Craig	HR	127	-	S	S	surface	S(R)	S(T)	surface (R)
Silverton	HR	179	30.3	P	P	P	P(Z)	P(Z)	P(Z)
Durango	HR	236	38.7	P	P	P	P(Z)	P(R)	P(R)
Denver	Alluv.	254	-	P	P	surface	P(R)	P(R)	surface (T)
Rawlins	Alluv.	273	-	P	P	P	P(Z)	P(Z)	P(Z)
Farmington	Alluv.	296	46.6	P	P	P	P(Z)	P(Z)	P(Z)
Farmington	HR	296	46.8	P	P	P	P(Z)	P(Z)	P(Z)
Salt Lake City	Alluv.	367	-	surface	surface	surface	surface (Z)	surface (Z)	surface (Z)

NR = Noisy record, data are unreliable

** = Trace clipped, or not recorded

* = Spike on record but waveform not obscured

- = Arrival time not recorded due to poor or missing time signal

1. The peak vector particle accelerations correlate almost exclusively with the P wave time windows over the entire distance range.

2. The peak vector particle velocities correlate principally with the body wave (P and S) time windows. Exceptions close-in include Grand Junction where the peak vector particle velocity occurs in the surface wave time window.

3. The peak vector particle displacements correlate mainly with the body wave time windows, particularly at close-in distances. Exceptions close-in include Mobil Mine and Rulison, where the peak displacement occurs in the surface wave window. The peak vector displacements tend to correlate with the surface wave at distant stations such as Denver (254 km) and Salt Lake City (367 km), a normal phenomenon.

4. The vertical components exhibit the largest velocities at all stations inside 10 km and the largest accelerations at all stations, except Richardson Ranch, inside 32.4 km.

Figure 4-26 shows the relationship between the regression line representing the mean peak vector particle velocity corresponding to each of the three wave mode time windows, observed at various sites. The data shown in this figure illustrate that the peak vector particle velocities are caused mainly by P and S waves. The surface wave causes the peak vector velocity at only a few sites.

Table 4-2 lists the correlation of the peak vector ground motion and the wave mode time windows for the Gasbuggy detonation. The results are generally comparable with those listed above for the Rulison detonation. The peak particle velocity

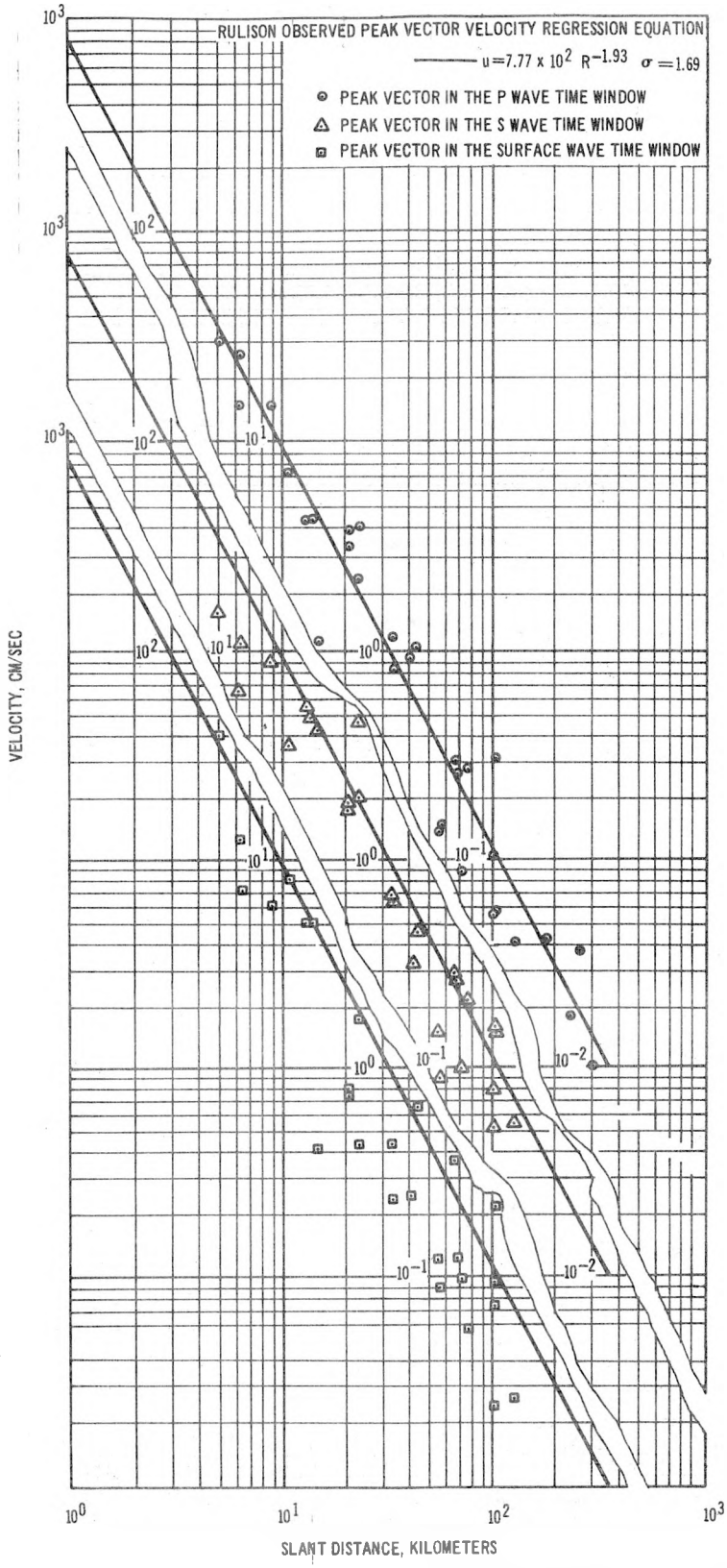

Figure 4-26. Comparison of Peak Vector Velocity in P, S, and Surface Wave Time Windows with the Regression Line Derived from the Peak Vector Particle Velocity, Rulison Event, Piceance Creek Basin Sites

TABLE 4-2.

CORRELATION OF PEAK GROUND MOTION PARAMETER
WITH WAVE MODE TIME WINDOWS,
GASBUGGY EVENT

RECORDING STATION	SITE GEOLOGY	SLANT DISTANCE	FIRST ARRIVAL TIME	WAVE MODE WINDOW WHERE THE PEAK VECTOR PARTICLE MOTION OCCURS			WAVE MODE WINDOW AND COMPONENT WHERE THE PEAK PARTICLE MOTION OCCURS		
				ACCELERATION	VELOCITY	DISPLACEMENT	ACCELERATION	VELOCITY	DISPLACEMENT
Gaswell #6	HR	1.5		P	**	**	**	**	**
Gaswell #16	HR	1.8	-	P	**	**	**	**	**
Gaswell #7	HR	1.8	-	P	**	**	**	**	**
GB #6	HR	4.3	-	P	**	P	P(R)	**	P(Z)
GB #7	HR	7.8	-	P	**	**	P(Z)	**	S(?)(R)
GB #5	HR	10.0	-	P	**	P	P(R)	**	P(R)
GB #8	HR	11.6	-	P	**	P	P(Z)	**	P(R)
LaJara Lake Ranch	HR	20.9	-	P	**	P	P(R)	**	P(T)
Lowry Camp	HR	30.3	7.0	P	P	surface	P(Z)	P(Z)	surface(Z)
Dulce	HR	34.1	-	P	P	P	P(R)	P(Z)	P(R)
Dulce School	HR	35.4	6.9	P	P	P	P(E/W)	P(E/W)	surface(Z)
Dulce	HR	35.6	-	P	P	surface	P(R)	P(R)	P(N/S)
Navajo City	HR	35.9	7.4	P	P	P	P(Z)	P(R)	P(Z)
Lumberton	HR	40.6	-	P	P	P	P(R)	P(R)	P(R)
Lindrith	HR	44.0	8.7	P	P	S	P(Z)	P(Z)	S(T)
Blanco	Alluv.	55.2	10.4	P	P	P	P(R)	P(R)	P(R)?
Blanco	HR	55.2	10.4	P	P	P	P(T)	P(Z)	P(Z)
Lybrook	HR	59.0	11.1	P	P	surface	P(Z)	P(Z)	surface(Z)?
Tierra Amarilla	Alluv.	60.0	10.7	P	**	surface	P(Z)	**	surface(R)
Huerfano T.P.	Alluv.	65.5	11.8	P	P	surface	P(Z)	P(Z)	surface(Z)
EPNG Pump Station	HR	67.5	12.7	P	P	P	P(R)	P	P(Z)
Pagosa Springs	HR	68.2	12.5	S	P	surface	surface(T)	P(Z)	surface(Z)
Bloomfield	Alluv.	68.6	12.8	P	P	P	S(R)	P(R)	P(R)
Bayfield	Alluv.	70.3	12.8	P	P	surface	P(R)	P(R)	surface(R)
Aztec	Alluv.	71.8	13.9	**	**	**	S(R)	S(R)	surface(Z)
Aztec	HR	72.8	13.9	P	P	P	P(R)	P(R)	P(R)
Cuba	Alluv.	76.3	13.9	P	P	P	P(Z)	P(R)	P(R)
Farmington	HR	88.4	15.9	P	P	P	P(Z)	P(Z)	P(Z)
Farmington	Alluv.	88.4	15.9	P	P	surface	P(Z)	P(Z)	surface(Z)
Farmington	Alluv.	89.7	15.9	P	P	surface	P(Z)	P(Z)	surface (Z)
Durango	HR	90.0	16.0	P	surface	surface	P(Z)	P(Z)	surface (Z)
Durango	Alluv.	90.0	15.9	surface	surface	surface	surface(T)	surface(T)	surface (Z)

** = Trace clipped, or not recorded

- = Arrival time not recorded due to poor or missing time signal

correlates primarily with the body waves; however, the seismograms show that the surface waves tend to exhibit somewhat larger relative peak vector particle velocities at several recording stations throughout the 90 km distance range.

The fact that the peak vector particle velocities observed from the Gasbuggy and Rulison detonations correlate primarily with the body wave time windows differs from the relationship observed from nuclear excavation detonations. Both Schooner and Cabriolet generate velocity time histories, recorded over a distance range of 340 km, which almost exclusively exhibit the peak vector velocity in the surface wave time window (Hays, et al., 1969).

This general correspondence of the peak vector particle velocities with the relatively high frequency body wave time windows for overburied detonations and with the relatively low frequency surface wave time window for underburied (cratering) detonations agrees qualitatively with scaling theory (Mueller, 1969a). An event of a fixed yield detonated at a shallower than normal depth of burial has a lower seismic energy efficiency. The level of motion is reduced and the dominant seismic energy occurs at lower frequencies. The same detonation at a greater than normal depth of burial causes the dominant seismic energy to occur at high frequencies, enhancing the level of peak acceleration and velocity. The combination of the depth of burial and the spectral composition of the

dominant energy relates, at least qualitatively, to the mechanism for generation of surface waves. The surface waves decay with depth beneath the surface (Ewing, et al., 1957). This phenomenon may be thought of in terms of an excitation mechanism for surface waves; the deeper the depth of burial, the relatively weaker excitation of surface waves, and conversely. This relationship appears to be generally verified by the relationship of the elastic waves generated by Cabriolet, Schooner, Gasbuggy, and Rulison, cratering and overburied detonations, respectively. Also, it is a well-known fact (Richter, 1957) that in some cases, deep focus earthquakes generate no surface waves. However, the fundamental mechanisms for earthquakes and nuclear explosions are different.

4.2.1 Shear (SH) Waves

Significant SH shear energy (i.e., shear motion polarized in the horizontal plane) was observed at several recording sites, generally in a NE-SW direction from Rulison ground zero (see Table 4-3). This phenomenon is not expected for the case of a compressive source acting in an infinite, homogeneous, isotropic, and perfectly elastic medium (Grant and West, 1965). However, this phenomenon has been observed before, both from underground high explosive and nuclear detonations (Press, et al., 1962; Kisslinger, et al., 1961; and others), and is a subject presently under investigation at NTS.

TABLE 4-3

RULISON SITES WHICH RECORDED SIGNIFICANT SH GROUND MOTION

Station	Distance (km)	Azimuth
Rulison	8.7	N6°47'E
Grand Valley	10.6	N59°43'W
Anvil Points	13.3	N10°53'E
Mobil Mine	14.6	N1°49'W
Rifle	20.2	N45°38'E
Debeque	22.8	S71°05'W
Harvey Gap Dam	32.4	N48°34'E
Cedaredge	55.4	S2°07'E
Glenwood Springs	56.2	N73°15'E
Grand Junction	65.8	S54°50'W
Delta	75.2	S7°45'W

Several mechanisms have been proposed to explain the generation of SH energy by an underground nuclear detonation. These include:

1. Asymmetry of the explosion; i.e., the explosion is not a radially symmetric simple expansion about a point (Leet, 1946).

2. Rotation of the surface of the equivalent cavity or the elastic radius (Kisslinger, et al., 1961).

3. Faulting with a horizontal component of slip (McKeown and Dickey, 1969).

4. Cracking or propagating faulting with displacement normal to the fault surface (Knopoff, et al., 1960; Kisslinger, et al., 1961).

5. Wave propagation in pre-stressed media (Kim and Kisslinger, 1967); Thompson, et al., 1969; Beaudet, 1970).

Certainly, any one or a combination of these mechanisms could be responsible for the significant SH energy observed from the Rulison event. Although no specific explanation to account for the occurrence of this energy is available at this time, short-induced movement along a general NE-SW and NW-SE fracture pattern found on aerial photographs of the area may be the primary source of the shear energy observed at some sites.

Estimates of the crustal thickness can be made based on the combined use of the characteristics of the amplitude and phase spectra (Ibrahim, 1969). Phinney (1964), Fernandez (1967), and Ibrahim (1969) have shown that a change in the thickness of the crust has a noticeable effect on the spacing of the minima of the amplitude spectra. A change in the velocity will hardly effect the position of the minima, but will change the value of the amplitude spectra.

Unfortunately, significant SH energy was not observed at the relatively few recording sites located beyond 200 km, the critical distance; therefore, the technique cannot be adequately applied to determine crustal thickness using Rulison generated seismic data. A limited study made using the Fourier amplitude spectra of the shear wave window

observed on the transverse component at the Rawlins (273 km) and Farmington (296 km) stations did not yield conclusive results.

4.2.2 Characteristics of the First Arrival (P Wave)

The peak particle velocity of the first 1-1/2 cycles of the first arrival observed at sites both inside and beyond 200 km was determined for each component of motion and for the resultant vector (see Figure 4-27). Over the distance range 0-200 km, the first arrival (called the direct arrival), P_g, is a P wave which travels primarily within the upper crustal layers. Beyond 200 km, the first arrival represents the refraction from the Mohorovicic discontinuity, P_n. The first arrival represents the radiating portion of the seismogram and is considered to be relatively sensitive to variations in the physical properties of the source environment (Springer, 1966) and to geologic variations along the transmission path and at the recording site. The data shown in Figure 4-27 verify this sensitivity. The data exhibit a fair amount of scatter about the regression line representing the average decay of amplitude with distance. For P_g, the decay rate is $R^{-1.9\pm0.5}$. Because of the limited data related to P_n, the decay rate cannot be determined.

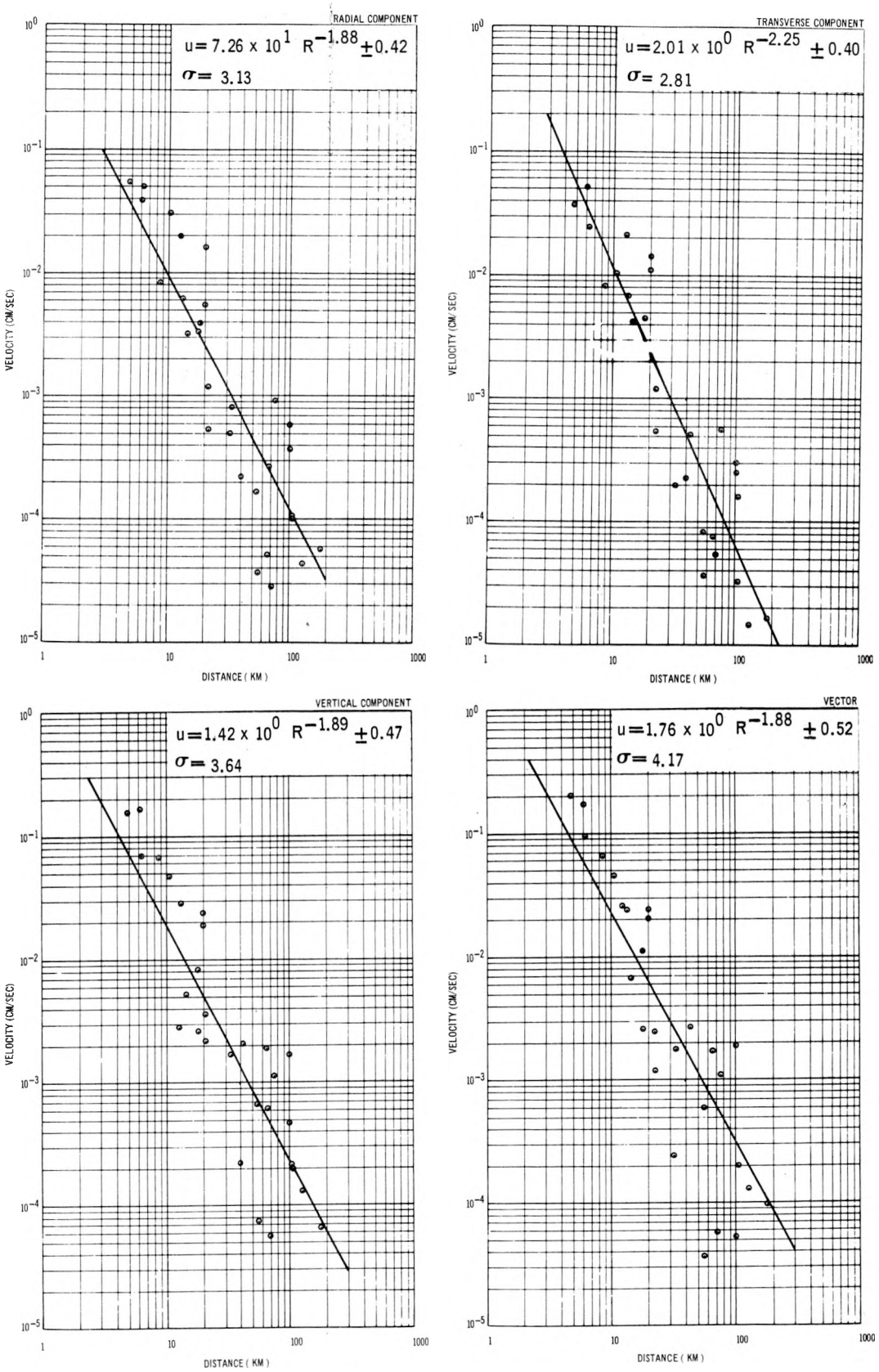

Figure 4-27. Variation of the Peak Particle Velocity of P_g with Distance, Rulison Detonation

These results for P_g may be compared to corresponding data obtained from analysis of seismograms from NTS detonations (Hays, 1969). On the basis of NTS experience, P_g and P_n decay approximately as $R^{-1.8\pm0.4}$ and $R^{-3.0\pm0.7}$, respectively. The more rapid decay rate for P_n is expected on the basis of its travel path (Heelan, 1953).

Figure 4-28 illustrates the smoothed Fourier amplitude spectra of the P wave time windows observed at a number of recording sites located over the distance range 5-300 km. As noted earlier, the composition of the P wave time window varies from site to site. In the most general sense, the amplitude spectrum of a seismic signal observed at a recording site can be written as the product of a source spectrum and a number of transfer functions representing the effects of processes that the signal has undergone. Thus,

$$B(f,R) = S(f)\cdot T_1(f)\cdot T_2(f,R)\cdot G(R)\cdot X(f,R)\cdot A(f,R) \quad (4\text{-}1)$$

where $B(f,R)$ is the spectral amplitude at frequency f and range R, $S(f)$ is the source spectrum, $T_1(f)$ is the crustal transfer function at the source, $T_2(f,R)$ is the crustal transfer function at the receiver, $G(R)$ is the geometric spreading, $X(f,R)$ is the reflection coefficient, and $A(f,R)$

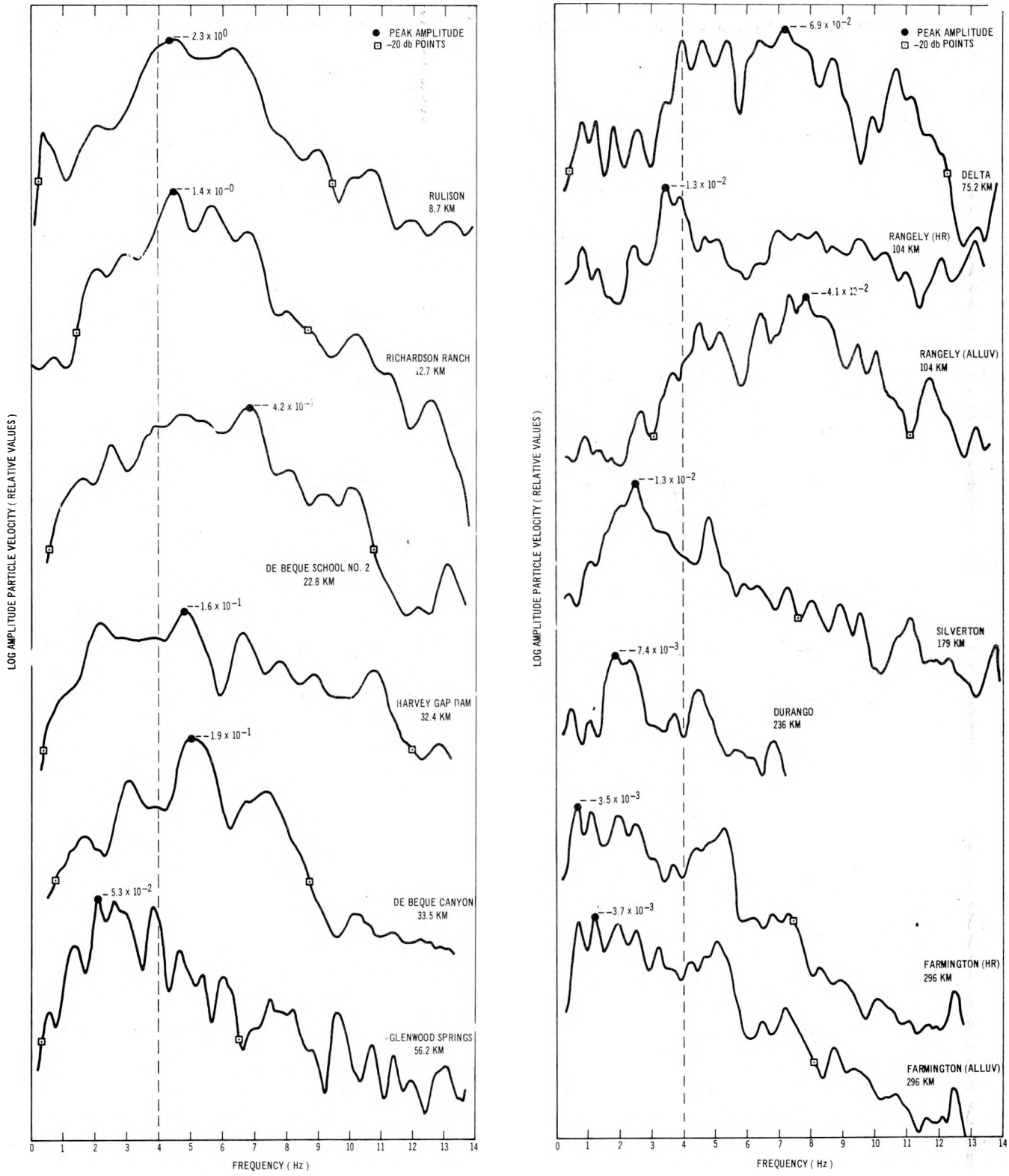

Figure 4-28. Smoothed Fourier Amplitude Spectra of the P Wave Time Window Observed at Various Recording Sites, Rulison Detonation

is the attenuation due to anelasticity, scattering, etc. It is virtually impossible to evaluate more than a few of the terms in Equation (4-1) (for example, attenuation will be evaluated in Section 4.2.3) due to the complex physical processes involved and the lack of specific data. However, it is sufficient to note that the amplitude spectrum represents the output of a complex physical system.

The Fourier amplitude spectra for the P wave window shown in Figure 4-28 illustrate the following:

1. The composition of the amplitude spectra varies somewhat with distance, reflecting the complex interaction of various systems along the total propagation path.

2. The maximum spectral response occurs at frequencies in the range of 2-7 Hz.

3. The spectra observed at close-in stations tend to have a greater high frequency composition than those for the distant stations, illustrating the well known low-pass filter action of the earth.

With respect to NTS experience for a typical 40 kt detonation, the Rulison detonation generated a higher level of high frequency P wave ground motion. On the basis of NTS experience, the dominant P wave energy for a typical 40 kt detonation observed over corresponding distance ranges would occur around 1-2 Hz. As noted earlier, the higher relative level of high frequency energy for Rulison ground motions can be explained in terms of scaling theory (Mueller, 1969a).

4.2.3 Attenuation of Seismic Waves in the Earth's Crust

Information about the dissipative nature of the earth's crust can be obtained by studying the attenuation of propagating seismic waves, using either body or surface waves. If there is no effect of attenuation due to geometrical spreading, scattering, or diffraction, etc., amplitudes of propagating elastic waves should diminish exponentially with distance (Knopoff, 1964 and 1969) as

$$e^{-\alpha R} \tag{4-2}$$

where $\alpha = \frac{\omega}{2CQ}$ is the distance attenuation factor, C is the wave velocity, R is the distance of propagation, ω is the angular frequency, and Q is the specific dissipation function. The attenuating effect of a transmission path upon a propagating seismic wave can be determined by evaluating an expression of the form

$$S(\omega,R) = S_o(\omega) \cdot T(\omega,R) \tag{4-3}$$

where $S(\omega,R)$ is the Fourier transform of the recorded signal, $S_o(\omega)$ is the Fourier transform of the source term, and $T(\omega,R)$ is the transfer function for the transmission path. The characteristics of the transmission path can be described (Press, 1964) with the expression

$$T(\omega,R) = R^{-n} \exp \frac{-\omega R}{2CQ} \tag{4-4}$$

Evaluation of Q independent of the properties of the source is accomplished by considering the spectra of signals recorded at a pair of stations from the same source. Thus,

$$\frac{S(\omega,R_1)}{S(\omega,R_2)} = \left(\frac{R_2}{R_1}\right)^n \exp\left[-\frac{\omega(R_1-R_2)}{2CQ}\right] \qquad (4\text{-}5)$$

Hence, Q can be expressed as

$$Q = \frac{\pi(R_2-R_1)}{c\cdot\frac{\partial}{\partial f}\left\{\ln\left[\frac{S(\omega,R_1)}{S(\omega,R_2)}\right]\right\}} \qquad (4\text{-}6)$$

Results of experiments upon a large number of solid materials, metals, non-metals, granular rocks, glasses, and single crystals, in the laboratory and upon relatively homogeneous formations at shallow depths in the field indicate that the parameter Q is essentially independent of frequency or wavelength over a wide range of frequencies (White, 1965). Values of Q for the crust obtained by various investigators include:

1. Values for Q of 169±42 and 116±38 determined from data recorded from the Gnome and Shoal events using compressional wave data in the 100-600 km range, i.e., P_g and P_n waves (Long and Berg, 1969).

2. An average Q of 260±40 determined for the crust, using the P_g phase recorded from the Clearwater, Shoal, Aardvark, Cimarron, Stillwater, and Ardmore events (Press, 1964) at NTS.

3. An average Q of 450±30 determined for the crust, based on the L_g phase from the Clearwater, Shoal, Aardvark, Cimarron, Stillwater, and Ardmore events (Press, 1964) at NTS.

4. A value of about 375 for Q, based on observations and a study of P_n (Werth, et al., 1962).

Values of Q have been calculated for the BPF line, an instrument array located slightly north of Nevada Test Site along one of the simplest geologic travel paths from Nevada Test Site. Figure 4-29 shows the radial component of particle velocity observed for each of the six recording sites for the Boxcar event. The smoothed Fourier amplitude spectra of the corresponding P wave windows are shown in Figure 4-30. The values of Q determined for the line vary somewhat due to the complex physical processes involved, and yield an average Q of 135. The largest value of Q determined along the line is 212. These values seem reasonable considering the relatively short travel paths involved.

Values of Q were determined for the crust at the Rulison site, using selected P wave amplitude spectra from Figure 4-28. This analysis yields a Q of about 190.

Figure 4-31 illustrates graphically the relationship between amplitude, Q, and frequency for three fixed distances. It is concluded that the relationship depicted for Q = 200 is representative of the crustal attenuation in the Piceance Creek Basin.

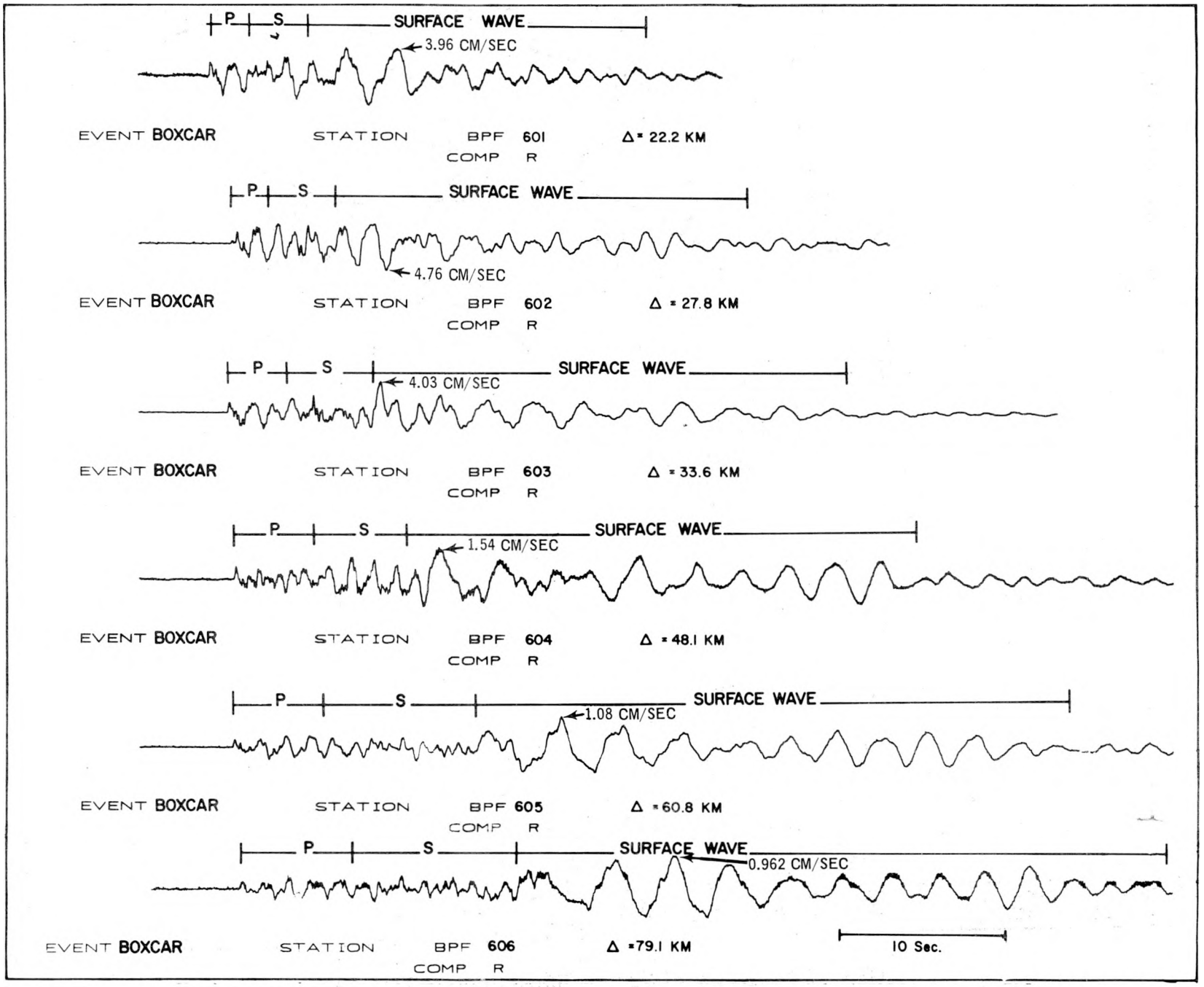

Figure 4-29. Radial Component of Particle Velocity Observed at Stations on the BPF Line, Boxcar Detonation

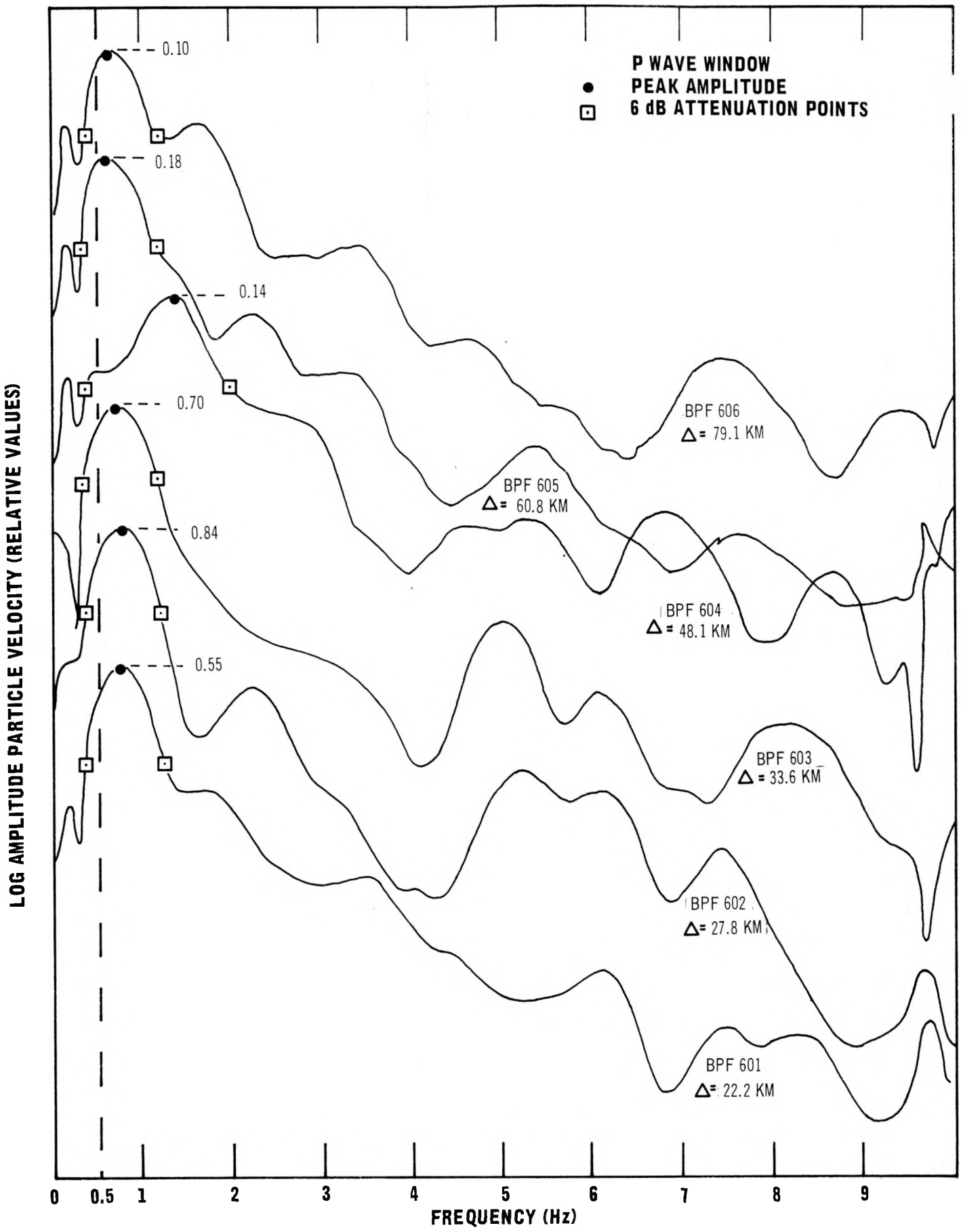

Figure 4-30. Smoothed Fourier Amplitude Spectra Corresponding to the P Wave Time Window Observed at Stations on the BPF Line, Boxcar Detonation

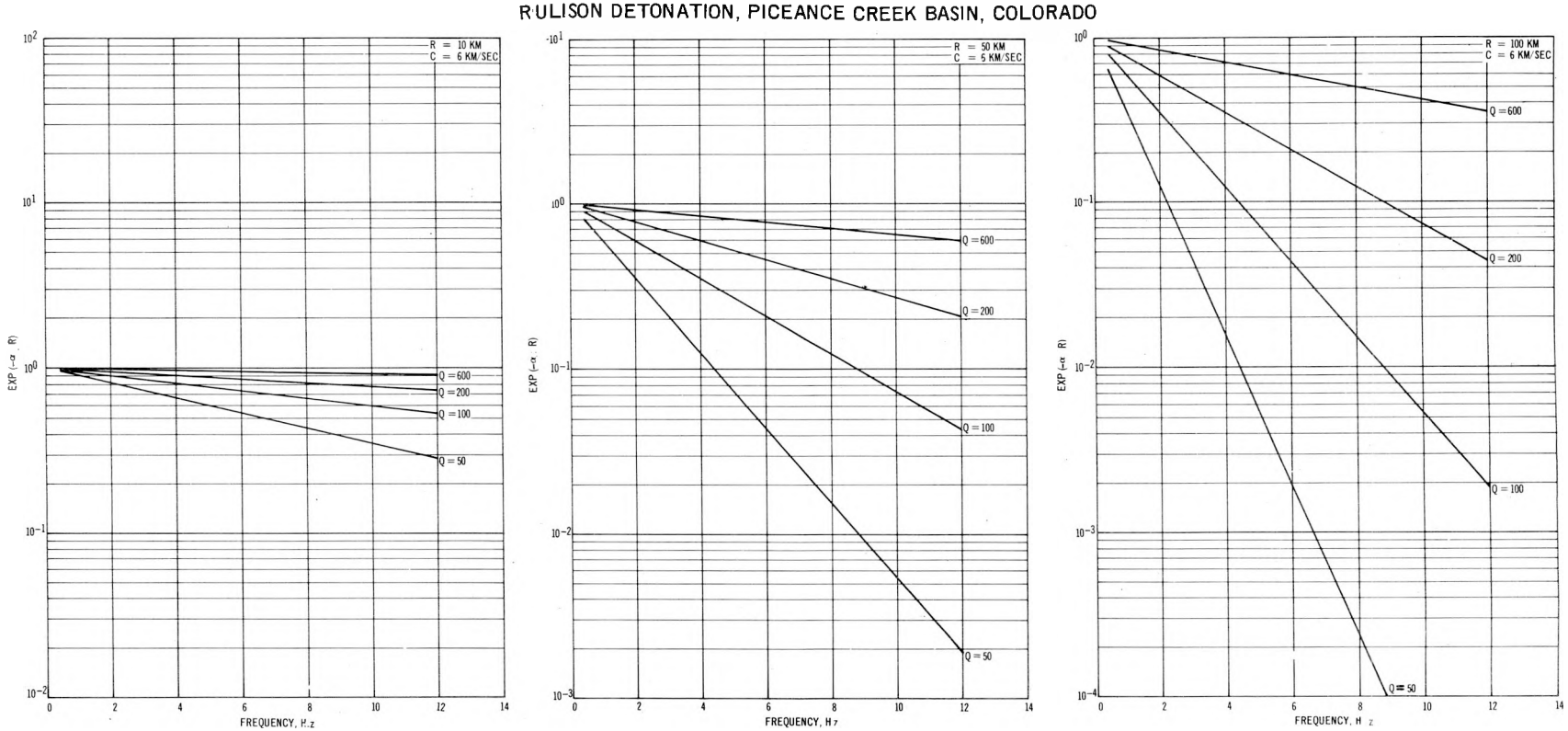

Figure 4-31. The Relationship between Amplitude, Q, and Frequency for Three Fixed Distances

4.3 FREQUENCY DEPENDENT AMPLIFICATION OF GROUND MOTION

Amplification of seismic motion at recording stations located on alluvium or a low velocity material has been noted since the early days of seismology. Haskell(1953), Hannon (1964), Schultz (1967), Davis and Murphy (1967), Murphy and Davis (1969) and a number of others since 1930 have shown that the shallow low-velocity layers of the earth's crust act as a filter with respect to the seismic energy arriving at a seismograph station and significantly affect the ground motion. Various investigators have shown that the transfer function of the near surface, low-velocity, layered system is a complex function which involves several variables:

1. The elastic wave type (P,SH,SV, Rayleigh, Love).
2. The angle of incidence of the incident wave.
3. The physical parameters (thickness, density, rigidity, compressional and shear wave velocities) of the layered sequence and the underlying rock.

Experience at predicting the ground motion from Nevada Test Site events has confirmed that the presence of thin layers of low-velocity material (usually alluvium) at the recording site can lead to significant local amplification. Perhaps the most dramatic example of this effect is for the

pair of recording stations located in Tonopah, Nevada. The two stations, located 600 feet apart, are sited, respectively, on andesite and a 39 foot layer of mine tailings overlying the andesite. Examination of the ratio of Fourier spectra derived from ground motion data recorded at these two stations indicates that the thin layer of tailings causes frequency dependent amplification which attains a maximum of a factor of 5 at 7 Hz, relative to the andesite layer (Figure 4-32).

Knowledge of the existence of thin intermittent alluvial layers at sites in the San Juan (Gasbuggy site) and Piceance Creek (Rulison site) basins caused concern about possible local amplification of the ground motion, perhaps leading to resonances coinciding with the natural period of structures. As little or no information on the thickness and physical properties of the shallow low-velocity layered system at sites of interest was available, refraction surveys were used to gain the desired information.

Refraction surveys were conducted at seven sites in the Piceance Creek Basin (Weetman, et al., 1969) and six sites in the San Juan Basin (Foote, et al., 1969). The sites were selected in terms of the relative sensitivity of structures to possible frequency dependent amplification of ground motion.

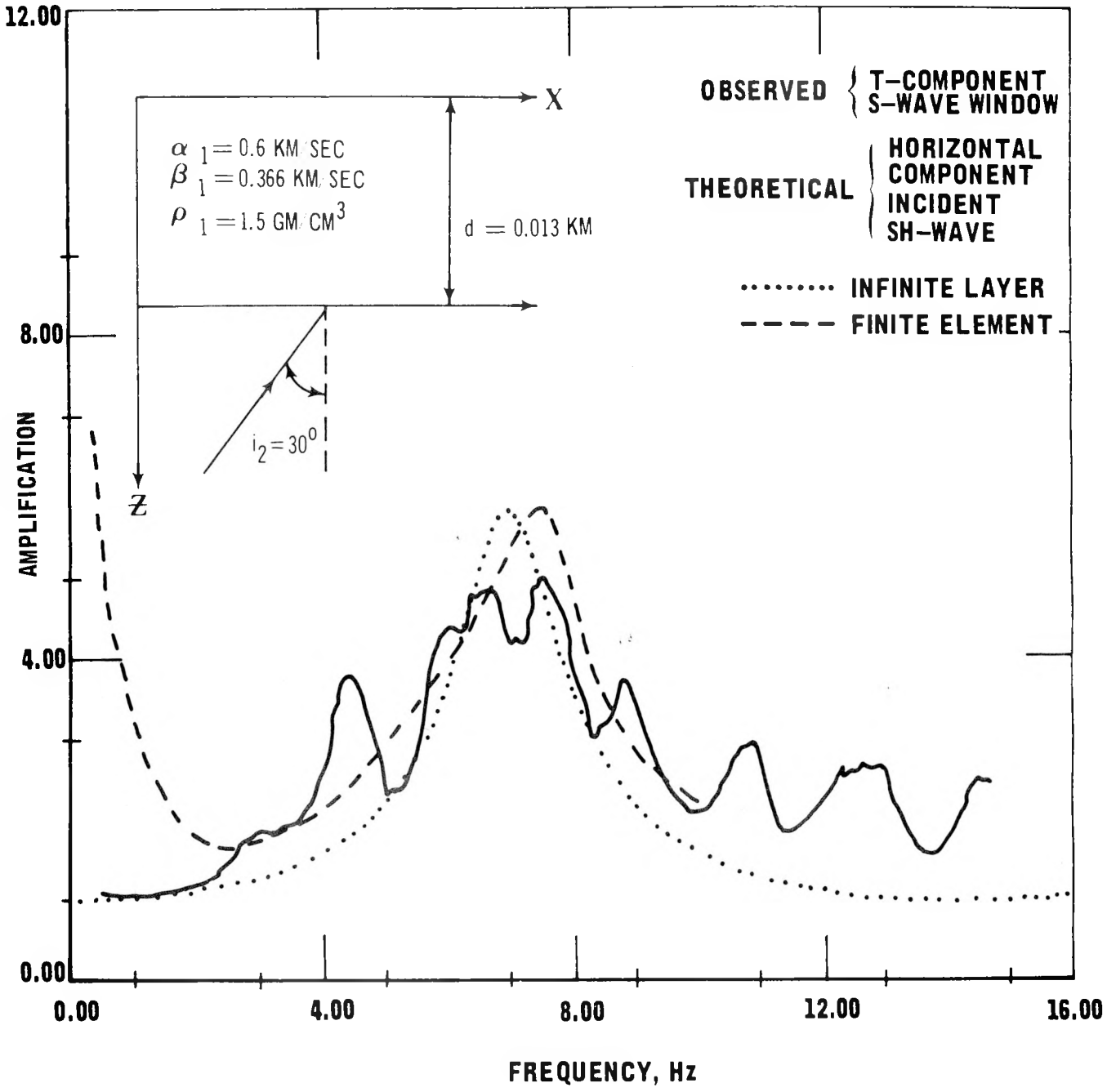

Figure 4-32. Frequency Dependent Amplification Observed at Tonopah, Nevada, from Underground Nuclear Detonations

Rulison sites selected were: Rifle, Rulison, Grand Valley, Holmes Mesa, Morrisania Mesa, the Union Carbide Plant at Rifle, and Harvey Gap Dam.

Figures 4-33 through 4-35 illustrate the interpretation of the refraction results obtained at the seven Rulison sites. The parameters (thickness, velocity) derived from the refractor survey data, were used as input parameters to compute the transfer function of the near surface layered system. Theoretical transfer functions (Figures 4-36 and 4-37) were computed for body waves, using a model based on the Haskel-Thompson matrix formulation (Haskell, 1953). Body wave models were used because of the relative thinness of the layers involved and the proximity of the stations to the source. The model assumes an input plane wave (a Dirac delta function) incident at some designated angle at the base of a sequence of plane parallel, perfectly elastic layers; this is clearly a simplification of the real physical processes.

These calculations indicated that significant local amplification in the 7 Hz range was to be expected at two locations, Harvey Gap Dam and Rifle. Consequently, the spectral predictions at these two locations were modified to account for this possibility. (see Weetman, et al., 1969, for details)

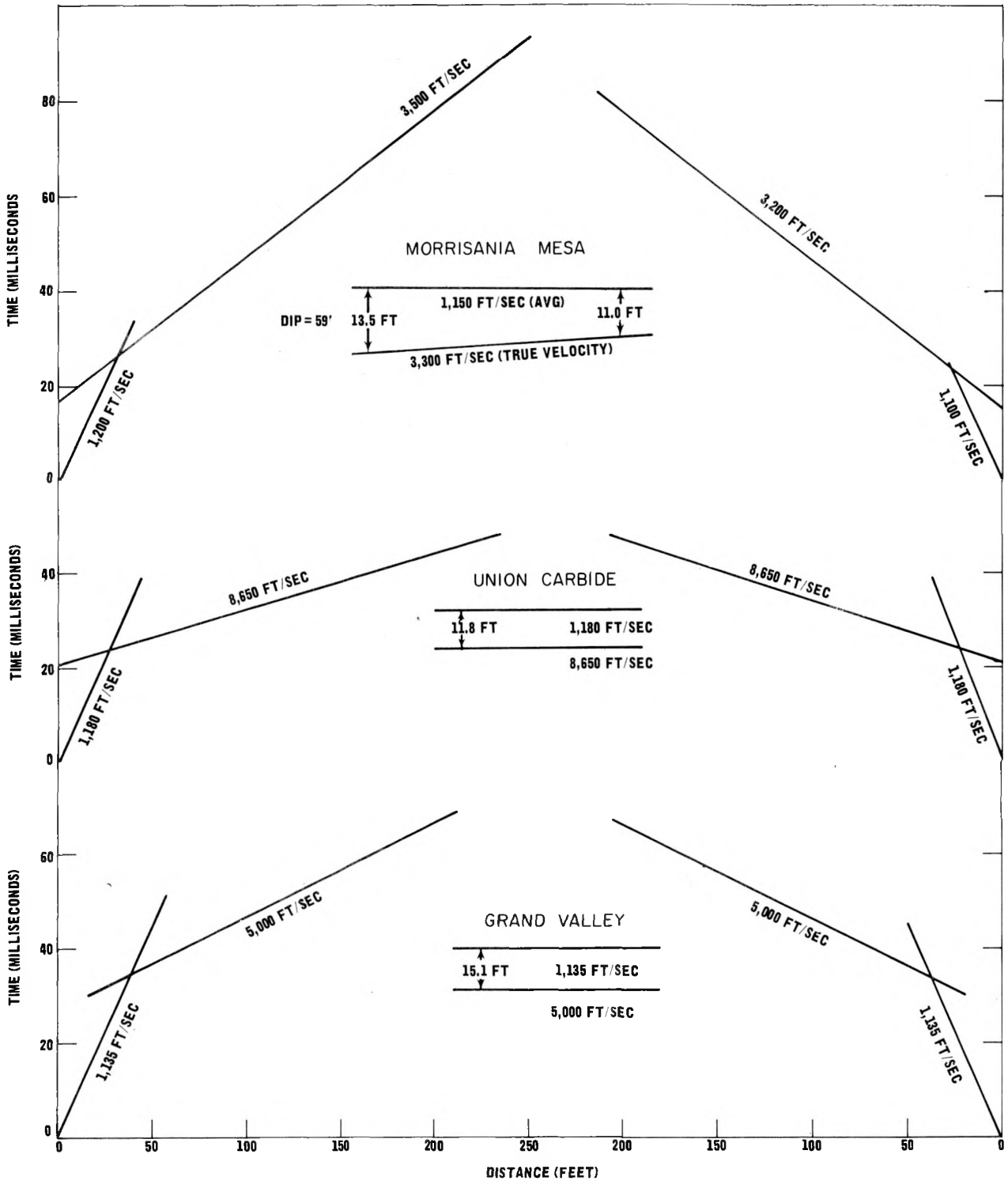

Figure 4-33. Interpretation of Refraction Surveys at Selected Rulison Sites

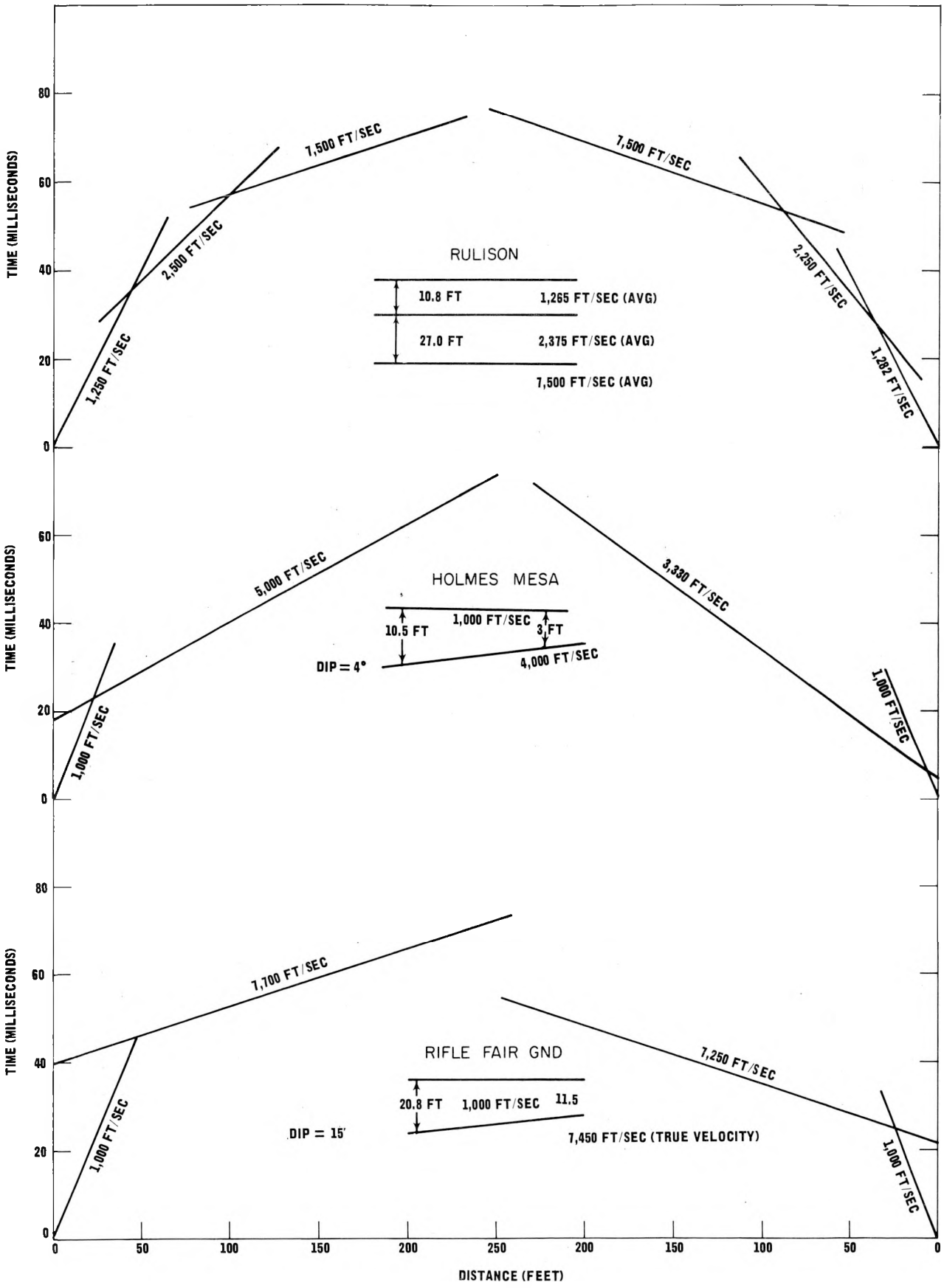

Figure 4-34. Interpretation of Refraction Surveys at Selected Rulison Sites

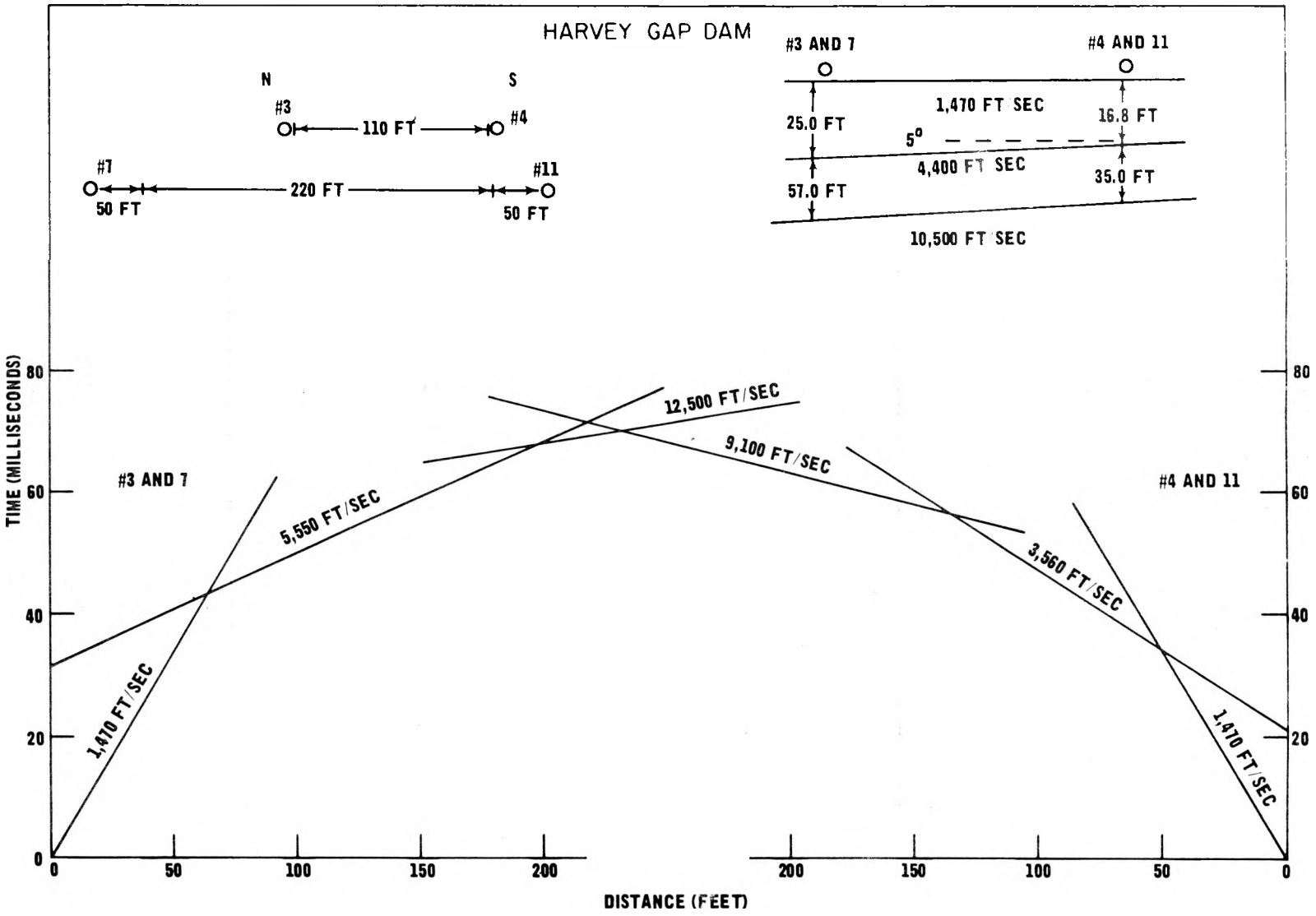

Figure 4-35. Interpretation of Refraction Survey at Selected Rulison Site

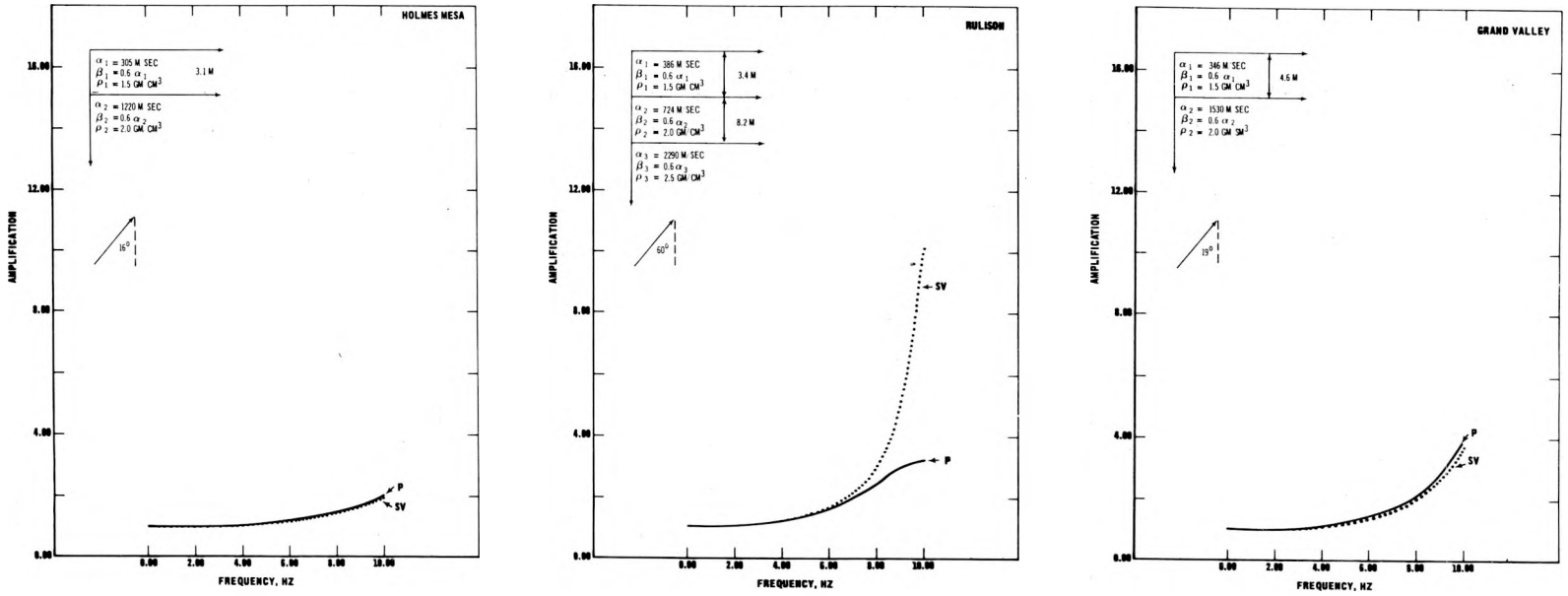

Figure 4-36. Theoretical Transfer Functions Calculated for Selected Rulison Sites

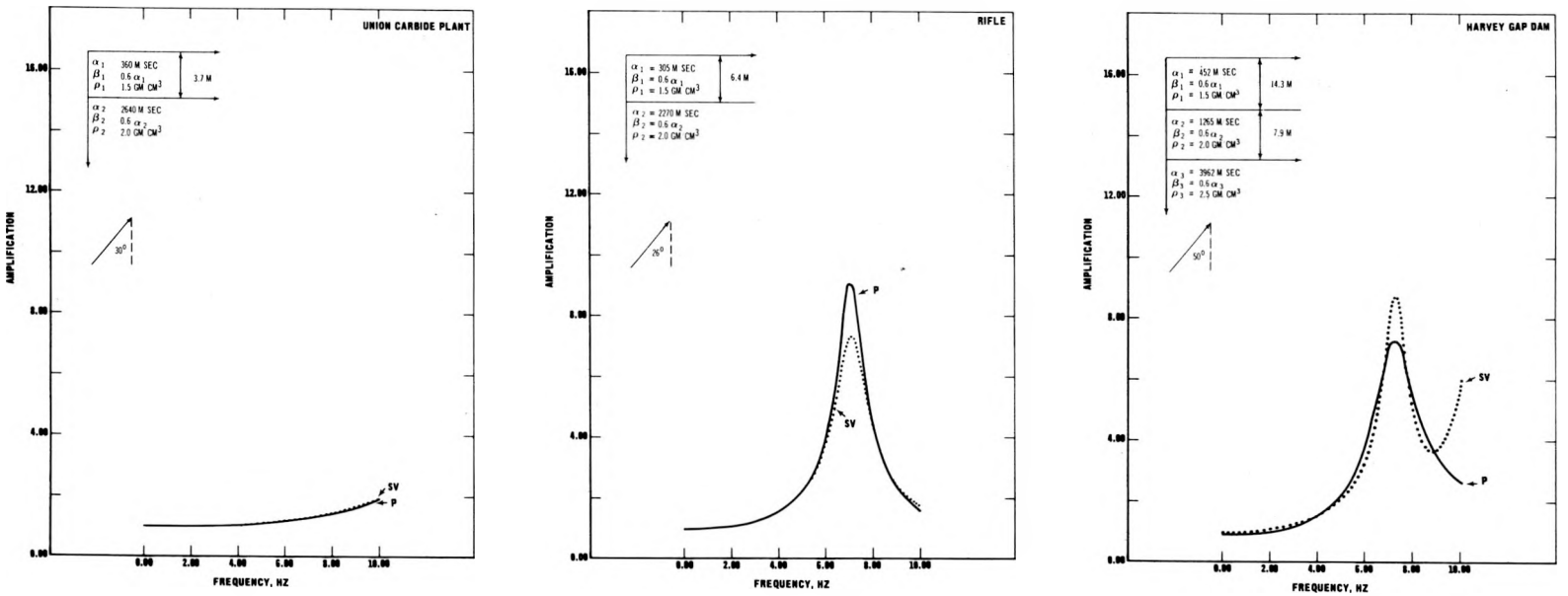

Figure 4-37. Theoretical Transfer Functions Calculated for Selected Rulison Sites

Figures 4-38 and 4-39 illustrate the comparison of the PSRV spectra derived from the ground motion observed at Harvey Gap Dam and Rifle with the predicted spectra. The spectra which would have been predicted without accounting for the frequency dependent amplification are shown for reference. The data of these figures show that good agreement is obtained between the observed PSRV spectra and the spectral predictions. Amplification effects can be estimated well on the basis of amplification models, using data derived from refraction surveys as the input parameters.

Pairs of instruments were deployed at Rangely, Colorado, and Farmington, New Mexico, to record the ground motion from the Rulison detonation. Deployment of an instrument pair allows one to monitor the ground motion at two closely spaced sites, one site on hardrock and one site on the alluvial layer overlying the hardrock. Transfer functions of the layered system can then be computed by taking the ratio of the PSRV spectrum of the ground motion recorded at the alluvium site to the spectrum of the motion recorded at the hardrock site (Davis and Murphy, 1967). Figure 4-40 shows the amplification observed at these two sites, indicating that substantial amplification occurred at Rangely and little amplification occurred at Farmington. In the case of Farmington, the amplification expected on the basis of amplification

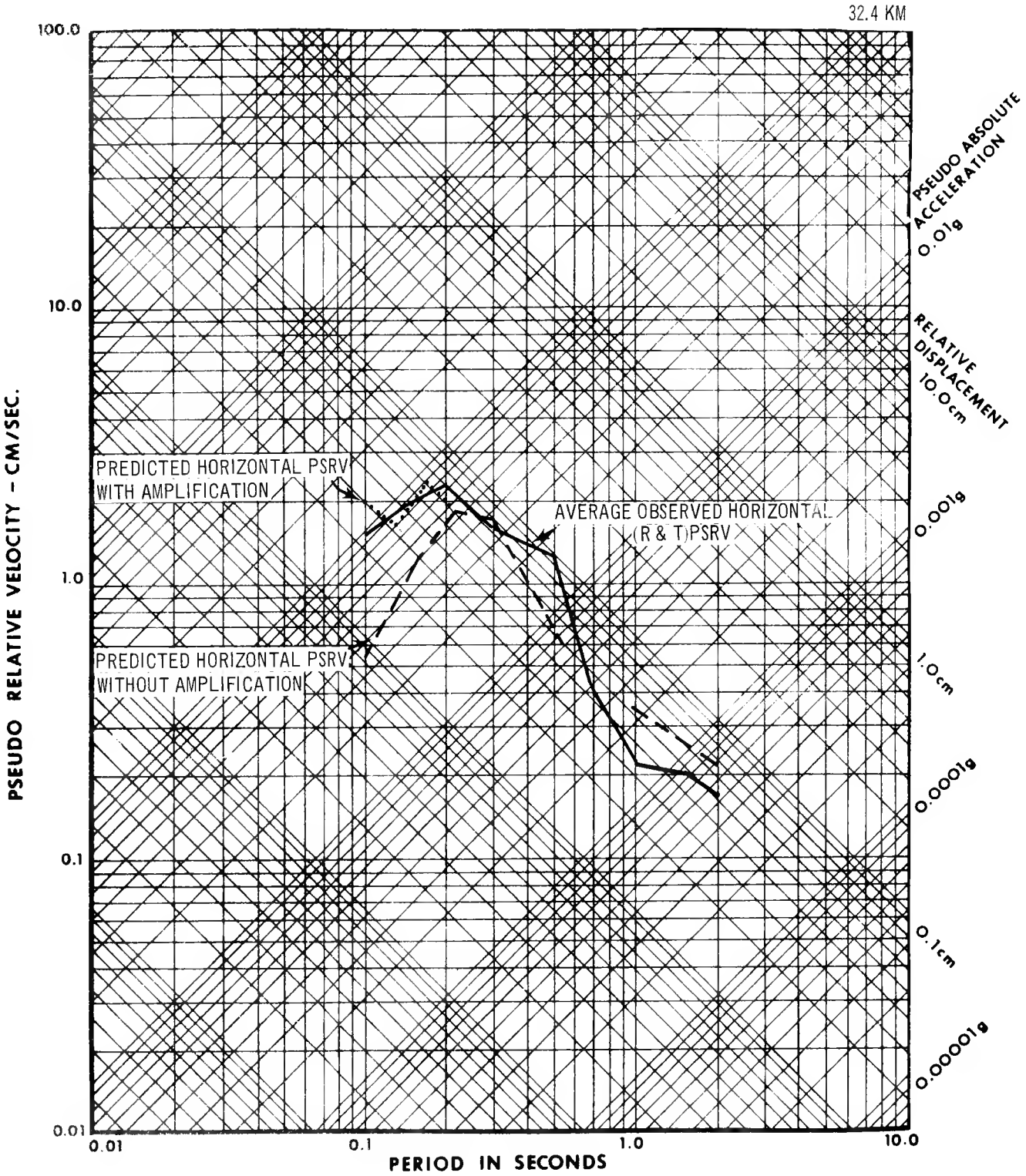

Figure 4-38. Comparison of the Observed and Predicted PSRV Spectra at Harvey Gap Dam (East End), Rulison Detonation

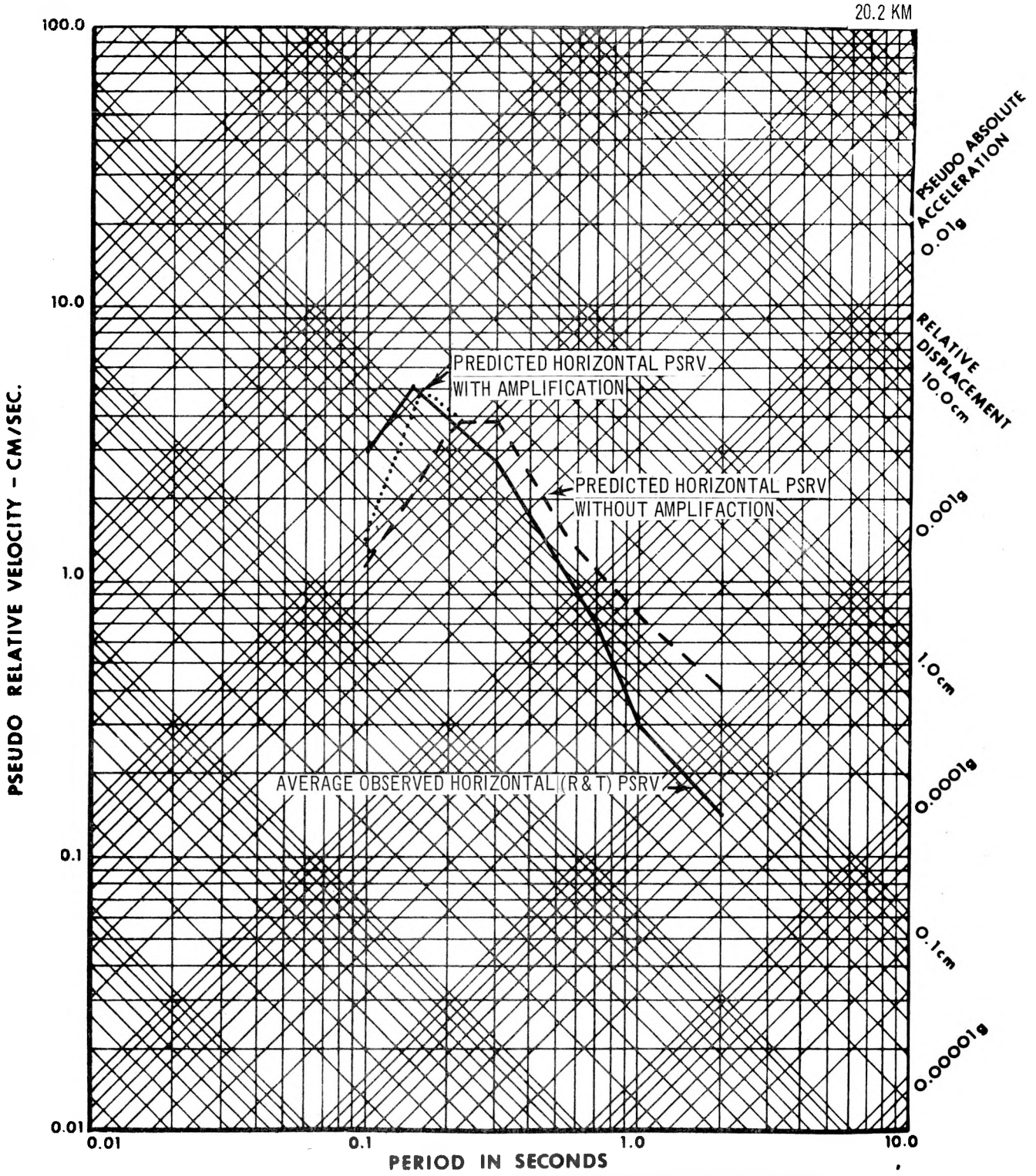

Figure 4-39. Comparison of the Observed and Predicted PSRV Spectra at Rifle (Church), Rulison Detonation

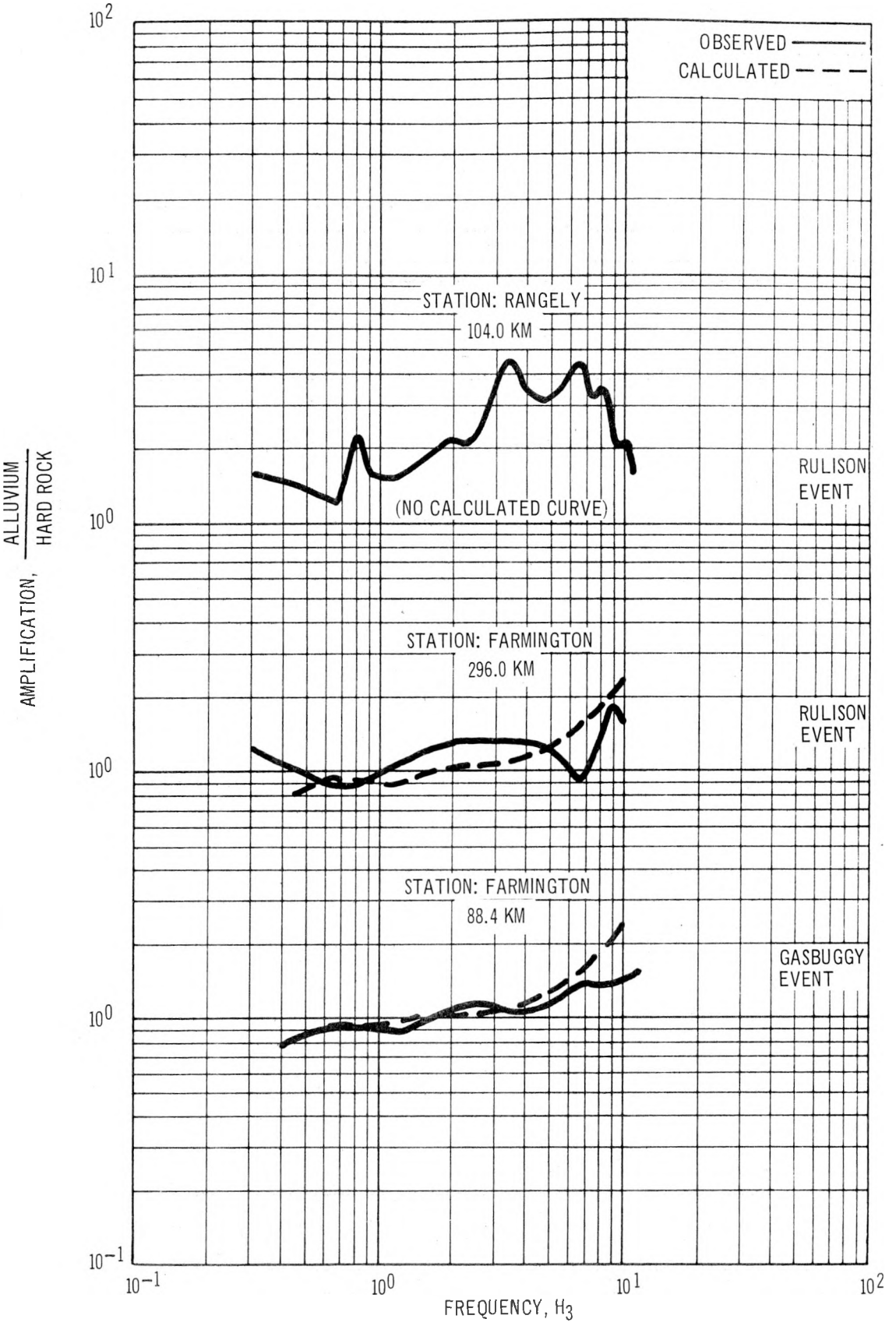

Figure 4-40. Frequency Dependent Amplification Observed at Rangely, Colorado, and Farmington, New Mexico

modeling, using refraction surveys to define the input parameters, is shown for comparison. Good agreement between theory and observation is obtained.

4.3.1 Analysis of the Ground Motions at Harvey Gap Dam

Analysis of the ground motions at Harvey Gap Dam, an earthen embankment located some 30 km from Rulison ground zero, was extremely important. The dam, constructed originally in the period 1906-1910, serves to create a reservoir to collect water. This water is the main irrigation supply during the dry season.

Due to the irregular geometry, and the overall two component nature of the embankment (see Figure 4-41), a finite element analysis is the only feasible approach to an analysis of the ground motions at the dam. The rocks exposed in the vicinity of the dam exhibit moderate dip changes over a short distance. The dam consists primarily of clayey materials (see report by John A. Blume and Associates, JAB-99-63, for details) sited on a sandstone-shale bedrock. The two global regions are identified in Figure 4-42.

The finite element technique (Zienkiewicz and Cheung, 1967) allows one to approximate the infinite degrees of

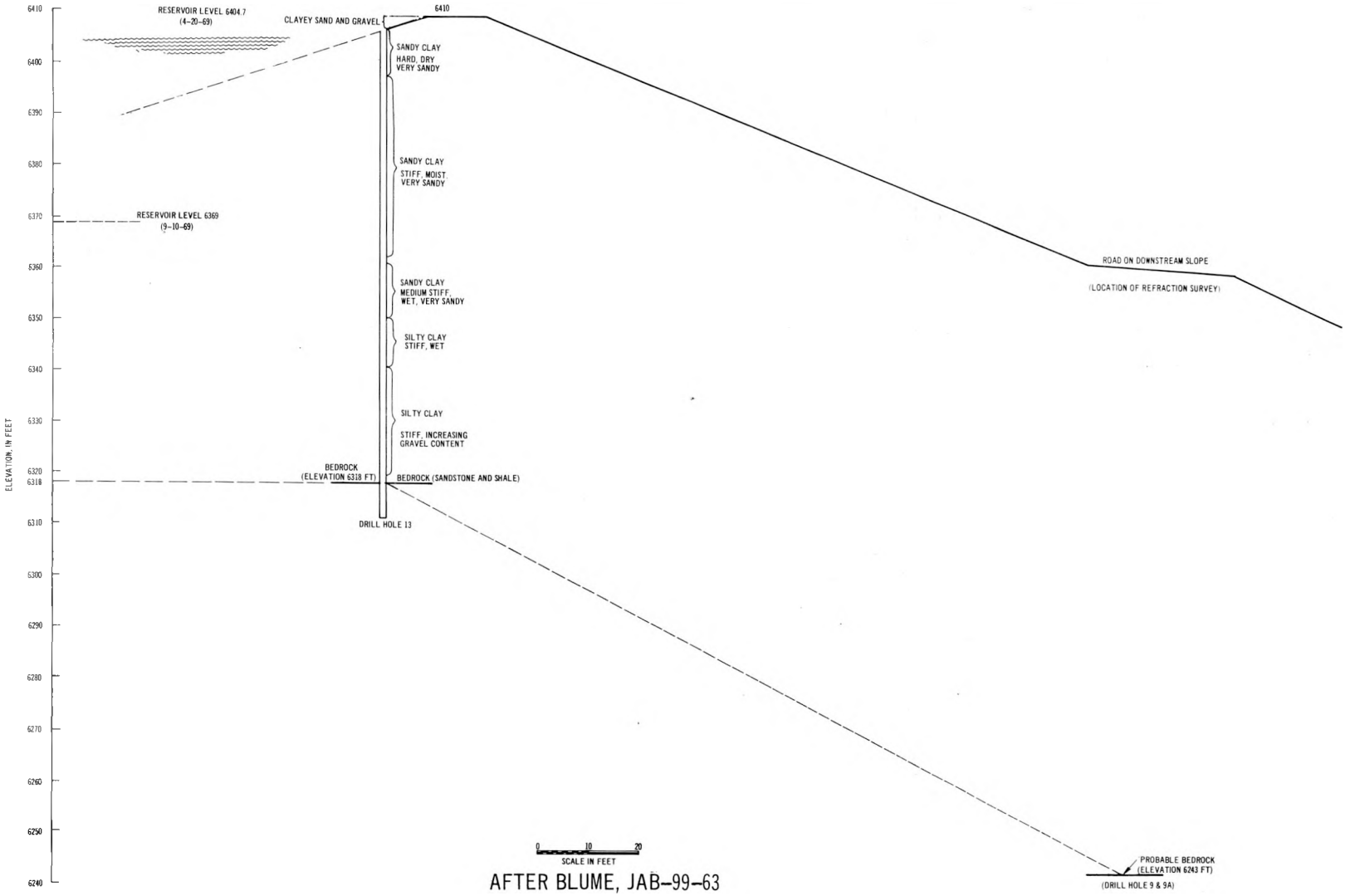

Figure 4-41. Cross-Sectional View of Harvey Gap Dam

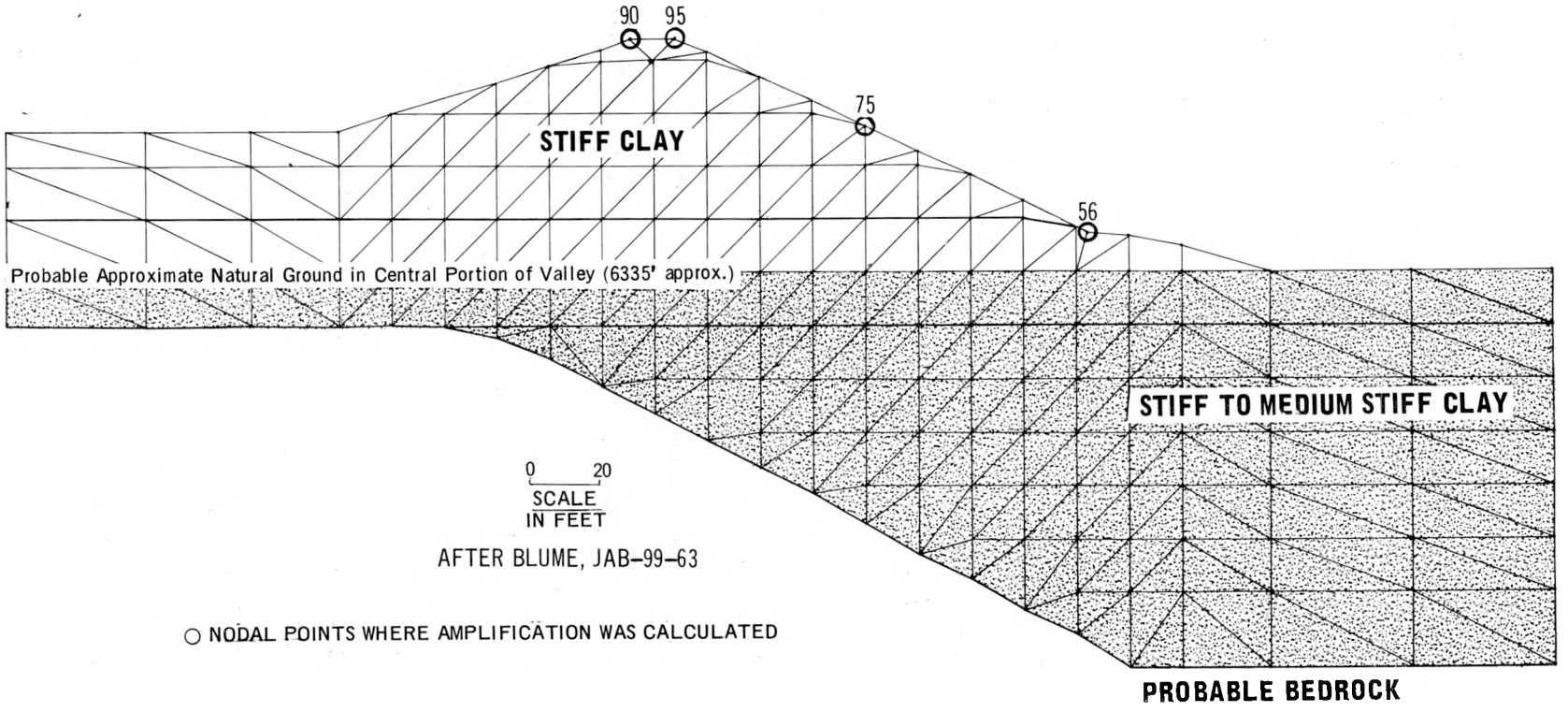

Figure 4-42. Finite Element Representation of Harvey Gap Dam

freedom of a continuum in terms of the degrees of freedom at a finite number of nodal points. The basic computational procedure consists in partitioning the structure into a discrete set of finite elements of certain basic geometrical shapes (e.g. triangles, quadrilaterals, etc.). Due to its computational simplicity, the most widely used element is the three-node triangle. Thus, any arbitrary continuum (or structure) with varying properties can be meaningfully approximated by assigning to each finite element the average physical properties of the pertinent section in the actual structure.

Figure 4-42 exhibits a partitioning of Harvey Gap Dam into a finite element net assembled from basic triangles. The elemental properties assigned to each triangle are derived from (1) knowledge of the shallow-layered systems gained from the refraction surveys (see Figure 4-41), (2) information contained in JAB-99-63, and (3) engineering experience. Nodal points, at which amplification curves were obtained, are identified in the figure.

Figures 4-43 and 44 display the computed amplification at the nodes of interest for modal dampings of 5% and 17%; the fundamental vibration mode of the dam was calculated to be 3.35 Hz. A comparison between Figures 4-43 and 4-44 reveals

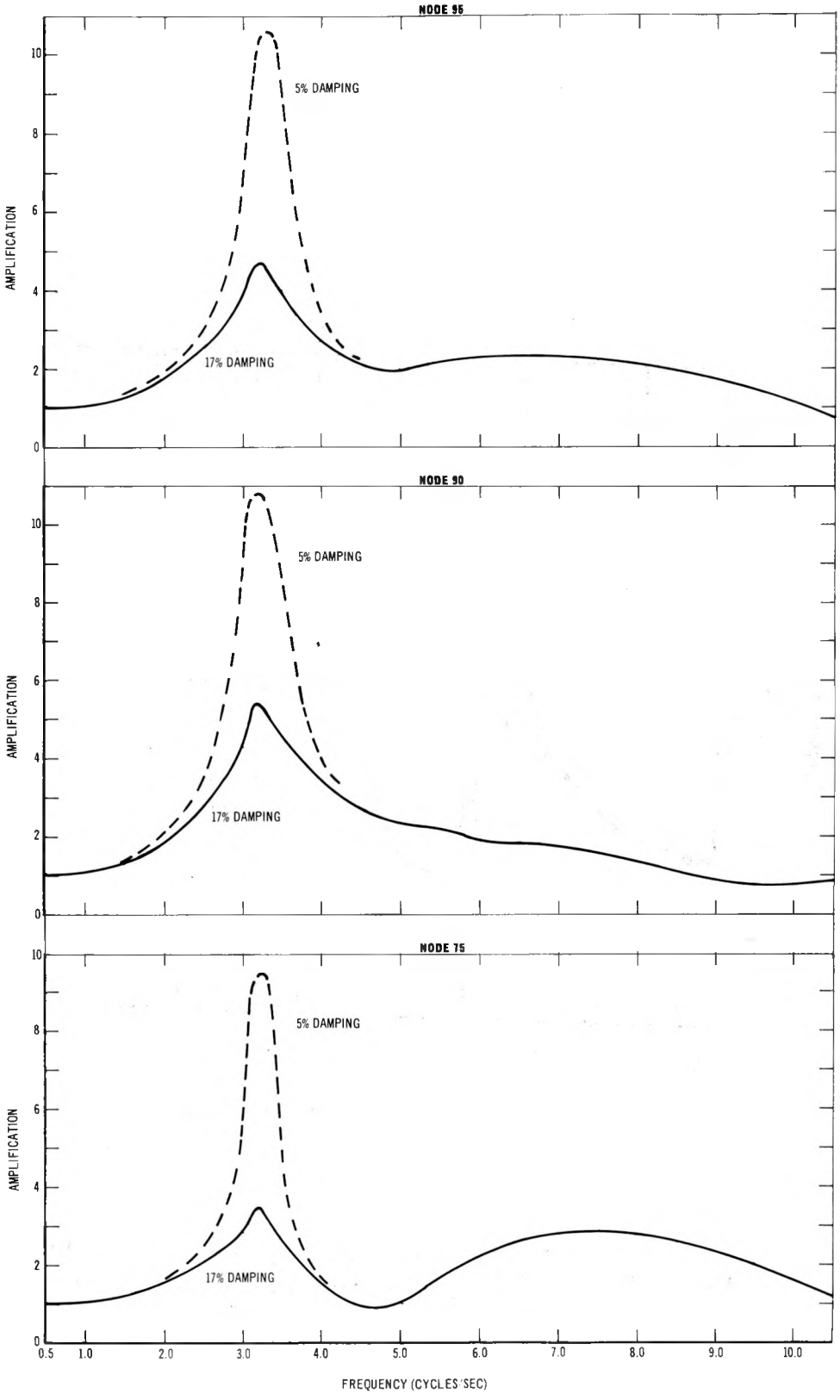

Figure 4-43. Amplification Versus Frequency Close to Crest of Harvey Gap Dam, Rulison Event

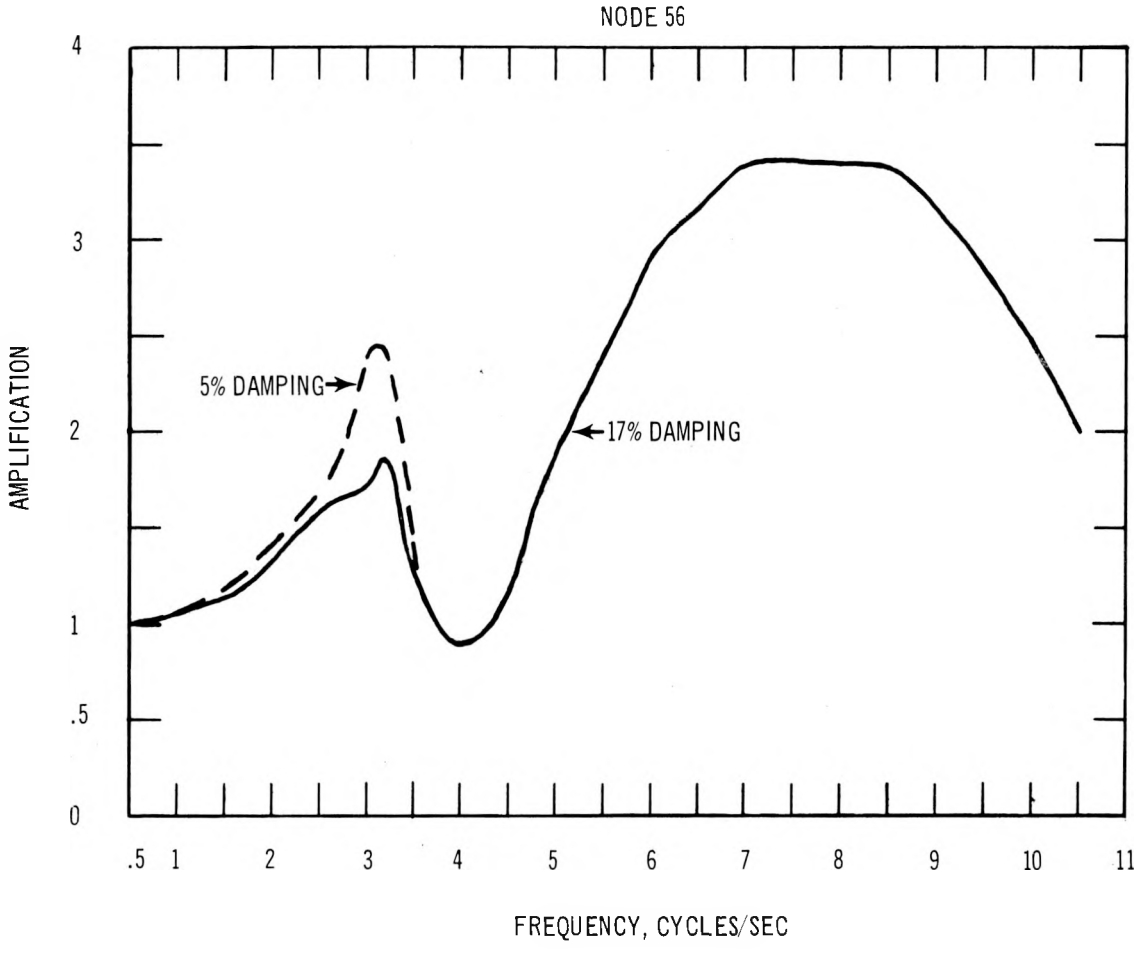

Figure 4-44. Amplification Versus Frequency, Harvey Gap Dam (Node 56), Rulison Event

that (1) as expected, the amplification versus frequency curves peak in the 3 Hz range, and (2) the most significant amplification occurs at (or near) the crest of the dam. In particular, the amplification at nodes 90 and 95 is four times larger than at node 56. Thus, for recording instruments deployed at all three of these nodes, the present finite element analysis would prescribe suitably higher gain settings at the crest of the dam, than at the location of node 56. The experimental fact that the recorded signals at the crest were clipped, while at node 56 unclipped seismograms were obtained is in total accord with our present conclusions.

It is possible to carry the present analysis one step further; since the finite element displacement equations are linear, and since the principle of superposition holds, it is possible to perform a semiempirical calculation in the following fashion. From the amplification versus frequency curve at node 56 (Figure 4-44) and the Fourier transform of the measured seismogram at that point, it is easy to calculate a unique "equivalent" input signal to the entire dam. The response of the finite element ensemble of Figure 4-43 to this equivalent input will give rise at the

nodes 90 and 95 to a time history which should be rather close to the actual seismic motion experienced by the crest of the dam during the Rulison event. Thus, it is perfectly feasible to regenerate analytically the clipped portions of the seismogram.

Consideration of the ground motions at Harvey Gap Dam provided an opportunity to test a new method for generating synthetic seismograms. A representative time history, when available, permits the response of structural models, such as the finite element model of Harvey Gap Dam, to be simulated before a detonation, thereby, providing useful information.

Several techniques for generating representative time histories are available (see Jennings et al., 1968; Beaudet et al., 1968; Iyengar et al., 1969). The technique employed in this case to generate a seismogram representing the ground motion input to the dam is an extension of the technique by Jennings et al. It involves scaling an observed seismogram satisfying basic requirements (e.g., the distance from the source, the geologic configuration of the station site, etc.). The constraint in the procedure is that the PSRV spectrum of the scaled seismogram must agree with the PSRV spectrum defined as the target. In this case, the

station at Harvey Gap Dam which recorded useable data was situated so that the ground motion observed there approximates the input to the dam. Because of the close agreement between the observed PSRV spectrum and the predicted spectrum, incorporating anticipated amplification effects (see Figure 4-38), the predicted spectrum was selected as the target.

Particle velocity data recorded on the radial component at station 15 from the Gasbuggy detonation was selected as the basic time history to be scaled. Figure 4-45 shows the comparison of the three time histories: (1) the observed Rulison seismogram, (2) the synthetic seismogram, and (3) the observed Gasbuggy seismogram. The comparisons of the PSRV spectra are also shown in Figure 4-45. The good agreement obtained indicates that this scaling technique can be utilized to generate realistic synthetic seismograms which closely approximate observed seismograms. This fact increases the assurance with which they can be utilized in the future to represent the dynamic input to structural models in order to assess the amplification.

4.4 AZIMUTHAL VARIATION OF GROUND MOTIONS

Contour maps of the peak vector particle acceleration, velocity, and displacement recorded, at sites both in and outside the Piceance Creek Basin, were prepared to determine

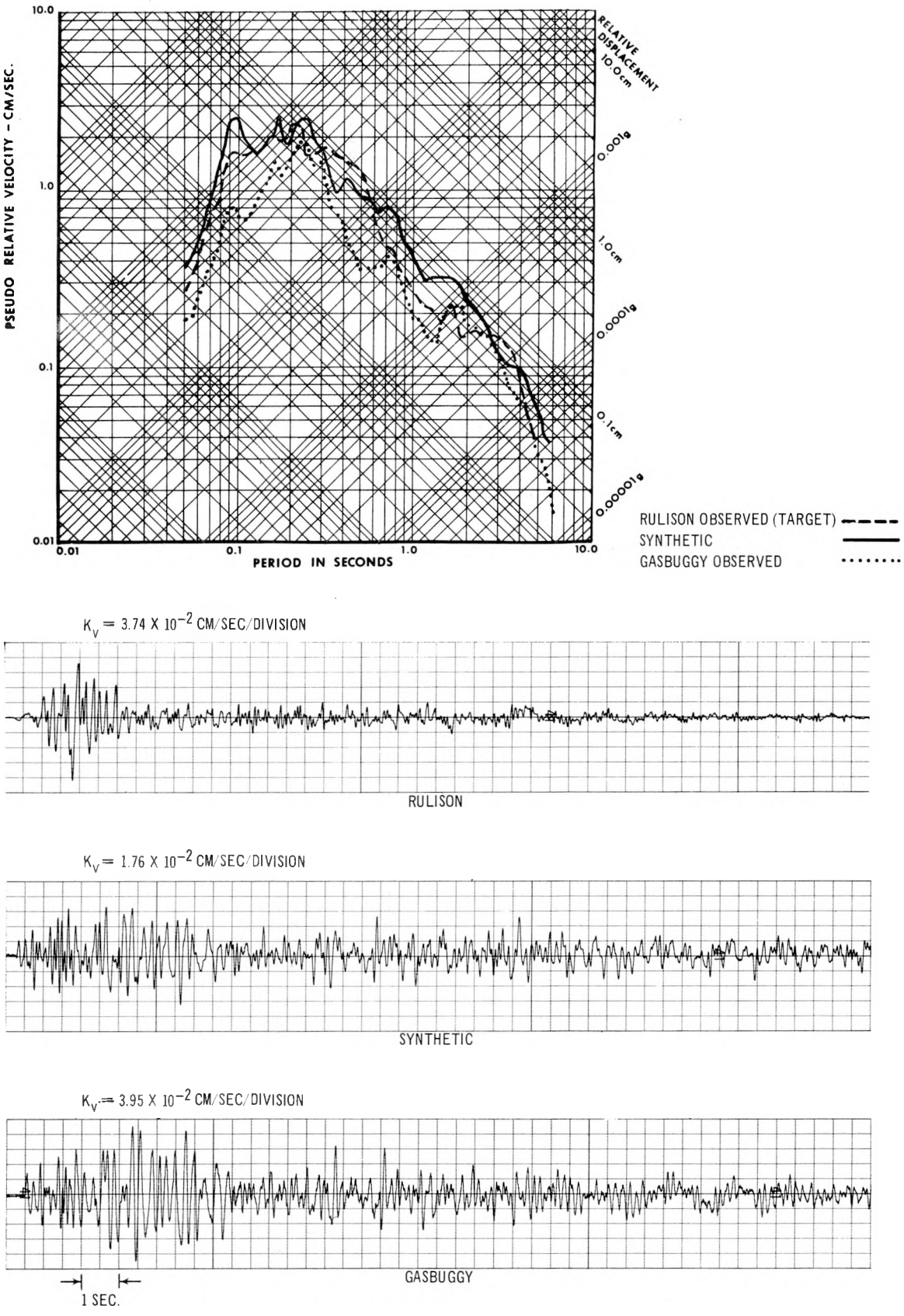

Figure 4-45. Comparison of Seismograms and PSRV Spectra, Harvey Gap Dam

if azimuthal variations existed. The results are displayed in Figures 4-46 through 4-48. In general, the seismic radiation pattern is roughly elongate about the Rulison source, and indicates a fairly uniform radiation pattern. The asymmetry of the radiation pattern tends to correspond to the general outline of the basin. This general correspondence was also noted for the Gasbuggy detonation (Foote, et al., 1969).

To the north of the Rulison site, all three maps show a subtle to pronounced change in the orientation of the isolines, indicating a possible regional anomaly. These changes are primarily the result of high peak vector particle values for the Rawlins, Wyoming station (see Figure 4-1 through 4-3 for a measure of the anomalous motions). However, the peak vector particle motions for the Craig and Meeker, Colorado stations are also slightly high. The cause of this possible anomaly may be related in some manner to the transmission of the seismic energy from the Piceance Creek Basin to the Colorado Plateau. Additional data points would be helpful in defining the presence of the anomaly, its extent and intensity. The influence of other nearby regional geologic features, such as the Uncompahgre Uplift, on the transmission of the seismic energy cannot be defined because of the lack of data.

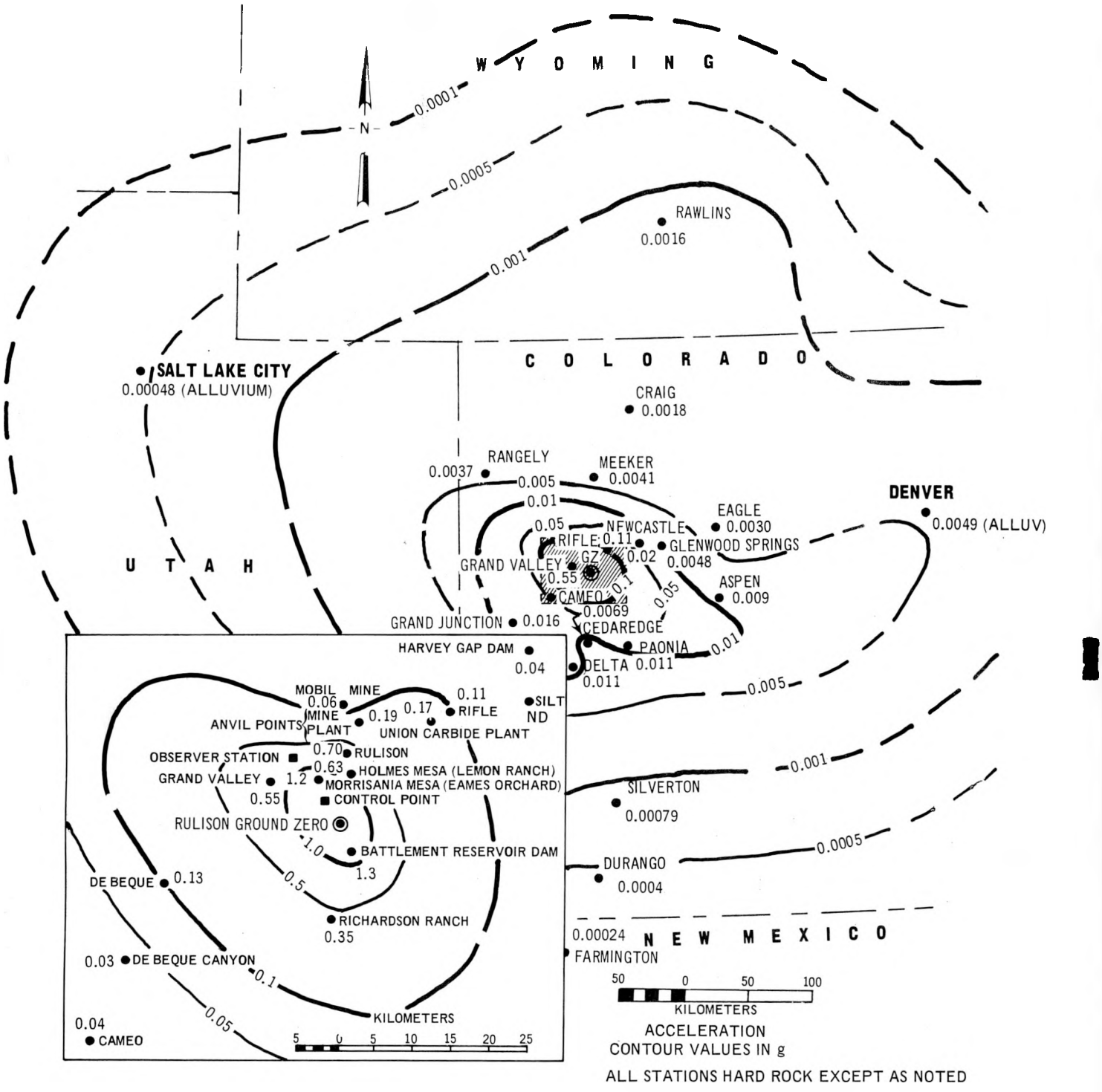

Figure 4-46. Azimuthal Variation of the Peak Vector Particle Acceleration, Rulison Detonation

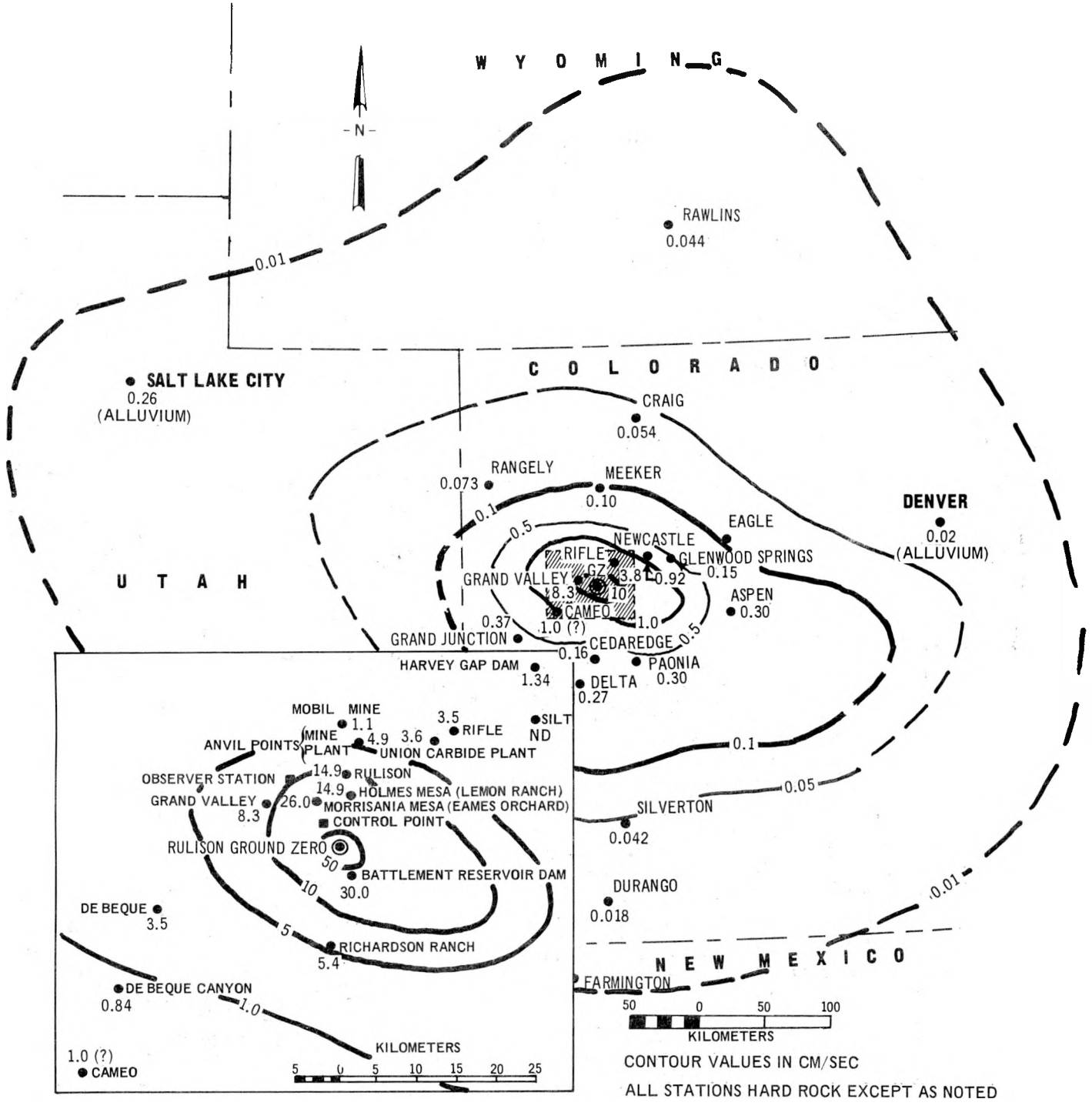

Figure 4-47. Azimuthal Variation of the Peak Vector Particle Velocity, Rulison Detonation

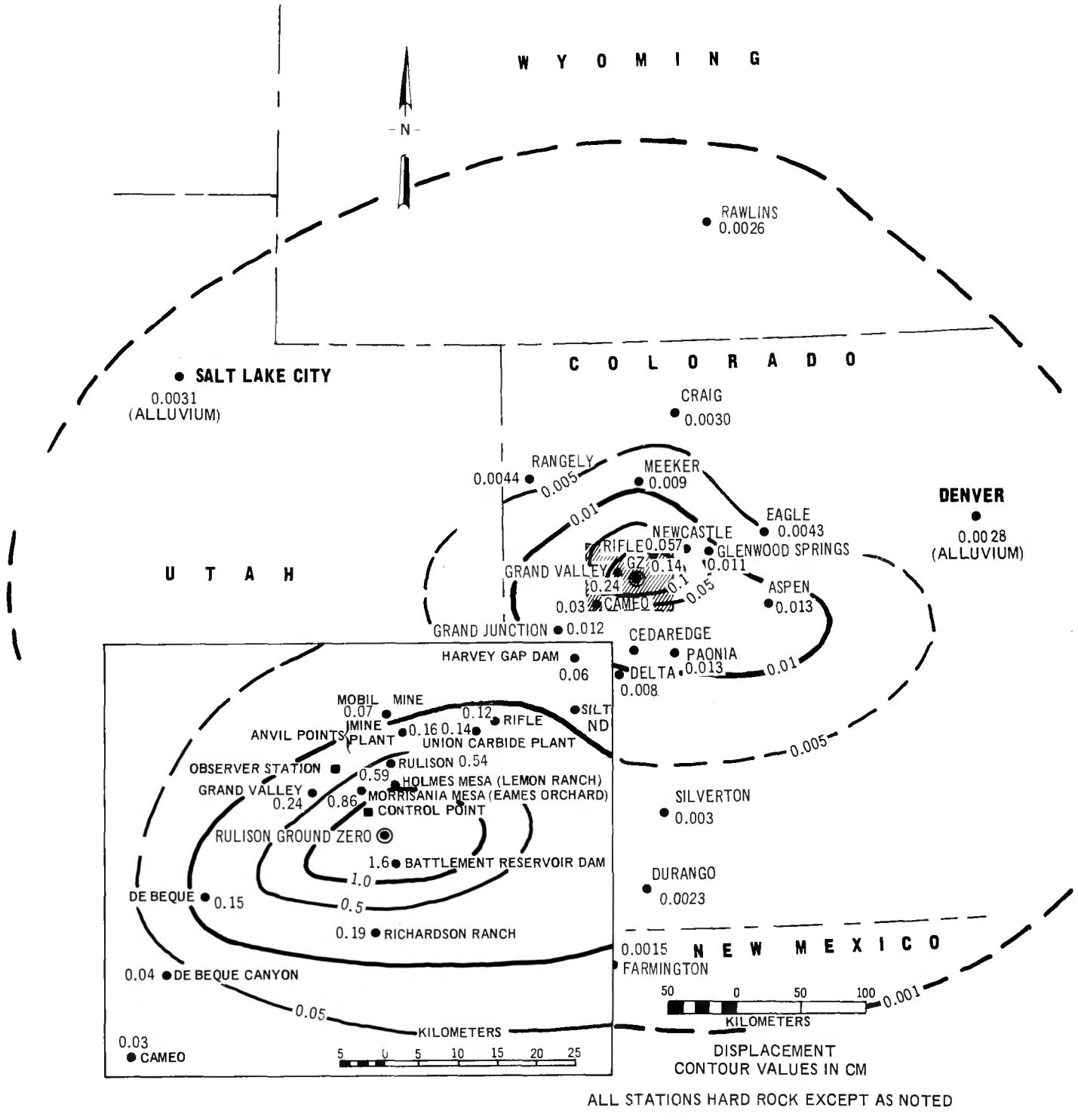

Figure 4-48. Azimuthal Variation of the Peak Vector Particle Displacement, Rulison Detonation

Azimuthal variation in the ground motions observed from Rulison is due to several factors:

1. Horizontal and vertical anisotrophy of velocity and elastic properties caused by spatial variation in the geological processes of sedimentation.

2. The amplifying effect of variable, shallow low-velocity alluvial layers at some sites (as indicated in Section 4-3).

3. Variation in the structural attitude of acoustic impedance contrast interfaces, caused by tectonic activity.

For the relatively high frequency ground motions generated by Rulison, the azimuthal variation appears to be minimal within the Piceance Creek Basin.

Stations located outside the Piceance Creek Basin (i.e., Denver, Farmington, Rawlins, etc.) tend to exhibit higher ground motion levels than the trend exhibited on the basis of the ground motions observed in the basin (Figures 4-46 through 4-48). The sites outside the basin are located on substantial alluvium deposits and, therefore, were expected to exhibit somewhat higher levels of peak vector ground motions. The sites inside the basin are on hardrock or very thin alluvial layers, as noted in Appendix A.

4.5 SEISMIC ENERGY EFFICIENCY

The seismic energy measured in the far field is related to the energy coupled into the earth at the elastic radius, the region where the material begins to behave elastically. This percentage of the original energy available (seismic energy efficiency) which ends up forming the far field seismic radiation can be determined from the amplitude spectra of the compressional waves generated by the detonation (see Mueller, 1969b, for a detailed description of the method). The procedure used to compute the seismic energy efficiency is summarized below, for completeness, and applied to the Rulison and Gasbuggy detonations. These results are compared to corresponding results obtained for Boxcar, Benham, and Duryea, three NTS detonations.

The method is based on the spherically symmetric model of Sharpe (1942) which describes the displacement potential produced by an exponential pressure function acting in an ideally elastic medium. Using this model, the expression for the energy radiated into the far field from an underground nuclear detonation is

$$E = \frac{\pi P_o^2 a^3}{2\mu} K \qquad (4\text{-}7)$$

where

$$K = \frac{1+k}{1+k+3k^2/4}$$

P_o = the peak pressure at the elastic radius, a

μ = the modulus of rigidity

k = the constant of proportionality between the decay constant $\alpha = T_o^{-1}$, and the natural frequency $\omega_o = c/a$.

c = compressional wave velocity

The frequency of maximum amplitude (ω_m) for the Fourier amplitude spectrum of the particle velocity can be obtained from the solution of the equation

$$\beta^2 \left(\frac{\omega_m}{\omega_o}\right)^6 - (k^2-2\beta k^2+1) \left(\frac{\omega_m}{\omega_o}\right)^2 - 2k^2 = 0 \qquad (4-8)$$

where

$\omega_o = c/a$, $\beta = \frac{\lambda+2\mu}{4\mu}$, and λ and μ are Lame's constants.

The frequency of maximum aplitude (ω_m) is determined from the compressional wave (P) time window, as this model is valid only for compressional waves. The observation distance must be in the far field; however, it must also be small with respect to the differential attenuation effects of the earth. If α, the decay constant, is known from free field measurements, than k can be found from the equation

$$\beta^2 \left(\frac{\omega_m}{\alpha}\right)^6 k^4 + (2\beta-1) \left(\frac{\omega_m}{\alpha}\right)^2 k^2 - \left(\frac{\omega_m}{\alpha}\right)^2 - 2 = 0 \qquad (4\text{-}9)$$

Thus, given values ω_m and k, the elastic radius can be determined from equation (4-10).

Free field measurements of α and the peak pressure at the elastic radius are not available for the Rulison and Gasbuggy detonations. Thus, approximations derived by Mueller (1969b) are used to estimate the elastic radius and the radiated energy, respectively. These relations are

$$a = 1.5\ c/\omega_m \pm 13\% \qquad (4\text{-}10)$$

and

$$E = \frac{3\pi P_o^2 c^3}{4\mu\omega_m^3} \pm 10\% \qquad (4\text{-}11)$$

If material properties other than density are unavailable, then the rigidity μ may be approximated by $\rho_c^2/3$ (assuming Poisson's ratio = 0.25). Then,

$$E = \frac{9\pi P_o^2 c}{4\rho\omega_m^3} \qquad (4\text{-}12)$$

The peak pressure P_o at the elastic radius is approximated by

$$P_o = 1.5\ OBP \qquad (4\text{-}13)$$

where OBP is the overburden pressure. The newly refined factor of 1.5 was obtained by averaging P_o/OBP data reported for the Salmon and Shoal events, (Weart, 1965; Perret, 1967; Rogers, 1966; Perret, 1968).

Figure 4-49 shows smoothed Fourier amplitude spectra at the P wave time windows observed on the radial component particle velocity seismograms of selected Rulison and Gasbuggy stations. The frequency of maximum amplitude varies somewhat, as noted earlier, for the four stations and occurs in the range 3.0 - 5.15 Hz for Rulison and 2.8 - 4.1 Hz for Gasbuggy. The average value (4.3 and 3.4 Hz) was determined

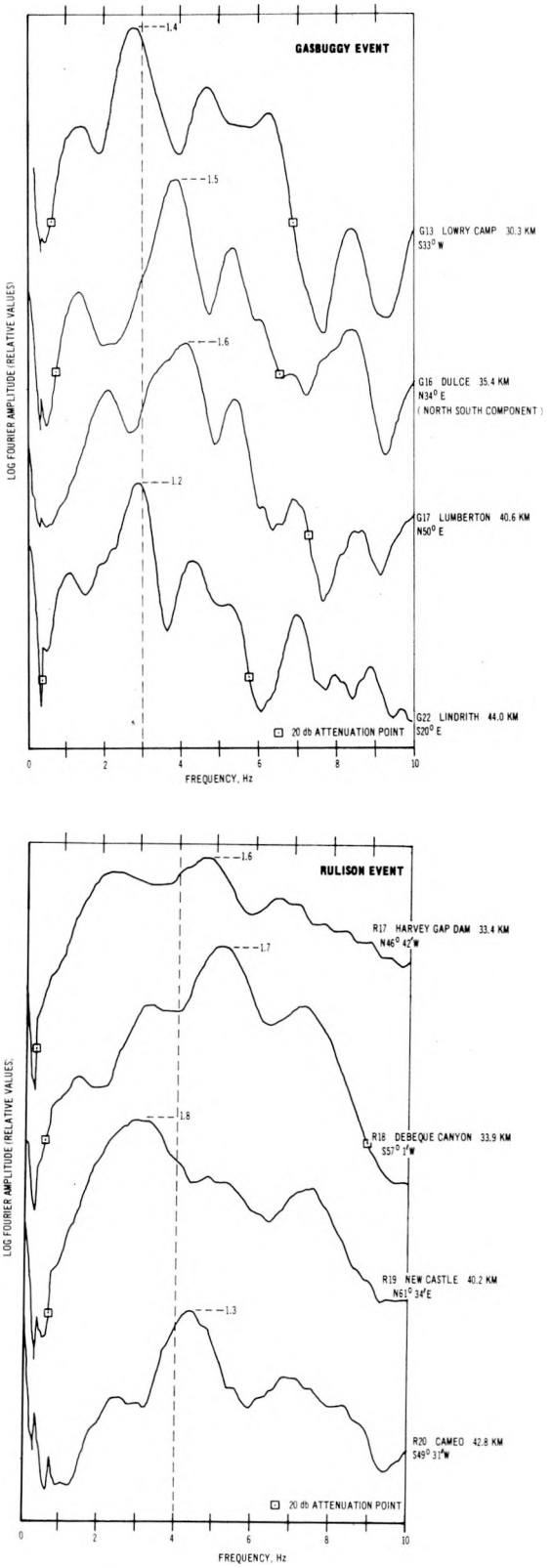

Figure 4-49. Smoothed Fourier Amplitude Spectra of P Wave Time Windows Observed at Selected Sites, Gasbuggy and Rulison Detonations

and used in each case to determine the elastic radius (equation 4-10), radiated energy (equation 4-11) and seismic energy efficiency. These values are shown in Table 4-4. The corresponding values determined for the Boxcar, Benham, and Duryea events are also listed for comparison in the table.

Keeping in mind the high degree of uncertainty involved in the determinations due to the lack of free-field data, the data of Table 4-4 appear reasonable. (The numerical results reported in Chapter 3 are also in relative agreement.) The elastic radius determined for Rulison is smaller (255 meters versus 334 meters) than the elastic radius for Gasbuggy and the frequency of maximum spectral amplitude is higher. The seismic energy efficiency is also slightly larger for Rulison as a consequence of the trade off between the frequency of maximum amplitude and the overburden pressure. These results are consistent with scaling theory (Mueller, 1969a) which predicts an increase in the dominant frequency of the seismic energy for Rulison relative to Gasbuggy and NTS experience. As noted in earlier sections of this chapter, the characteristics of the observed ground motion verify this expectation.

TABLE 4-4. SEISMIC ENERGY EFFICIENCY

EVENT	RULISON	GASBUGGY	DURYEA	BOXCAR	BENHAM
Shot Location	Piceance Creek Basin, Colorado	San Juan Basin, New Mexico	Pahute Mesa, Nevada	Pahute Mesa, Nevada	Pahute Mesa Nevada
Yield (kt)	40	26	65	1200	1100
Depth of Burial (ft)	8442.5	4240	1795	3822	4630
Scaled Depth ($ft/kt^{1/3}$)	2468.6	1431.2	446.2	359.5	447
Medium	Mesaverde Shale	Lewis Shale	Rhyolite	Rhyolite	Tuff
Density (gm/cc)	2.35	2.58	2.05	2.1	2.25
Overburden pressure (bars)	592.5	308.7	109.9	240	311
Compressional Velocity (km/sec)	4.6(1)	4.75(2)	3.51	3.84	3.66
fm (Hz)	4.3	3.4	2.1(3)	0.75	0.80
Elastic Radius (m)	255	334	398	1222	1093
Seismic Energy Radiated (kt)	1.31	0.68	3.4	33.1	46.5
Seismic Energy Efficiency (%)	3.3	2.6	4.9	3.4(4)	4.2(4)

[1]Rulison Well Data.

[2]Personal Communication, W.R. Perret (1969).

[3]Based on one Fourier Amplitude Spectrum.

[4]Refined from values reported in Mueller (1969b) on basis of equation (4-13).

CHAPTER 5

SUMMARY AND RECOMMENDATIONS FOR ADDITIONAL WORK

Ground motion data, recorded at 36 instrument stations for the Rulison event, were processed, analyzed, and compared with data observed from the Gasbuggy event and from selected detonations at Nevada Test Site.

5.1 SUMMARY OF CONCLUSIONS

The primary conclusions which result from the analyses may be summarized as follows:

1. Peak Vector Particle Motion

The level of peak vector particle acceleration and velocity significantly exceeded the level expected on the basis of NTS experience, as predicted. The peak vector particle acceleration observed at 10 km is about 8 times greater than the level expected at that distance from a normally buried 40 kt contained device detonated on the NTS, and the peak vector particle velocity at 10 km is about 5 times greater than expected. The peak vector particle displacement at 10 km is somewhat less (0.8 times) than the level expected.

The observed peak vector accelerations, velocities, and displacements compare well with the levels expected on the basis of scaling theory, i.e., scaling the corresponding Gasbuggy ground motions for differences in yield (26 kt versus 40 kt) and device depth of burial (4240 ft versus 8425 ft).

2. Pseudo-Relative Velocity Spectra

The horizontal spectra observed at Rulison sites are significantly different from the spectra expected on the basis of a typical 40 kt detonation at NTS. The peak spectral response from Rulison has a higher level and occurs at shorter periods (0.1 - 0.4 second) than the periods (0.2 to 1.0 second) of the peak spectral response typically observed for a 40 kt NTS detonation. Differences are greatest at distances inside 30 km. These differences include a slightly higher peak spectral response (a difference of less than a factor of 2 at most stations) than expected and a relative shift of the period of maximum spectral response to the short period end of the spectrum (the Gasbuggy maximum spectral response typically occurred at periods of 0.2 - 0.5 second).

The Rulison spectra exhibit characteristics which are comparable to those expected on the basis of Gasbuggy experience and scaling theory; scaling to account for the greater

device depth of burial for Rulison enhances the level at the short period end of the spectrum and reduces the level at the long period end. An effect of the dominant high frequency content is to enhance the peak vector accelerations and velocities, as noted above.

3. Numerical Computation of Close-in Physical Effects

Numerical simulation with a one-dimensional, shperically symmetric Lagrangian model provides estimates of the cavity radius, cracking radius (analogous to the elastic radius), pressure profiles, and the percentage of energy input to the seismic region. Simulation for Rulison leads to a cavity radius of 48-58^{+} meters, a cracking radius of 273^{+}-289 meters, and approximately 3% energy input into the elastic region. The corresponding values calculated for Gasbuggy are, respectively, 35 meters, 290 meters, and 2%. The relative order of magnitude of these values for the two detonations is supported by calculations of the seismic energy efficiency, and agrees qualitatively with the results expected on the basis of scaling theory.

4. Signal Duration

Determination of the duration of the ground motions observed from Rulison indicates that the duration is independent of frequency. The signal duration in the neighborhood of a given frequency band persists for approximately 3.25 cycles at Rulison. However, the observed values of 2.75 cycles for Gasbuggy and 3.90 cycles for NTS experience are somewhat different.

5. Characteristics of Elastic Wave Types

The peak vector particle accelerations correlate almost exclusively with the P wave time windows over the entire distance range. The peak vector particle velocities correlate primarily with the body wave (P and S) time windows. The peak vector particle displacements correlate mainly (with two exceptions) with the body wave windows at close-in distances. The peak vector displacements tend to correlate more with the surface wave at distant stations, a normal phenomenon. The vertical component exhibits the largest accelerations and velocities inside 10 km.

Significant shear (SH) energy was generated by the Rulison detonation, particularly, in a NE-SW azimuth from ground zero. The specific cause, unknown at this time, may be related to shot induced movement along existing fracture patterns.

The surface waves observed from Rulison are generally small relative to the body waves and NTS experience. The reason may relate to the greatly overburied nature of the Rulison detonation which probably affects the excitation mechanism of surface waves.

6. Attenuation of Seismic Waves in the Earth's Crust

A value of about 200 was obtained for the Q (the specific dissipation constant) of the earth's crust in the Rulison area. This value is in general agreement with the values of Q determined by other investigators in various crustal studies.

7. Frequency Dependent Amplification

Good agreement was obtained between the observed PSRV spectra and the spectral predictions which incorporated amplification effects expected on the basis of analytical amplification modeling, using the results of refraction surveys at selected sites as input. The agreement was especially good at the City of Rifle and at Harvey Gap Dam.

The results of the finite element analysis of the Harvey Gap Dam, located about 32 km from ground zero, indicate that considerable amplification of the ground motions should occur at the crest of the dam in comparison to the east end. These observations agree with the observed ground motion data.

A synthetic seismogram was generated to approximate the ground motion input into Harvey Gap Dam, using a time history scaling technique. The technique, based on scaling a seismo-

gram observed from the Gasbuggy detonation, leads to a fairly close agreement between the observed and synthetic seismograms and their PSRV spectra.

8. Azimuthal Variation

The seismic radiation pattern within Piceance Creek Basin is elongate in an east-west direction about the Rulison source. The asymmetry of the ground motions corresponds to the shape of the basin, a phenomenon noted for the ground motions generated by Gasbuggy. Sites on alluvium outside the basin exhibit systematically higher motions, as expected.

9. Seismic Energy Efficiency

Calculations of the seismic energy efficiency (radiated energy/initial energy available) of the Rulison and Gasbuggy detonations yield values of 3.3% and 2.6%, respectively. These values, although somewhat uncertain due to the lack of free field measurements, agree generally with the results obtained from numerical simulation of the two detonations (as described above). Values of the elastic radii determined from analysis of the seismic data of the two detonations are, respectively, 255 meters and 334 meters. An effect of the smaller elastic radii for Rulison is a higher dominant frequency of generation of the seismic energy relative to both Gasbuggy and NTS experience, a phenomenon noted earlier.

5.2 PREDICTION METHODOLOGY FOR FUTURE DETONATIONS

In order to predict accurately the ground motions expected from proposed detonations in the Piceance Creek Basin, or in other sedimentary basins having a similar geological environment, prediction techniques must be developed on the basis of empirical and theoretical considerations. The characteristics of the amplitude and frequency composition of the ground motions observed from the Rulison and Gasbuggy detonations, the total experience available to date for detonations in sedimentary (sand-shale) media, must be incorporated with analytical techniques in order to simulate the proposed situation.

Regression equations (listed in Table 5-1 and 5-2) derived from the Rulison ground motions will be used in conjunction with similar equations representing Nevada Test Site and Gasbuggy experience (see Tables 1-1 and 1-2, Chapter 1) to provide the empirical basis for making predictions. The level of peak ground motion and the spectral composition expected at selected sites from similar Plowshare experiments can be predicted with these equations. Scaling theory (Mueller, 1969a), which accounts for the difference in the major source parameters (device depth of burial, the yield of the device and the detonation medium) will be incorporated with the empirical relationships to provide the best estimate of the ground

TABLE 5-1. Regression Equations Relating the Parameter of Observed Ground Motion to Distance (km), Rulison Event

Ground Motion Parameter	Regression Equation	Site Geology Data Sample	Range (R) of Data Sample (km)
Acceleration			
1. Peak Resultant Vector	$5.269 \times 10^{1} R^{-2.09}$ $\sigma = 1.67$	Hard Rock	4.9-296.0
2. Radial	$2.24 \times 10^{1} R^{-1.96}$ $\sigma = 1.67$	Hard Rock	4.9-296.0
3. Transverse	$1.37 \times 10^{1} R^{-1.86}$ $\sigma = 2.36$	Hard Rock	4.9-296.0
4. Vertical	$3.35 \times 10^{1} R^{-2.04}$ $\sigma = 1.94$	Hard Rock	4.9-296.0
5. Horizontal (R and T)	$1.99 \times 10^{1} R^{-1.94}$ $\sigma = 2.04$	Hard Rock	4.9-296.0
Velocity			
1. Peak Resultant Vector	$7.77 \times 10^{2} R^{-1.93}$ $\sigma = 1.69$	Hard Rock	4.9-296.0
2. Radial	$5.12 \times 10^{2} R^{-1.89}$ $\sigma = 1.71$	Hard Rock	4.9-296.0
3. Transverse	$3.69 \times 10^{2} R^{-1.85}$ $\sigma = 1.96$	Hard Rock	4.9-296.0
4. Vertical	$6.46 \times 10^{2} R^{-1.95}$ $\sigma = 1.81$	Hard Rock	4.9-296.0
5. Horizontal (R and T)	$4.38 \times 10^{2} R^{-1.87}$ $\sigma = 1.83$	Hard Rock	4.9-296.0
Displacement			
1. Peak Resultant Vector	$1.64 \times 10^{1} R^{-1.69}$ $\sigma = 1.50$	Hard Rock	4.9-296.0
2. Radial	$9.64 \times 10^{0} R^{-1.62}$ $\sigma = 1.54$	Hard Rock	4.9-296.0
3. Transverse	$6.50 \times 10^{0} R^{-1.59}$ $\sigma = 1.73$	Hard Rock	4.9-296.0
4. Vertical	$1.04 \times 10^{1} R^{-1.66}$ $\sigma = 1.53$	Hard Rock	4.9-296.0
5. Horizontal (R and T)	$8.04 \times 10^{0} R^{-161}$ $\sigma = 1.66$	Hard Rock	4.9-296.0

TABLE 5-2. Regression Equations Relating the Observed PSRV Amplitude at Each Period to Distance (km), Rulison Event

Period (Second)	Regression Equation	Standard Error of Estimate
0.050	$4.53 \times 10^{2}\ R^{-2.09}$	1.85
0.055	$5.10 \times 10^{2}\ R^{-2.08}$	1.80
0.061	$5.95 \times 10^{2}\ R^{-2.08}$	1.83
0.067	$6.23 \times 10^{2}\ R^{-2.05}$	1.84
0.075	$7.07 \times 10^{2}\ R^{-2.05}$	1.82
0.082	$7.74 \times 10^{2}\ R^{-2.03}$	1.93
0.091	$9.29 \times 10^{2}\ R^{-2.02}$	2.02
0.101	$1.17 \times 10^{3}\ R^{-2.04}$	2.03
0.111	$1.41 \times 10^{3}\ R^{-2.04}$	2.09
0.123	$1.29 \times 10^{3}\ R^{-1.98}$	2.13
0.136	$1.25 \times 10^{3}\ R^{-1.94}$	2.08
0.150	$1.63 \times 10^{3}\ R^{-1.99}$	2.01
0.166	$1.86 \times 10^{3}\ R^{-2.01}$	1.98
0.183	$1.62 \times 10^{3}\ R^{-1.96}$	1.99
0.203	$1.30 \times 10^{3}\ R^{-1.90}$	2.00
0.224	$1.05 \times 10^{3}\ R^{-1.86}$	2.13
0.248	$7.62 \times 10^{2}\ R^{-1.81}$	2.07
0.274	$6.33 \times 10^{2}\ R^{-1.81}$	2.04
0.302	$4.61 \times 10^{2}\ R^{-1.74}$	2.08
0.369	$3.08 \times 10^{2}\ R^{-1.68}$	2.17
0.408	$2.57 \times 10^{2}\ R^{-1.67}$	2.17
0.451	$2.10 \times 10^{2}\ R^{-1.66}$	2.22
0.499	$1.62 \times 10^{2}\ R^{-1.63}$	2.17
0.551	$1.44 \times 10^{2}\ R^{-1.63}$	2.12
0.609	$1.14 \times 10^{2}\ R^{-1.63}$	2.02
0.673	$1.01 \times 10^{2}\ R^{-1.64}$	1.86
0.744	$7.19 \times 10^{1}\ R^{-1.58}$	1.80
0.822	$5.35 \times 10^{1}\ R^{-1.55}$	1.71
0.908	$4.83 \times 10^{1}\ R^{-1.54}$	1.68
1.004	$4.45 \times 10^{1}\ R^{-1.56}$	1.64
1.110	$3.58 \times 10^{1}\ R^{-1.54}$	1.61
1.226	$4.12 \times 10^{1}\ R^{-1.60}$	1.70
1.355	$2.93 \times 10^{1}\ R^{-1.54}$	1.83
1.498	$2.33 \times 10^{1}\ R^{-1.49}$	1.71
1.655	$2.51 \times 10^{1}\ R^{-1.54}$	1.74
1.829	$1.82 \times 10^{1}\ R^{-1.48}$	1.81
2.022	$2.27 \times 10^{1}\ R^{-1.56}$	1.73
2.234	$1.63 \times 10^{1}\ R^{-1.51}$	1.76
2.469	$1.47 \times 10^{1}\ R^{-1.51}$	1.79

motion characteristics expected from other proposed detonations having a different yield and device depth of burial than Rulison or Gasbuggy.

The procedures to predict the ground motions from future detonations in the Piceance Creek Basin are currently being developed at ERC. Tables and graphs will be presented in a future report to illustrate, for planning purposes, the predictions at 12 selected recording sites (Rulison, Grand Valley, Anvil Points, Mobil Mine, Union Carbide, 2 Rifle sites, Harvey Gap Dam, New Castle, Cameo, Glenwood Springs, and Grand Junction) as well as for arbitrary sites over the distance range 10-60 km. These predictions correspond to three arbitrary detonations having yields of 40, 80, and 160 kt and device depths of burial of 4000, 8000, and 12000 feet. Because the procedures will presented in detail in the future report, only a brief discussion will be included here.

The essence of the prediction procedure involves the scaling of ground motion data observed from Rulison (Gasbuggy or NTS data in applicable cases) to account for the difference in yield (W) and device depth of burial (h) of the proposed detonation. Either ground motion data (peak amplitudes or PSRV spectra) observed at individual sites or predicted on the basis of mean regression equations (see

Tables 5-1 and 5-2) can be utilized as the basic data. The procedure for scaling is as follows:

1. Peak Vector Ground Motion Scaling

   a) Displacement -- The scaling factor for peak particle displacement is

$$\left(\frac{W_1}{W_2}\right)^{0.87} \cdot \left(\frac{h_2}{h_1}\right)^{0.33} \qquad (5\text{-}1)$$

   where the subscripts 1 and 2 relate, respectively, to the parameters of the detonation to which ground motion is being scaled and the parameter of the detonation giving the observed ground motion, Expression (5-1) gives a multiplicative factor which is applied at all distances to the regression equation or the data to be scaled. As an example, the factor required to scale the regression equation of the peak displacements observed from Rulison (W_2 = 40 kt, h_2 = 8425 feet) to another detonation with a yield (W_1) of 80 kt and a device depth of burial of 12,000 feet (h_1) is

$$\left(\frac{80}{40}\right)^{0.87} \cdot \left(\frac{8425}{12000}\right)^{0.33}$$

   The resulting factor multiplies the values given by the regression equation to give the predicted peak vector displacements for 80 kt and depth of burial of 12,000 ft.

   b) Acceleration -- The scaling factor to obtain the predicted peak vector particle acceleration is given by*

$$\left(\frac{W_1}{W_2}\right)^{0.33} \cdot \left(\frac{h_1}{h_2}\right)^{0.58} \qquad (5\text{-}2)$$

   c) Velocity -- The scaling factor for the peak vector particle velocity is determined empirically from the PSRV spectra. The ratio of the peak spectral response of the PSRV spectrum,

---

*Note: $\left(\frac{W_1}{W_2}\right)^{0.33}$ is an adequate approximation for the range of yields to be considered in the future report. The exponent (0.56) would be used in actual practice.

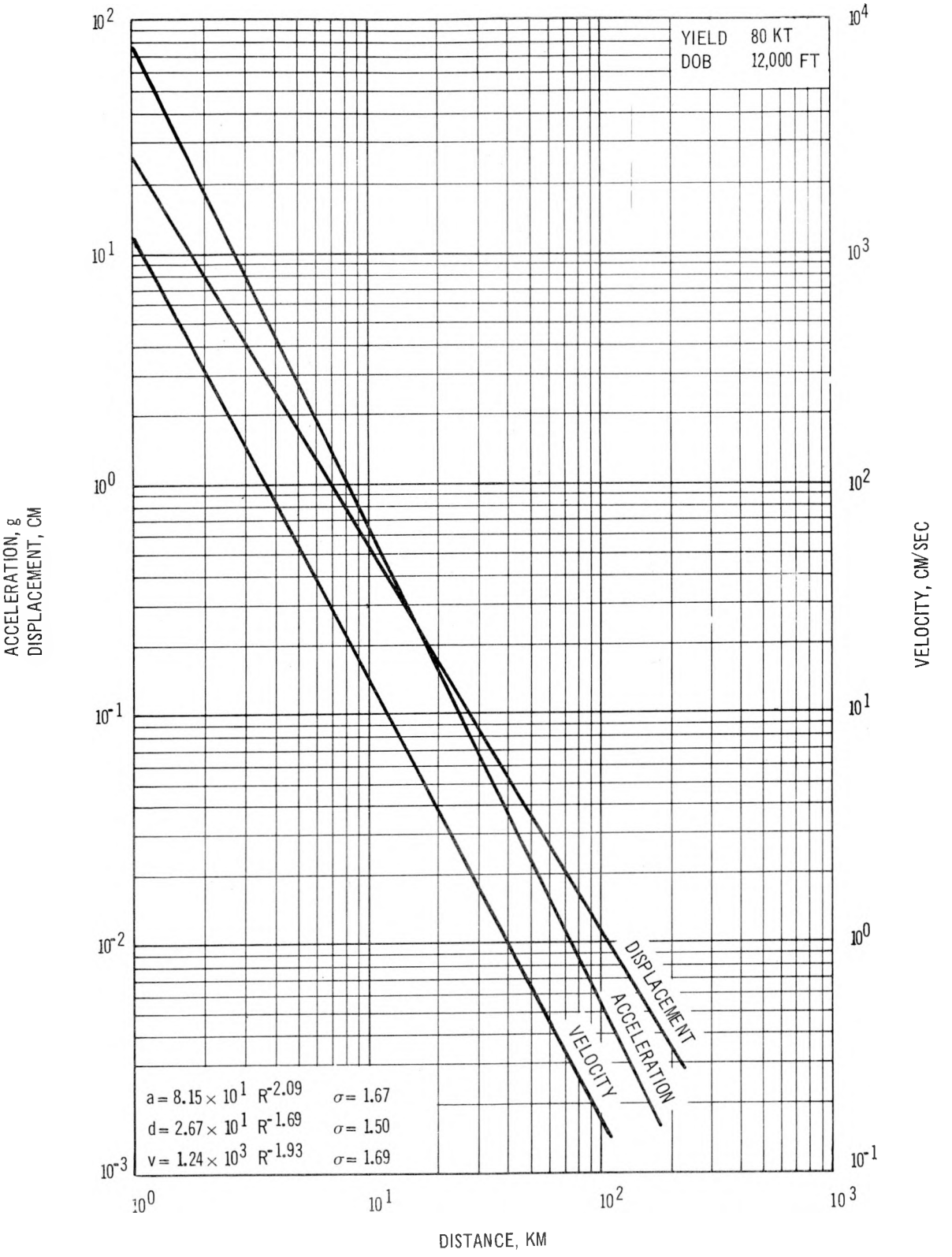

Figure 5-1. Ground Motion Levels Predicted for an Arbitrary 80 kt Detonation Buried at 12,000 ft, Using Observed Rulison Data as the Basis

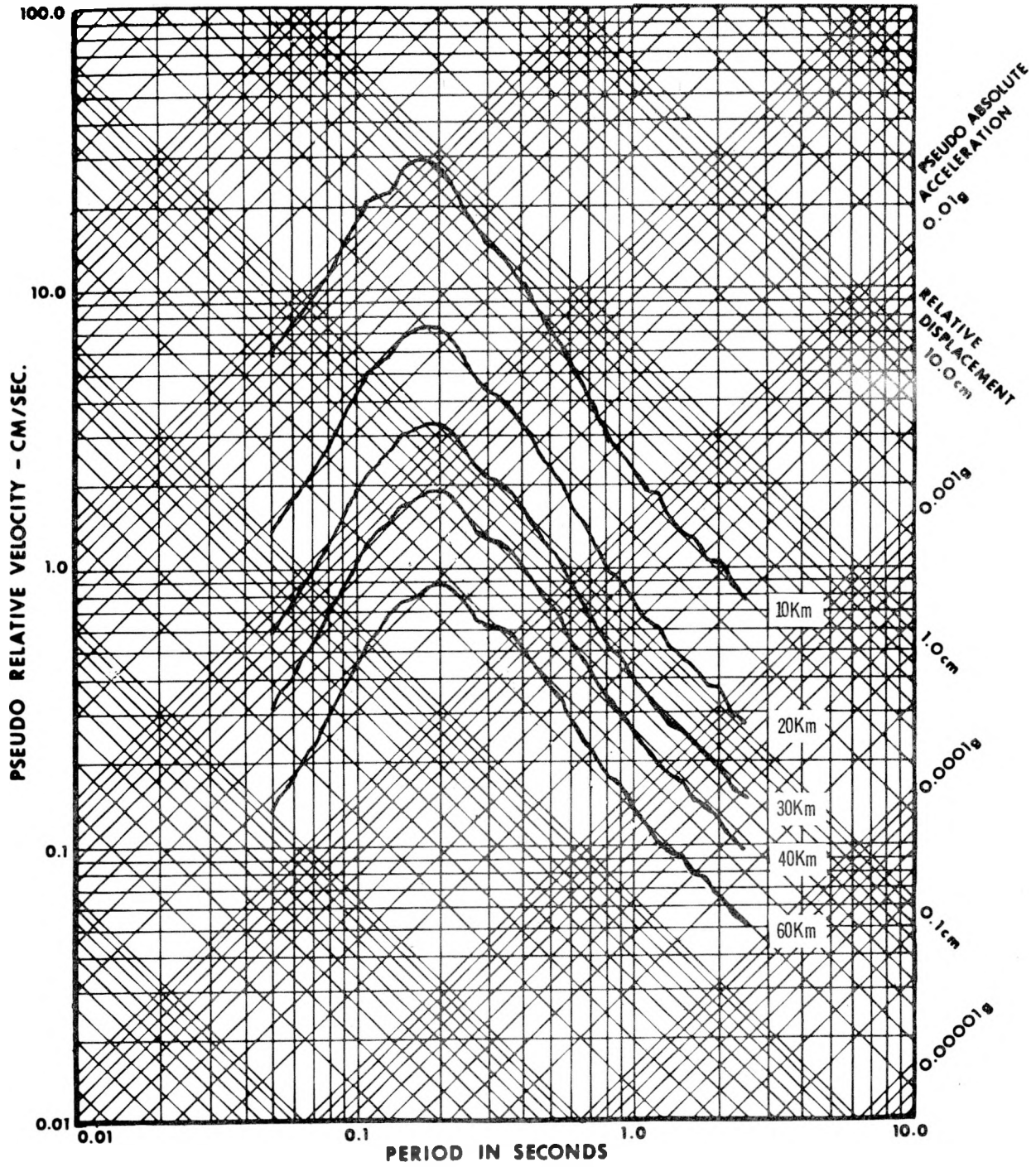

Figure 5-2. 5% PSRV Spectra Predicted for an Arbitrary 80 kt Detonation Buried at 12,000 ft, Using Observed Rulison Data as the Basis

Rulison data (regression equations) to a new yield (80 kt) and device depth of burial (12,000 feet). Other graphs will be shown in the forthcoming report. It should be emphasized that these graphs are applicable only for detonations located in the Piceance Creek Basin and in the same detonation media as Rulison.

Predictions for detonations in sedimentary basins other than the Piceance Creek Basin can be based upon the characteristics of the data observed for the Rulison and Gasbuggy detonations, the scaling techniques described above, and other considerations. Consideration must be given to source variables (yield, device depth of burial, detonation media), transmission path variables (effect of basin parameters, attenuation, geometric travel path), and recording site variables (thickness and physical properties of the layered sequence underlying the recording site). If this is done, realistic predictions of the ground motion can be made.

5.3 RECOMMENDATIONS FOR ADDITIONAL WORK

Analysis of the Rulison data, when related to the Gasbuggy and NTS experience, provides significant physical insight into the geological and geophysical parameters which must be considered in order to extend significantly the ability to predict accuragely the ground motions of nuclear events, especially those detonated in sedimentary basins. Although the present level of understanding is substantial, additional data from future underground events, detonated in either sedimentary basins or on large structurally uplifted areas, will materially advance the safety and scientific objectives of the Plowshare program.

Specific redommendations to be considered for future detonations are as follows:

1. In advance of future detonations, conduct scientific surveys to provide supplemental date to assist in preparation of the predetonation evaluations. These surveys should include the following:

    - The physical properties and thicknesses of the near-surface layers should be determined by refraction surveys, core analysis and various logging techniques for specific sites which may exhibit local frequency dependent amplification. Several sites

instrumented for Rulison should be investigated to determine the local amplification. These include Rawlins, Rangely, Silt, New Castle, and Paonia.

- Finite element analyses, utilizing data gained from the surveys discussed above, should be made for high risk and/or cost structures, such as dams, buildings, and mine tunnels, which have been built on sites that may exhibit local frequency dependent amplification.

2. Process and compile representative ground motion data samples for underground nuclear detonations in sedimentary basins and structurally uplifted areas. From these data, statistically derived peak amplitude (acceleration, displacement, and velocity) and PSRV equations can be derived for an evaluation of the observed motion and for calibration of proposed events.

3. Determine the similarities and differences of the amplitude and frequency characteristics of ground motions from underground detonations as a function of device yield, burial depth of device, detonation medium, distance from source to recording station, and geologic conditions surrounding the recording station.

4. Determine the experimental and theoretical effect of the physical properties of the source medium on factors such as the amplitude and frequency characteristics, seismic energy efficiency, and wave mode generation of cratering detonations.

The basis for making ground motion predictions of future underground nuclear events will be significantly improved by implementation of these recommendations.

REFERENCES

Beaudet, P. R., 1970, Wave Propagation in Heterogeneous Media, Environmental Research Corporation Report; NVO-1163-202.

Beaudet, P. R., Cassity, C. R., Davis, A. H., and de Caprariis, P. P., 1969, Models for Calculating Close-In Motions from Underground Nuclear Explosions; Environmental Research Corporation Report, NVO-1163-165.

Beaudet, P. R., Hays, W. W., Lynch, R. D., and Williams, S. L., 1968, An Application of Non-Stationary Process to Generate Synthetic Seismograms; Environmental Research Corporation Report, NVO-1163-156.

Bishop, R. H., 1963, Spherical Shock Waves from Underground Explosions; Sandia Corporation Report, SC-4907 (RR), Section 4.

Blume, John A., and Associates, 1969, Harvey Gap Dam Safety Study; John A. Blume Report, JAB-99-63.

Blume, John A., and Associates, 1970, Structural Effects of the Rulison Event; John A. Blume Report, JAB-99-76.

Cassity, C. R., Davis, A. H., and McQuinn, L. D., 1969, One-Dimensional Earth Motion Calculations; Environmental Research Corporation Report, NVO-1163-TM-11 (in press).

Cherry, J. T., 1967, Computer Calculations of Explosion-Produced Craters; International Journal of Rock Mechanics and Mining Sciences, V. 4, p. 1.

Cherry, J. T., and Hurdlow, W. R., 1966, Numerical Simulation of Seismic Disturbances; Geophysics, V. 31, p. 33.

Davis, A. H., and Murphy, J. R., 1967, Amplification of Seismic Body Waves by Low Velocity Surface Layers; Environmental Research Corporation Report, NVO-1163-130.

Environmental Research Corporation Report, NVO-1163-124, Summary Report of Predictions, Gasbuggy Event, November, 1967.

Environmental Research Corporation Report, NVO-1163-197; Observed Seismic Data, Rulison Event; December, 1969.

Ewing, W. M., Jardetzky, W. S., and Press, F., 1957, Elastic Waves in Layered Media, McGraw-Hill Book Company.

Fernandez, L. M., 1967, Master Curves for the Response of Layered Systems to Compressional Seismic Waves; Bulletin of the Seismological Society of America, V. 57, p. 515.

Foote, R. Q., Hays, W. W., and Klepinger, R. K., 1969, Analysis of Ground Motions and Close-in Physical Effects, Gasbuggy Event; PNE-1010.

Germain, L. S., and Kahn, J. S., 1969, Phenomenology and Containment of Underground Nuclear Explosions; Technical Discussions of Off Site Safety Programs for Underground Nuclear Detonations, United States Atomic Energy Commission, Nevada Operations Office, NVO-40, p. 13.

Geologic Map of Colorado; United States Geological Survey (Reprinted, 1967).

Grant, F. S., and West, G. F., 1965, Interpretation Theory in Applied Geophysics; McGraw-Hill Book Company, New York.

Hannon, W. J., 1964, An Application of the Haskell-Thompson Matrix Method to the Synthesis of Surface Motion Due to Dilational Waves; Bulletin of the Seismological Society of America, Vol. 54, p. 2067.

Haskell, N. A., 1953, The Dispersion of Surface Waves on Multilayered Media, Bulletin of the Seismological Society of America, V. 43, p. 17.

Hays, W. W., 1969, Amplitude and Frequency Characteristics of Elastic Wave Types Generated by the Underground Nuclear Detonation, Boxcar; Bulletin of the Seismological Society of America, V. 59, p. 2283.

Hays, W.W., 1968, Identification of Elastic Wave Types Generated by Underground Nuclear Explosions; Environmental Research Corporation Report, NVO-1163-157.

Hays, W. W. Mueller, R. A., and Spiker, C. T., 1969, Schooner Event, A Contribution to the Analysis of Seismic Data from Cratering and Contained Events; Environmental Research Corporation Report, NVO-1163-188 (in press).

Heelan, P. A., 1953, On the Theory of Head Waves; Geophysics, V. 18, p. 871.

Herrin, E., 1969, Regional Variations in P Wave Velocity in the Upper Mantle Beneath North America, The Earth's Crust and Upper Mantle; Geophysical Monograph 13 of the American Geophysical Union, p. 242.

Ibrahim, A. B., 1969, Determination of Crustal Thickness from Spectral Behavior of SH Waves; Bulletin of the Seismological Society of America, V. 59, p. 1247.

Iyengar, R. N., and Iyengar, K.T.S., 1969, A Nonstationary Random Process Model for Earthquake Accelerograms; Bulletin of the Seismological Society of America, V. 59, p. 1163.

Jennings, P. C., Housner, G. W., and Tsai, N. C., 1968, Simulated Earthquake Motions; California Institute of Technology Report, Earthquake Engineering Research Laboratory.

Kim, W. H., and Kisslinger, C., 1967, Model Investigation of Explosions in Prestressed Media; Geophysics, V. 32, p. 633.

King, K. W., 1969, Ground Motion and Structural Response Instrumentation; Technical Discussions of Off Site Safety Programs for Underground Nuclear Detonations, Atomic Energy Commission, Nevada Operations Office, NVO-40, p. 83.

Kisslinger, C., Mateker, E. J., and McEvilty, T. V., 1961, SH Motion from Explosions in Soil; Journal of Geophysical Research, V. 66, p. 3487.

Knopoff, L., 1969, Attenuation of Seismic Waves in the Mantle; The Earth's Crust and Upper Mantle, Geophysical Monogram 13 of the American Geophysical Union, p. 273.

Knopoff, L., 1964, Q, Reviews of Geophysics, V. 2, p. 625.

Knopoff, L., and Gilbert, F., 1960, First Motion from Seismic Sources; Bulletin of the Seismological Society of America, V. 50, p. 117.

Latter, A. L., Martinelli, E. A., and Teller, E., 1959, Seismic Scaling Law for Underground Explosions; Physics of Fluids, V. 2, p. 280.

Leet, L. D., 1946, Earth Motion from the Atomic Bomb Test; American Scientist, V. 34, p. 198.

Long, L. T., and Berg, J. W., 1969, Transmission and Attenuation of the Primary Seismic Wave, 100-600 km; Bulletin of the Seismological Society of America, V. 59, p. 131.

Loux, P. C., and Davis, L. L., 1969, Ground Motion; Technical Discussions of Offsite Safety Programs for Underground Nuclear Detonations, Atomic Energy Commission Nevada Operations Office, NVO-40, p. 99.

Lynch, R. D., 1965, A Statistical Relationship between Band-Pass Filter and Pseudo-Relative Velocity Spectra; Environmental Research Corporation Report, NVO-1163-88.

Lynch, R. D., 1969, Response Spectra for Pahute Mesa Nuclear Events; Bulletin of the Seismological Society of America, V. 59, p. 2295.

McKeown, F. A., and Dickey, D. D., 1969, Fault Displacements and Motion Related to Nuclear Explosions; Bulletin of the Seismological Society of America, V. 59, p. 2253.

Mueller, R. A., 1969a, Seismic Scaling Law (Abstract) Transactions of the American Geophysical Union; Vol. 50, No. 4, p. 248.

Mueller, R. A., 1969b, Seismic Energy Efficiency of Underground Nuclear Detonations; Bulletin of the Seismological Society of America, V. 59, p. 2311.

Murphy, J. R., and Davis, A. H., 1969, Amplification of Rayleigh Waves in a Surface Layer of Variable Thickness; Environmental Research Corporation, NVO-1163-175.

Murphy, J. R., and Lahoud, J. A., 1969, Analysis of Seismic Peak Amplitudes from Underground Nuclear Explosions; Bulletin of the Seismological Society of America, V. 59, p. 2325.

Navarro, R., and Wuollet, G., 1969, "Rulison Seismic Effects," (Preliminary), CGS-746-2, U. S. Coast & Geodetic Survey.

46

Perret, W. R., 1968, Free-Field Particle Motion from a Nuclear Explosion in Salt, Part I, Project Dribble, Salmon Event; VUP 3012, Sandia Laboratory.

Perret, W. R., 1967, Surface Motion Response Spectra, Project Shoal, SC-RR-66-696, Sandia Laboratory.

Phinney, R. A., 1964, Structure of the Earth's Crust from Spectral Behavior of Long Period Body Waves; Journal of Geophysical Research, V. 60, p. 2997.

Press, F., 1964, Seismic Wave Attenuation in the Crust; Journal of Geophysical Research, V. 69, p. 4417.

Press, F., and Archambeau, C., 1962, Release of Tectonic Stress by Underground Nuclear Explosions; Journal of Geophysical Research, V. 67, p. 337.

Reily, D., and Cushing V., 1967, Characteristic Emissions from an Underground Explosion; Engineering Physics Company Report, DA-49-146-XZ-089.

Richter, C., 1957, Elementary Seismology, Freeman Press.

Rogers, L. A., 1966, Free-Field Motion Near a Nuclear Explosion in Salt: Project Salmon, Journal of Geophysical Research, V. 71, p. 3415.

Rulison Project Definition Plan; December 9, 1968.

Schultz, A., 1967, Magnification of Love Waves; Environmental Research Corporation Report, NVO-1163-80.

Sharpe, J. A., 1942, The Production of Seismic Waves by Explosion Pressures. I. Theory and Empirical Field Results; Geophysics, V. 18, p. 144.

Springer, D. L., 1966, P. Wave Coupling of Underground Nuclear Explosions; Bulletin of the Seismological Society of America, V. 56, p. 861.

Stuart, D. J., Roller, J. C., Jackson, W. H., and Mangan, G. B., 1964, Seismic Propagation Paths, Regional Traveltimes, and Crustal Structure in the Western United States, Geophysics, V. 29, p. 178.

Sutton, G., and Pomeroy, P., 1963, Analog Analysis of Seismograms Recorded on Magnetic Tape; Journal of Geophysical Research, V. 68, pp. 2791-2815.

Tentative Operational Plan--Project Rulison (Draft); November 27, 1967.

Thompson, K. C., Ahrens, T. J., and Toksoz, M. N., 1969, Dynamic Photoelastic Studies of P and S Wave Propagation in Prestressed Media, Geophysics, V. 34, p. 696.

United States Coast and Geodetic Survey Seismic Stations, Event Rulison (Final Station Coordinates), December, 1969.

Voegeli, Sr., P. T., 1969, "Geology and Hydrology of the Project Rulison Exploratory Hole, Garfield County, Colorado," Open File Report 474-16 (Rulison 1), USGS.

Weart, W.D., 1965, Free-Field Earth Motion and Spalling Measurements in Granite, Project Shoal, VUF-2001, Sandia Corporation.

Weetman, B. G., and others, 1969, Predictions of Seismic Motion and Close-in Effects, Rulison Event; Environmental Research Corporation Report, NVO-1163-180.

Werth, G. C., Herbst, R. F., and Springer, D. L., 1962, Amplitudes of Seismic Arrivals from the M Discontinuity; Journal of Geophysical Research, V. 67, p. 1587.

White, J. E., 1965, Seismic Waves: Radiation, Transmission, and Attenuation, McGraw-Hill Book Company, New York.

Yeend, Warren E., 1967, "Quarternary Geology of the Grand-Battlement Mesa Area, Colorado," USGS Report--Open File Series No. 945.

Yeend, W. E., and Donnel, J. R., 1968, "Rulison Area Geologic Maps," USGS--Open File.

Zienkiewicz, O. C., and Cheung, Y. K., 1967, The Finite Element Method in Structural and Continuum Mechanics, McGraw-Hill Publishing Co., Ltd., London.

APPENDIX A

GEOLOGIC ENVIRONMENT

A.1 Introduction

The three main regions, which play an important role in shaping the resultant ground motion observed at a site, are as follows: (1) the source and hydrodynamic region, (2) the elastic-wave-transmission region, and (3) the receiver and near-surface region. The geologic environment of these regions is described below.

A.2 Regional Geologic Environment of the Rulison Detonation

The Rulison Project occurred in northwestern Colorado in the Rulison gas field of the Piceance Creek Basin (Figure A-1). In general terms, this basin is geologically similar to the San Juan Basin of New Mexico where the Gasbuggy event took place. Both these geologic basins are characterized by thick sequences of sedimentary deposits which are evenly distributed over a wide area, gently downwarped, and display shallow dips toward the central portion of the structure. Essentially flat-lying beds of shale, sandstone, and siltstone predominate at both sites. Figures A-1 and A-2 illustrate the general basin configuration. The Mesaverde formation, lying

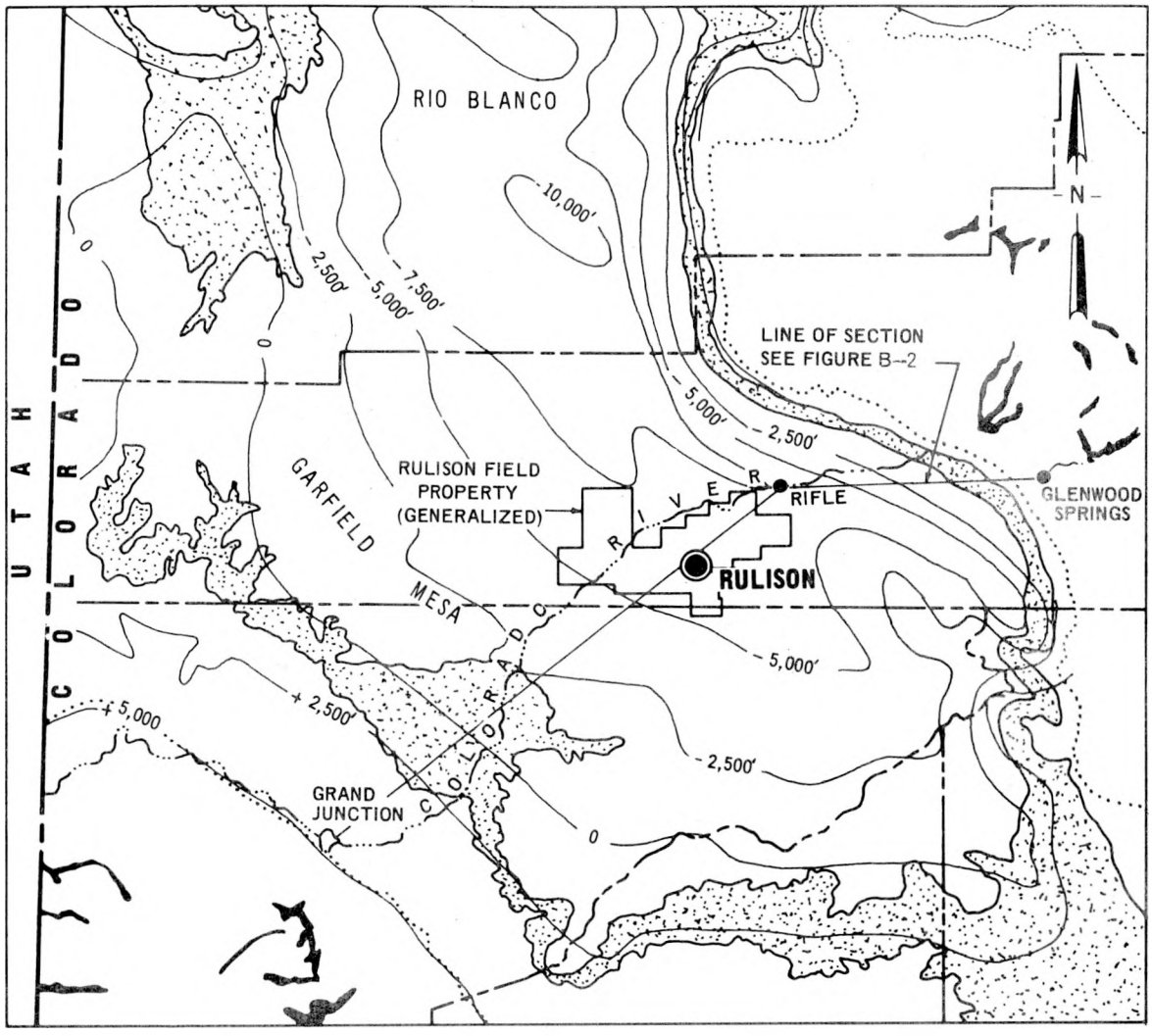

Figure A-1. Regional Geological and Structural Map of the Piceance Creek Basin, Northwestern Colorado, showing the Rulison Site

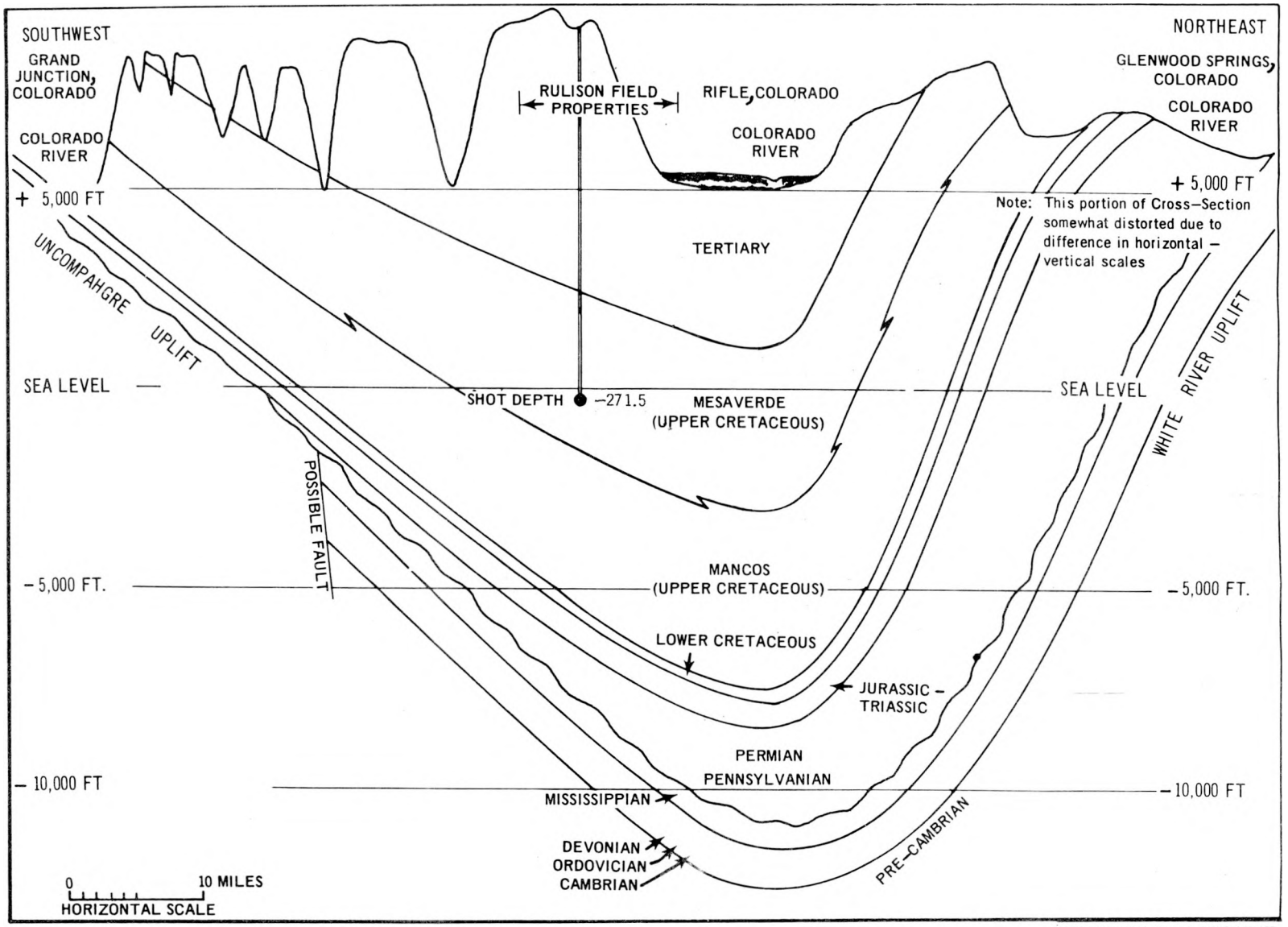

FROM RULISON PROJECT DEFINITION PLAN (1968)

Figure A-2. Generalized Cross-Section Across the Piceance Creek Basin, Colorado

at a depth of 6,188 feet under the Rulison site (Table A-1), crops out several tens of miles from the Rulison well and delineates the Piceance Creek Basin perimeter.

A.3 Geology of the Source Region

A.3.1 Location and Topography

The Rulison emplacement hole is in the upper reaches of Battlement Creek on the north slope of Battlement Mesa. The creek valley opens to the north-northwest and is bounded on the east, south, and west by slopes rising to above 9,600 feet (Tentative Operational Plan--Project Rulison, 1967).

A.3.2 Stratigraphy and Lithology

The emplacement hole, located on the southwest flank of the Piceance Creek Basin, penetrates relatively flat-lying upper Cretaceous beds which dip toward the northeast at an angle of 2° or less (Voegeli, 1969). Table A-1 summarizes the stratigraphy and lithology of the emplacement hole. Additional geologic information can be found in the Rulison Project Definition Plan (1968), Yeend (1967), Voegeli (1969), and Weetman, et al., 1969).

Table A-1

General Sequence of Rocks Overlying the Rulison Gas-Bearing Formation (Mesaverde)
(Voegeli, 1969 and Rulison Project Definition Plan, 1968)

System and Period	"Formations"	General Lithology of Piceance Creek Basin	Depth at Hole R-EX
Quaternary	"Recent"	Low Terrace, flood plain and alluvial deposits	
	"Pleistocene"	Terrace and fan sand and gravel, pediment gravel, colluvium, mudflow, and solifluction deposits	
Tertiary	Green River	Shales, marlstones, and minor sandstones siltstones, and limestone	1,700 ft.
	Wasatch	Bright colored clays and shale with minor sandstone lenses	
	(Unnamed)	Sandstone, shale and coal	6,134 ft.
	Ohio Creek	Sandstone, siltstone, and conglomerate	6,188 ft.
Cretaceous (Upper)	Mesaverde	Shale - sandstone	Shot Point 8,442.5 ft.

A.3.3 Physical Properties

Table A-2 lists the range and the average of physical properties determined from a Birdwell 3-D Computation log which was run in the detonation medium, the Mesaverda formation. In the log, properties were computed for every foot over the depth interval of 6,460 - 8,479 feet; however, only the 1,000-foot interval between 7,450 and 8,450 feet (W. P. at 8,442) was used to calculate the physical property values shown on the table. The figures given for the average values are the result of taking the numerical average of 1,000 values for each of the properties with the exception of the longitudinal and transverse velocities. The average velocities were derived by determining the travel times over small intervals and dividing the total 1,000-foot interval by the sum of these travel times.

The following physical properties of the Mesaverde formation (detonation medium) are averages taken from the Rulison Project Definition Plan, 1968. These are derived from wells in other parts of the Rulison field.

Median Porosity	9.7%
Average Water Saturation	45.0%
Average Gas Saturation	54.0%
Average Oil Saturation	2.0%
Average Overburden Density	2.35 gm/cc

Table A-2. Physical Properties of the Rulison W. P. Medium
(First 1,000 feet over the W. P. - Mesaverde formation)

Property	Units	Range of Values	Average Value
Longitudinal Velocity	ft/sec	12,270 - 19,350	15,200
Transverse Velocity	ft/sec	6,550 - 9,940	8,250
Bulk Modulus	psi x 10^6	2.46 - 9.19	4.93
Shear Modulus	psi x 10^6	1.26 - 3.41	2.19
Young's Modulus	psi x 10^6	3.31 - 8.95	6.09
Porosity	%	7.0 - 24.0	13.0
Density	g/cc	2.05 - 2.65	2.53

A.3.4 Structure

Bedding under the Rulison site is essentially parallel and displays a dip of approximately 150 feet per mile to the northeast. In the vicinity of the emplacement hole, stereo aerial photography disclosed lineations which were subsequently examined by field reconnaissance. Most of the lineations were found to be related to well-developed joint sets. Others were associated with slide margins and topographically controlled vegetation changes. No displacements or traces of faulting were found (Rulison Project Definition Plan, 1968).

A.3.5 Hydrology

Hydrologic tests in the Rulison exploratory hole indicated that little or no water occurs in the Ohio Creek conglomerate and Mesaverde group. These units were expected to be the stratigraphic units most likely to yield water to the hole (Voegeli, 1969). Six depth intervals, ranging from 6,129 feet to 8,018 feet were tested. While the test tool was open in the individual zones, the recorded pressures indicated little or no fluid entry (Voegeli, 1969).

A.4 Geology of the Elastic Wave Transmission Region

The Rulison detonation and the receiving stations of interest (see Section A.5) are located well within the more

geometrically regular portion of the Piceance Creek Basin. The Rulison site is underlain by about 18,000 feet of marine and non-marine sedimentary rocks which are essentially parallel, flat-lying, and areally extensive (Voegeli, 1969). Therefore, the geologic environment through which the seismic energy travels to the nearby recording stations may be considered to be more predictable as a transmitting medium, offering primarily variations in the elastic constants at the geologic "boundaries" (discussed in Chapter 4) to modify the seismic signals.

A.5 Geologic Environment of Recording Sites

In the Rulison area, many of the station sites are covered with a thin layer of relatively unconsolidated material, such as soil or alluvium. In a general way, the geologic configuration of the Rulison site is comparable to the sites in New Mexico which recorded the Gasbuggy event (Weetman, et al., 1969).

Brief generalized descriptions of the geologic characteristics of selected close-in stations which recorded the Rulison detonation are given in Table A-3. These stations are well within the perimeter of the Piceance Creek Basin. Data gained from refraction surveys conducted at seven sites

(Eames Orchard, Lemon Ranch, Rulison, Grand Valley, the Union Carbide plant, Rifle, and Harvey Gap Dam) to delineate near-surface layer thicknesses and compressional wave velocities, were incorporated (described in Chapter 4 of this report and by Weetman, et al., 1969). Additional information was taken from the color photographs and text by Navarro and Wuollet (1969). At sites where no detailed data were available, surface geology of the general station locality was taken from the Geologic Map of Colorado, USGS, Reprinted 1967. The description at Harvey Gap Dam is based on data presented in a report by John A. Blume and Associates (JAB-99-63).

TABLE A-3

DESCRIPTION OF THE GEOLOGIC CHARACTERISTICS OF SELECTED RULISON INSTRUMENT SITES

Recording Site	Description
Battlement Mesa	The instrument site was located at a slant range of 4.9 km on the shore of a reservoir. The site is underlain by an unknown thickness of alluvium underlain by slump blocks, talus, and solifluction deposits (Yeend and Donnel, 1968).
Eames Orchard (Morrisania Mesa)	The site was located at a slant range of 6.2 km on 8 to 13.5 feet of unconsolidated material underlain by older, more consolidated terrace and fan gravels of unknown thickness (Weetman, et al., 1969; Yeend and Donnel, 1968; Navarro and Wuollet, 1969).
Lemon Ranch (Holmes Mesa)	The seismometer was placed at a slant range of 6.4 km on 1.5 to 10.5 feet of unconsolidated surface material, underlain by an unknown thickness of older, probably more endurated terrace and fan gravels (Weetman, et al., 1969; Yeend and Donnel, 1968; Navarro and Wuollet, 1969).
Rulison	The instrument was located at a slant range of 8.7 km on approximately 11 feet of unconsolidated flood plain deposits underlain by 27 feet of what is probably terrace and fan gravels. This material, in turn, is underlain by shales and claystones (Weetman, et al., 1969; Yeend and Donnel, 1968).
Grand Valley	The instrument site was situated at a slant range of 10.6 km on approximately 15 feet of unconsolidated younger gravels and flood plain deposits underlain by either well consolidated older gravels or clays and shales (Weetman, et al., 1969; Yeend and Donnel, 1968).

TABLE A-3 (Continued)

Recording Site	Description
Richardson Ranch	The instrument was placed at a slant range of 12.7 km on an unknown thickness of terrace gravels underlain by sandstone (Yeend and Donnel, 1968).
Anvil Points	The seismometer was placed at a slant range of 13.3 km on thin soil over clays and shales (Navarro and Wuollet, 1969; U.S.G.S., 1967.
Mobil Mines	The instrument was placed at a slant range of 14.6 km. It was located in a mine tunnel, probably directly on competent rock of the Green River formation (shale, sandstone, or marlstone) (Navarro and Wuollet, 1969; U.S.G.S., 1967).
Union Carbide	The station was situated in the valley flat of the Colorado River at a slant range of 18.0 km. The surface is about 12 feet of unconsolidated valley fill over an unknown thickness of relatively indurated older alluvium or the clays and shales of the Wasatch formation (Weetman, et al., 1969; U.S.G.S., 1967).
Rifle	The seismometer was located at a range of 20.2 km on 11.5 to 21 feet of unconsolidated valley fill over an unknwon thickness of either well indurated older gravels or shales and siltstones (Weetman, et al., 1969; U.S.G.S., 1967).
De Beque	The instrument sites were located a distance of 22.8 km. They were apparently placed on relatively thick alluvial fill underlain by shales and clays (Navarro and Wuollet, 1969; U.S.G.S., 1967).

TABLE A-3 (Continued)

Recording Site	Description
Harvey Gap Dam	The station was located near the top of the dam at a range of 32.4 km. The dam consists of a homogeneous embankment of stiff clay which, at the crest, is approximately 80 feet thick. This dam embankment is probably underlain by the clays, shales, and siltstones of the Wasatch formation. This "bed rock" surface apparently parallels the 25-30 degree downstream slope of the embankment so that, at the foot of the dam, the underlying hardrock surface is approximately 85 to 110 feet below the ground surface. The overlying layers here consist of about 25 feet of relatively dry, loose silty-- to sandy clay underlain by 60 to 85 feet of saturated clay, silt, and some gravel (Weetman, et al., 1969; U.S.G.S., 1967; John A. Blume and Associates, 1969).

DISTRIBUTION - NVO-1163-206

Mr. R. A. Johnson, AEC/NVOO, Las Vegas, Nevada (3 copies)
Mr. R. R. Loux, AEC/NVOO, Las Vegas, Nevada (20 copies)
Dr. R. L. Aamodt, LASL, Los Alamos, New Mexico (1 copy)
Mr. Robert Campbell, LASL, Los Alamos, New Mexico (1 copy)
Mr. R. W. Newman, LASL, Los Alamos, New Mexico (1 copy)
Dr. W. E. Ogle, LASL, Los Alamos, New Mexico (1 copy)
Dr. J. W. Hadley, LRL, Livermore, California (1 copy)
Dr. W. J. Hannon, LRL, Livermore, California (1 copy)
Dr. G. H. Higgins, LRL, Livermore, California (1 copy)
Dr. Fred Holzer, LRL, Livermore, California (1 copy)
Dr. H. L. Reynolds, LRL, Livermore, California (1 copy)
Mr. D. Springer, LRL, Livermore, California (1 copy)
Dr. G. C. Werth, LRL, Livermore, California (1 copy)
Dr. J. R. Banister, Sandia Corp., Albuquerque, New Mexico (2 copies)
Dr. M. L. Merritt, Org. 5412, Sandia, Corp., Albuquerque, New Mexico (1 copy)
Dr. W. E. Weart, Org. 512, Sandia Corp., Albuquerque, New Mexico (1 copy)
Dr. L. K. Bustad, School of Vet. Med., U of C., Davis, Cal. (1 copy)
Dr. D. U. Deere, University of Illinois, Urbana, Illinois (1 copy)
Dr. C. Kisslinger, St. Louis University, St. Louis, Mo. (1 copy)
Dr. G. B. Maxey, University Station, Reno, Nevada (1 copy)
Dr. N. M. Newmark, University of Illinois, Urbana, Illinois (1 copy)
Dr. L. A. Sagan, Dept. of Environ. Health, Palo Alto Medical Clinic, Palo Alto, California (1 copy)
Dr. Vincent Schultz, Department of Zoology, Washington State University, Pullman, Washington (1 copy)
Mr. T. F. Thompson, San Francisco, California (1 copy)
Dr. W. G. Van Dorn, Scripps Inst. of Oceanography, La Jolla, California (1 copy)
Mr. L. G. vonLossberg, Sheppard T. Powell & Associates, Baltimore, Maryland (1 copy)
Dr. J. T. Wilson, University of Michigan, Ann Arbor, Mich. (1 copy)
Mr. S. D. Wilson, Shannon & Wilson, Inc., Seattle, Washington (1 copy)
Dr. M. B. Biles, AEC/DOS, Hq., Washington, D.C. (1 copy)
Maj. Gen. E. B. Giller, AEC/DMA, Hq., Washington, D.C. (2 copies)
Mr. Richard Hamburger, AEC/DPNE, Hq., Washington, D.C. (1 copy)
Mr. J. S. Kelley, AEC/DPNE, Hq., Washington, D.C. (1 copy)
Mr. P. L. Russell, USBM, Denver, Colorado (1 copy)
Mr. K. W. King, USC&GS, Las Vegas, Nevada (2 copies)
Mr. Wendell Mickey, USC&GS, Rockville, Maryland (1 copy)
Dr. W. S. Twenhofel, USGS, Denver, Colorado (1 copy)
DTIE, Oak Ridge, Tennessee (1 copy)

DISTRIBUTION - NVO-1163-206 (continued)

Mr. Eberhardt Rechtin, ARPA, Washington, D.C. (1 copy)
Mr. Lyman Heller, WES, Vicksburg, Mississippi (1 copy)
Dr. Benjamin Grote, TCD-B, DASA, Sandia Base, Albuquerque, New Mexico (2 copies)
Lt. Commander R. O. Johnstone, ACDA/WEC, Washington, D.C. (1 copy)
Dr. J. A. Blume, John A. Blume & Associates, San Francisco, California (2 copies)
Mr. L. E. Rickey, H&N, Las Vegas, Nevada (1 copy)
Dr. L. B. Werner, Isotopes, Inc., Palo Alto, California (1 copy)
Mr. Chalres Atkinson, USBM, Bartlesville, Oklahoma (1 copy)
Resident Manager, H&N, Inc., Mercury, Nevada (1 copy)
Environmental Research Corporation, Las Vegas, Nevada (1 copy)
Environmental Research Corporation, Alexandria, Virginia (5 copies)